Influence of Lamin A E145K progeria mutation on nuclear mechanics

Dissertation

submitted as a partial fulfillment
for procuring the degree

Doctor of Natural Sciences

–Dr. rer. nat.–

to
Fachbereich 2 Biologie/Chemie, Universität Bremen

by

Ketaki Apte

Bremen, December 2013

Contents

Summary

Lamins are intermediate filament proteins. They are structural components of the nuclear lamina, a filamentous meshwork beneath the inner nuclear membrane, which confers mechanical stability to the nucleus. Mutations in the human *LMNA* gene cause a wide range of diseases called laminopathies. Amongst these is the Hutchinson-Gilford progeria syndrome (HGPS), a rare premature aging disorder. One of the mutations causing HGPS is a heterozygous point mutation E145K within the central domain of the lamin A protein. The E145K mutation affects lamin filament assembly and induces profound changes in the composition and architecture of the patient cell nuclei. In vitro analyses of purified E145K lamin A reveal severe assembly defects into higher order lamin structures, indicating an abnormal lateral association of lamin protofilaments. Ex vivo expression of the wild-type and E145K lamin A in *Xenopus* oocytes showed influence of the mutant lamin A on the mechanical properties of the lamina as revealed by atomic force microscopy (AFM). Nuclear laminae made up of overexpressed E145K lamin A were stiffer than those harboring wild-type lamin A.

In this work, mechanical properties of somatic cell nuclei were studied using AFM. In pilot experiments with HeLa cells AFM data acquisition and analysis was optimized. Next, the mechanical properties of the dermal fibroblasts of a four years old progeria patient bearing the E145K lamin A mutation were analyzed using AFM. The abnormal shape of nuclei expressing E145K lamin A and alterations in the cellular actin network were revealed by fluorescence microscopy. Lamina thickness was assessed by transmission electron microscopy. AFM probing of entire dermal fibroblasts revealed minor differences in the elastic moduli of nuclear and cytoplasmic cell regions. Thus, isolation of the nuclei was done to directly measure their mechanical properties by AFM. Isolated nuclei of the progeria patient (age 4) and the old person (age 61) were significantly stiffer than those of a young person (age 10). These results indicated that lamin A E145K alters the mechanical properties of the nuclei of the dermal fibroblasts obtained from a progeria patient. Thus, it was shown that the process of aging, be it natural or abnormal, increases the stiffness of nuclei.

Zusammenfassung

Lamine gehören zur Familie der Intermediärfilamentproteine. Sie bilden den Hauptbestandteil der Kernlamina, einem Filamentnetzwerk unterhalb der inneren Kernmembran. Die Kernlamina gibt dem Kern mechanische Stabilität. Mutationen im *LMNA*-Gen verursachen eine Reihe menschlicher Erbkrankheiten, die als Laminopathien bezeichnet werden. Eine dieser Krankheiten ist das Hutchinson-Gilford Progerie Syndrom (HGPS), eine seltene Form des frühzeitigen Alterns. Eine für HGPS verantwortliche Mutation ist die Punktmutation E145K in der zentralen Domäne des Lamin A-Proteins. Diese Mutation beeinträchtigt die Filamentbildung und verursacht tiefgreifende Veränderungen im Aufbau des Zellkerns. In vitro-Assemblierungsversuche mit aufgereinigtem Lamin A E145K-Protein zeigten schwere Defekte in der Filamentbildung verursacht durch eine Störung der lateralen Assoziation von Protofilamenten. Kraftmikroskopische Messungen von *Xenopus* Oocytenkernen, die Lamin A E145K exprimierten, zeigten, dass eine aus Lamin A E145K bestehende Lamina steifer ist als eine Lamina aus Wildtyp Lamin A.

Im Rahmen dieser Arbeit wurden die mechanischen Eigenschaften somatischer Zellkerne mittels Kraftmikroskop (AFM) bestimmt. In Pilotversuchen mit HeLa-Zellen wurde die Durchführung der kraftmikroskopischen Analysen optimiert. Danach wurden die mechanischen Eigenschaften von Hautfibroblasten eines vier Jahre alten Progeriapatienten, der die Mutation E145K trug, durch kraftmikroskopische Experimente bestimmt. Fluoreszenzmikroskopische Untersuchungen der Fibroblasten zeigten eine abweichende Gestalt ihrer Kerne sowie die Veränderung ihres zellulären Aktinnetzwerks. Die Dicke der Lamina wurde durch transmissionselektronenmikroskopische Analysen bestimmt. Die nukleären und cytoplasmatischen Regionen der Hautfibroblasten zeigten nur minimale Unterschiede in den elastischen Moduli, wenn die Messungen an intakten Zellen vorgenommen wurden. Daher wurden die Kerne dieser Zellen isoliert und ihre mechanischen Eigenschaften durch AFM-Analysen bestimmt. Sowohl die Kerne des Progeria-Patienten als auch die Kerne einer 61 Jahre alten Person waren signifikant steifer als die Kerne einer 10-jährigen Person. Damit konnte bestätigt werden, dass Lamin A E145K die mechanischen Eigenschaften der Lamina somatischer Zellen verändert. Zudem konnte gezeigt werden, dass sich im Zuge des Alterungsprozesses – sei er natürlich oder krankheitsbedingt vorzeitig – die Steifigkeit der Zellkerne erhöht.

Acknowledgements

I express sincere gratitude towards Prof. Dr. Reimer Stick for giving me this wonderful opportunity to work in his group as a doctoral candidate. I thank you for being not only my research supervisor but for also being a kind, encouraging mentor. Those stimulating discussions, valuable critiques and advices have helped me develop a different perspective towards scientific research.

I am very grateful to Prof. Dr. Manfred Radmacher for allowing me to be a part of the fruitful collaboration between the Cell biology and Biophysics Institutes. I also thank you for reviewing my thesis and for your constructive suggestions during planning and development of this project. I am thankful to all the members of the Biophysics Institute who constantly helped and guided me while working with AFM. Special thanks to Ing. Holger Doschke for all the technical assistance and development of programs for analyzing the AFM data. I would like to thank Meenakshi for introducing the AFM to me and Dr. Jens Shäpe for his support with troubleshooting and valuable discussions in the lab.

I thank Prof. Dr. Andreas Dotzauer for agreeing to be the examiner in my thesis committee and for his valuable advices in cell culture maintenance. I also thank the University of Bremen for the financial support provided during the course of my studies. I am grateful to the members of eCOST action committee who provided funding for my visit to Dr. Laura Gasparini's lab in the Italian Institute of technology, where I could learn new techniques under the excellent guidance of Dr. Denise Ferrera and Dr. Claudio Canale.

I owe a lot to my dearest colleague, Dr. Annette Peter. Your constant support, encouragement upon failures and experienced suggestions during execution of the entire project were absolutely irreplaceable. I would also like to thank you for reading my thesis drafts in shortest possible time and for suggesting improvements in them.

A big thanks to all the current and past members of AG Stick. I would specially like to thank Ute for all the help with TEM, Regina and Bärbel for their support and help throughout my PhD. I really enjoyed working in the lab with my present and past colleagues- Kristina, Shweta, Eva, Amod, Jana, Emily, Carolyn, Nimesha, Paul and all the members of AG Reinhold especially- Teja and Mugdha.

I would not have reached this far without the perpetual support of my entire family and friends throughout my stay in Germany. I express deepest gratitude towards my parents including my uncle, aunt and cousin brother, as well as my in-laws for their endless encouragement which inspired me to pursue my interests in the field of science. Thank you for making me strong and giving me that boost of positivity from time to time. Last but definitely not the least, I am extremely grateful to Shaunak, the support system of my life, for always being there for me and taking care of everything else when I was busy with work.

1

Introduction

1.1 Aging

One of the key features of all living beings is aging. It is a complex process, which results in gradual modifications in the cellular functions that are necessary for survival. Aging can be defined as a decline in various biological functions along with reduction in the ability of a cell to adapt to metabolic changes. In prokaryotes, the effects of aging are not macroscopic but the biochemical changes occur in such a way that affects the proliferation capacity of the culture. Although they show morphologically similar divisions, the daughter cells show an uneven physiological distribution of the cellular contents [1]. In mammals, some of the metabolic alterations result into pronounced effects that are regarded as typical symptoms of aging. Major symptoms of human aging are wrinkled skin, hair loss eventually leading to balding, loss of bone rigidity and muscle strength, and changes in the elastic properties of the skin.

In human body, the cells belonging to different tissues, age at remarkably different rates. The epithelial cells of the intestine, which are repeatedly exposed to harsh conditions in the gut, are renewed every 3-6 days [2] in contrast to neurons, which do not show cell division after their formation at perinatal stage [3]. It has been shown that the muscle cells do not undergo mitosis and tend to seldom divide [4]. Turnover of the adipocytes and cardiomyocytes has also been shown to slow down as the age increases. Bergmann et al. have observed that turnover of the cardiomyocytes by age of 75 years can become as low as 0.45% [5]. A plethora of literature is available

about the studies done to characterize the tissue specific cell types, cell division, proliferation and the turnover of the cells originating from different tissues. But the biochemical interactions that occur as a part of metabolism of such long-lived or short-lived cells, have not been studied well. Moreover, it is of prime importance to discover the role of the proteins and biomolecules, in terms of their renewal and repair during development and cell growth, which are affected with increasing age. If the resynthesis of these macromolecules is altered, they can accumulate over time and disturb routine cellular functions which ultimately can affect the overall tissue function [6].

1.2 Aging disorders

Aging disorders are generally referred to as progeroid syndromes which mimic physiological senescence and are classified as rare genetic disorders [7]. These syndromes generally arise from a mutation in a single gene which either generates defects in DNA repair mechanism or in the human lamin A gene (*LMNA*). More than 75 types of progeroid syndromes have been described so far (for review, see [8]). Some of the premature aging disorders are: Werner's syndrome (WS), xeroderma pigmentosum, trichothiodystrophy, restrictive dermopathy, and Hutchinson-Gilford progeria syndrome (HGPS). These syndromes are differentiated into two types depending upon the number of organs that are affected. In case of the unimodal syndromes, only one type of organ is affected. For example in the disease xeroderma pigmentosum only the skin shows symptoms of accelerated aging. On the contrary, in the segmental progeroid syndromes, like HGPS and WS, multiple organs are affected simultaneously. Notably, not all of the symptoms of accelerated aging disorders resemble the symptoms of physiological aging. Typical symptoms of progeroid syndromes involve severe growth retardation, hair loss, diminished bone density and loss of subcutaneous fat. But these patients lack the features that are linked with normal senescence for example, reduction in cognitive abilities, cataract development, increased susceptibility to tumor formation and cardiovascular defects [9]. Since the past decade, various investigations have been undertaken for studying biochemical and mechanical properties of the cells of the progeroid patients to gain

insights into the mechanisms responsible for natural aging. HGPS is one of the premature aging disorders which is caused due to mutation in the *LMNA* gene [10]. Werner's syndrome on the other hand is caused due to an inherited autosomal recessive mutation in the *WRN* gene which encodes for a RecQ DNA helicase with exonuclease activity [11]. Atypical Werner's syndrome, however, develops due to missense mutations in the *LMNA* gene which cause amino acid changes either in the rod or the tail domain of lamin A.

1.3 Laminopathies

Genetic disorders that are caused due to mutations in the lamin genes are collectively termed as laminopathies. In 1999, Bonne et al. reported the first laminopathy mutation causing muscular dystrophy [12]. To date, at least 12 heritable diseases have been reported which are caused due to mutations in the human *LMNA* gene which are spread along the entire *LMNA* gene. Laminopathic mutations in the *LMNA* gene either selectively affect a particular type of tissue (for example lipodystrophy), or can alter function of multiple tissues simultaneously (progeroid syndromes). Depending on the type of the affected tissue and severity of the disease, laminopathies are classified into four different categories, namely, myopathies (affecting the striated muscle tissues), lipodystrophies (affecting adipose tissue), neuropathies (affecting peripheral nervous system) and the premature aging syndromes (systemic defects as multiple tissue types are affected simultaneously) [13], [14]. The myopathies involve diseases that cause abnormalities in the muscles, for example, autosomal recessive Emery-Dreifuss muscular dystrophy (EDMD), autosomal dominant limb girdle muscular dystrophy (AD-LGMD) and dilated cardiomyopathy (DCM), all of which include cardiac conduction defects [12]. Laminopathies in which the adipose tissue is affected, are autosomal dominant Dunnigan-type familial partial lipodystrophies (FPLD) [15], [16]. The neuropathic disorders include Charcot-Marie-Tooth disorder type 2 where axonal neurons are affected along with occurrence of EDMD in some patients [17]. The accelerated aging disorders are Hutchison-Gilford progeria Syndrome (HGPS), atypical Werner's syndrome, restrictive dermopahty (RD) and mandibuloacral dysplasia (MAD) [10].

In comparison to the mutations in the *LMNA* gene, fewer laminopathies linked to the mutations in the B-type lamin genes are known. An adult-onset autosomal dominant leukodystrophy (ADLD) associated with *LMNB1* duplication has been reported [18], but other mutations in *LMNB1* have not been explored to a larger extent yet. ADLD is neurological disorder with a slow progression pattern with excessive loss of myelin in the central nervous system [18]. Some mutations along the *LMNB2* gene have also been reported, that can lead to development of acquired partial lipodystrophy [19]. It has also been shown that ablations in the B-type lamin genes might be lethal [20] or can cause severe reduction in cell proliferative capacity [21].

HGPS is a premature aging disease with most devastating effects on a number of tissues like skin, bones, muscles and heart [22], [23], [10]. Children affected with progeria appear normal during birth but the progeric symptoms start to develop by an age of 2 years. Prominent symptoms are: delayed dentition, slow growth, alopecia, loss of subcutaneous fat and sclerodermatous skin changes. Patients normally die in their early teens due to myocardial infarction and/or a cerebrovascular accident. Additional features in the course of disease development are short stature, presence of beaked nose, overall aged appearance and during the final stages of the disease, angina and hypertension with a dilated heart [24]. To date many attempts have been made to decipher the connection between the various mutations in lamin genes and their severe effects on functioning of various types of cells and tissues. These mutations are observed to not only affect the structure of the lamin filaments but also cause abnormalities in the nuclei. The fibroblasts derived from HGPS patients show progressive lobulations and nuclear deformations as the cells age. Contrastingly, fibroblasts obtained from an old healthy person show very low percentage of nuclei with deformations upon aging [25]. The most frequent HGPS mutation is a de novo heterozygous point mutation wherein the nucleotide T replaces C at position 1824. Although the nucleotide change does not cause any change in the amino acid sequence, it activates a cryptic splice donor site resulting into abnormal splicing of the mRNA encoding lamin A. The splicing results into deletion of 150 nucleotides (corresponding exon 11 of the *LMNA* gene) in the lamin A transcript. This deletion results in a truncated protein designated as LAΔ50 or progerin which remains

permanently farnesylated [23], [10]. Progerin is shown to be responsible for nuclear deformations, and also causes onset of premature aging [25].

Another heterozygous HGPS mutation in the central domain of lamin A was reported by Eriksson et al. [23], in which the glutamate residue (E) at the amino acid position 145 is replaced by a lysine residue (K). Dermal fibroblasts of a progeria patient with the lamin A E145K mutation also show severe lobulations in the nuclear envelope [26]. The cells show a reduced proliferative capacity with significant increase in senescence associated β-galactosidase activity. Additionally, the E145K mutation was shown to be responsible for centromere clustering and telomere mislocalization in the nuclei. Nuclear invaginations developed post mitotically with a reduction in the total amount of lamin B1 in the progeria cell nuclei [26]. Moreover, in vitro assembly experiments conducted with the purified human lamin A E145K progeria mutant protein also revealed defects in the lamin filament assembly and ultimately formed unstructured paracrystalline arrays as compared to the well structured wild-type lamin A arrays [26]. Thus, lamins play a critical role in nuclear and cellular functions as the abnormalities in their functioning are shown to be responsible for disease development.

1.4 Lamins

The central functional unit of an eukaryotic cell is the nucleus which is delimited by a nuclear envelope from the corresponding cytoplasmic compartment. The nuclear envelope consists of outer and inner nuclear membranes with the nuclear pore complexes. Underneath the inner nuclear membrane, a protein meshwork is located which is called the nuclear lamina (see Figure 1.1). It serves as a platform for interactions between the peripheral chromatin and its intranuclear binding partners. Lamins are major structural components of the nuclear lamina and are an inherent part of the nuclear envelope. They are members of the intermediate filament (IF) protein family [27]. Lamins are thought to be involved in a number of processes such as DNA replication [28], [29], cell division etc. and are shown to confer structural stability of the nucleus [30]. Lamins interact with both, the integral proteins of the inner nuclear membrane and with chromatin binding proteins [31]. Lamins

also play a vital role in determining the shape and size of the nucleus along with other cytoplasmic factors [25], [32] and in the assembly-disassembly of the nuclear envelope during mitosis [33].

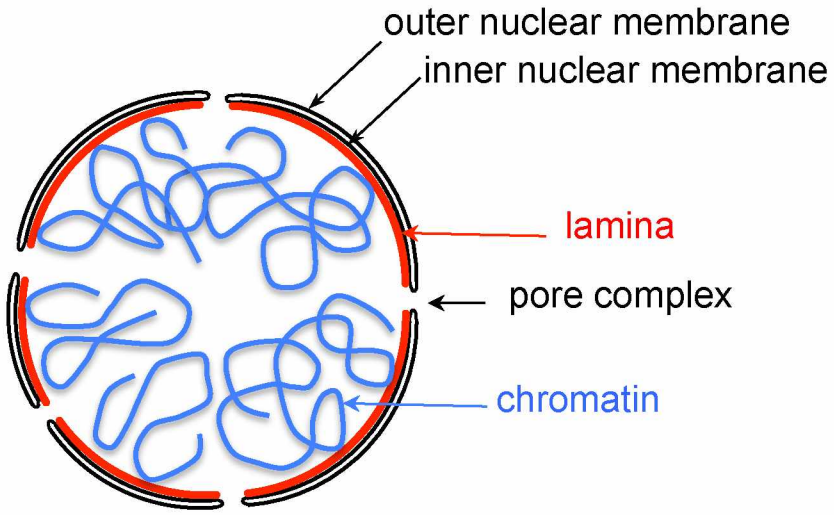

FIGURE 1.1 Schematic representation of the nuclear envelope. The nuclear envelope consists of an outer nuclear membrane, an inner nuclear membrane, the lamina *(red)* which underlines the inner nuclear membrane with the nuclear pore complexes embedded in the membranes. The nucleoplasm mainly contains the chromatin *(blue)*.

Lamins belong to the class V of the IF proteins. They are shown to be the ancestors of the cytoplasmic IF proteins [34], [35], [36]. A lamin monomer is comprised of a non-helical N-terminal domain, an α-helical central rod domain, which can form coiled coils, and a C-terminal domain, as shown in Figure 1.2. A globular immunoglobulin (Ig)-like fold and a nuclear localization signal (NLS) are present in the tail domain of the protein [37], [38]. Entry of lamins into the nucleus and their targeting to the inner nuclear membrane depends respectively on the presence of an NLS and lipidation of the C-terminal CaaX motif. A CaaX motif denotes the last four amino acid residues of the lamin protein sequence which is a target for posttranslational modifications which occur in three consecutive steps. The lipidation of the cysteine residue (C) is followed by removal of the last three amino acid residues (-aaX) by an endoplasmic reticular endoproteolytic enzyme

Rce1 or Zmpste24. In the third step, the prenylated cysteine is carboxymethylated by a methytransfearse, Icmt1 [39].

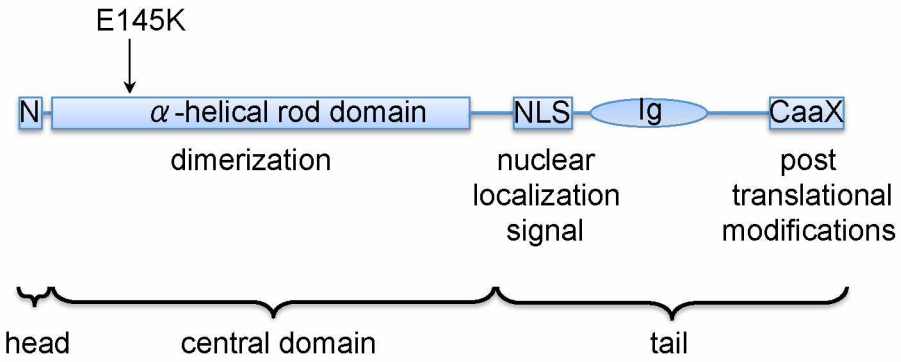

FIGURE 1.2 Schematic diagram of the structure of a lamin monomer. Lamins exhibit tripartite structure with a central α-helical rod domain flanked by an N-terminal head and C-terminal tail domain with the globular Ig-like fold. The CaaX indicates a set of four amino acid residues which are target for post-translational modifications. Lamins harbor a nuclear localization signal (NLS) required for their targeting to the nucleus. Location of the E145K HGPS mutation in the rod domain is indicated by a solid black arrow.

Based on their biochemical properties, like gel electrophoretic mobilities and domain structures, lamins can be generally divided into A-type and B-type [40]. A-type lamins are restricted to vertebrates. Their absence in invertebrates, for example in *Caenorhabditis elegans*, indicates that they evolved late in metazoan evolution [36]. A-type lamins have additional 50-100 amino acid residues in their tail domain as compared to B-type lamins. These amino acid residues are encoded by an additional lamin A specific exon. In humans the *LMNA* gene encodes four splice variants namely, lamin A, lamin AΔ10, lamin C and lamin C2. While lamin A and C are expressed by differentiated cells [41], expression of the C2 isoform is restricted to the germ line specific cells [42]. The lamin AΔ10 isoform has been poorly understood so far. In contrast, the B-type lamins are ubiquitously expressed in all the somatic cells and are essential for the cell survival. They represent the ancestral lamin type [43]. The mammalian lamin B1 and lamin B2 are encoded by two different genes, namely, *LMNB1* and *LMNB2* respectively. While the B-type lamins remain permanently isoprenylated, the lamin A loses its isoprene moiety due

to an additional proteolytic processing step. Lamin A is synthesized as prelamin A and undergoes one more proteolytic cleavage to yield the mature form of lamin A. As a result, the terminal 15 amino acid residues of prelamin A including the isoprenylated cysteine residue are removed by an endoproteolytic enzyme Zmpste24 [39]. The A-type lamins are generally absent in embryonic or undifferentiated cells. An ectopic expression of the prelamin A was reported to induce apoptosis in *Xenopus* embryos [44]. The prenyl moiety increases the hydrophobicity of the proteins, which enhances their association with nuclear membranes. The lipidation of the cysteine residue has been shown to be an essential step for membrane targeting of lamins [45]. The mature lamin A is believed to be targeted to the nuclear envelope via interactions with the B-type lamins or with other lamina associated proteins [46], [47].

Like all IF proteins, lamins are able to form filaments mainly via interactions between their rod domains as shown in case of the B-type lamin of *Caenorhabditis elegans* (Ce-lamin) in Figure 1.3. The head domain bears a set of conserved amino acid residues and the coiled rod domain comprises of the heptade repeats which allow their dimerization via coiled coil interactions [48]. Lamin dimers are formed by parallel non-staggered interactions between two monomers. The dimers further join in a head-to-tail manner to form a long and thin fibril. This head-to-tail fibril has a polar structure as it bears a head of a dimer at one end and the tail domain of the other dimer at the other end of the fibril. The head-to-tail fibril probably forms by a partial overlap between the paired tail domains of the previous dimer and the paired head domains of the subsequent dimer. The conserved regions in the head and tail domains are said to play a key role in these interactions. In the third step, the head-to-tail fibrils assemble in an antiparallel staggered way to form non-polar protofilaments. Lastly, a 10 nm thick lamin filament consisting of 3 to 4 protofilaments is formed [49], [50].

1.5 Role of lamins

Lamins are involved in a multitude of nuclear processes, such as DNA replication, transcription regulation, chromatin organization, and assembly-disassembly of the

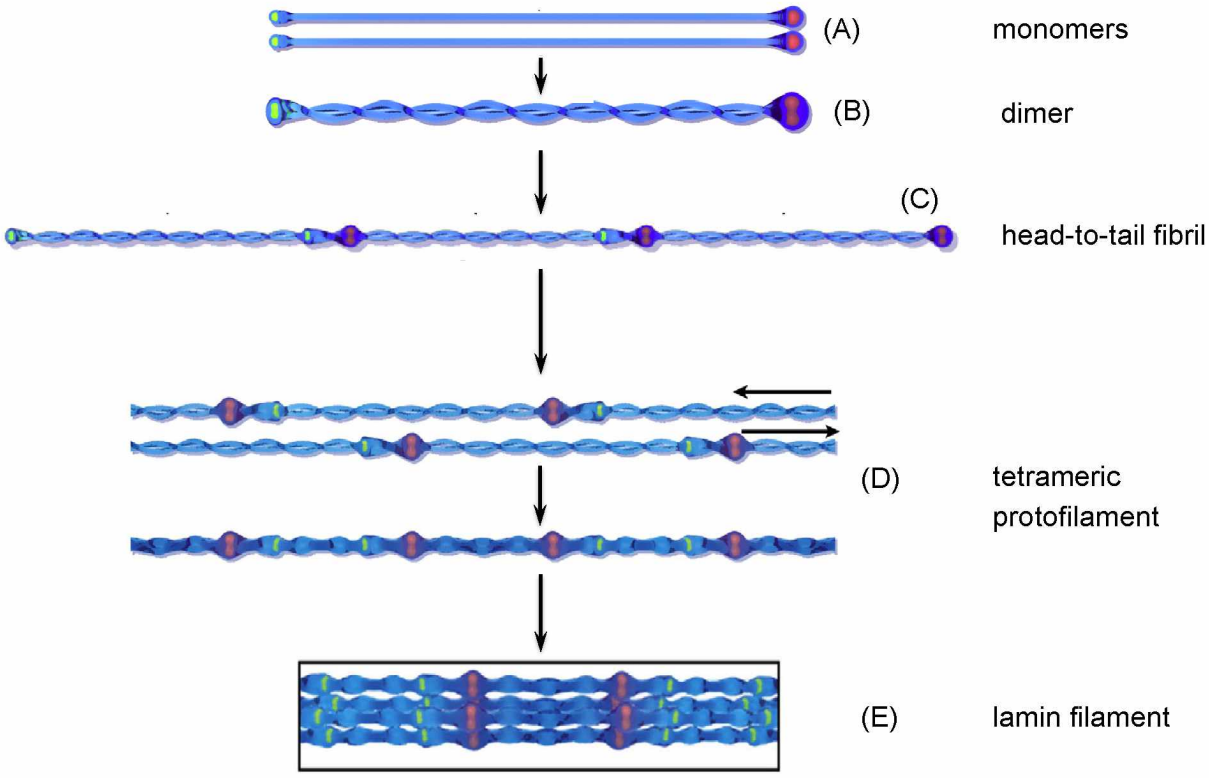

FIGURE 1.3 Lamin filament assembly pathway of the *Caenorhabditis elegans* lamin. The single B-type lamin of the nematode *C. elegans* can assemble into 10 nm thick filaments in vitro under specific buffer conditions. Lamin monomers *(A)* form dimers *(B)* via coiled coil interaction of their central rod domains. The dimers associate in a head-to-tail manner to form a polar fibril *(C)*. Two head-to-tail fibrils laterally associate in antiparallel direction to form a tetrameric protofilament *(D)*. Either three or four protofilaments further form a lamin filament *(E)*. The lamina is comprised of meshwork of these lamin filaments. Image adapted from [49].

nuclear envelope during cell division [28], [51], [52]. Besides their contribution to the biochemical processes occurring in the nucleus, they also provide structural integrity to the nucleus [30]. Experiments carried out with different mutant lamins have revealed their significance in maintaining the nuclear shape and positioning in the cell [53]. Despite availability of wide variety of literature on the characterization of the laminopathic mutations and their effects on the cellular processes, it is not quite clear how these mutations bring about perturbations in the normal functioning of the cells or a tissue. Moreover, some mutations lead to development of tissue specific defects (for example, FPLD) while some are shown to affect all types of tissues and organs of the organism simultaneously (for example HGPS). To this end, two hypotheses have been proposed [52].

According to the gene expression hypothesis, the disease development can be attributed to alterations in the expression and regulation of different genes depending on the mutation in the *LMNA* gene. Modifications in the expression pattern of particular set of genes can thus lead to tissue specific disease developments. A lipodystrophy for example, is caused due to mutations in the Ig-fold of the lamin A tail domain. Mutations in this region are shown to affect the renewal of adipocytes, as the capacity of preadipocytes to differentiate into mature ones is hampered due to the mutations [54]. The structural hypothesis, on the other hand suggests that the mutations in the *LMNA* gene are responsible for causing alterations in the mechanical properties of the cells thus making them susceptible to physical damage. Such a damage to the nucleus could even trigger cell death. Moreover, interactions between the lamina and its associated proteins along with the corresponding cytoskeletal elements might also be influenced [55]. Lamins are connected to the cytoskeleton via the SUN-proteins (anchored in the inner nuclear membrane) which interact with nesprins on the cytoplasmic side of the nuclear envelope. These proteins are collectively termed as LINC (linkers of nucleoskeleton and cytoskeleton) complex proteins. Nesprins, that are located in the outer nuclear membrane, are shown to interact with the IF and the actin network of the cell [56], [57]. Recently, it was reported that a myopathic mutation in lamin A disrupts its interaction with nesprin-2. Such a disruption in the nucleo-cytoskeletal coupling has been suggested to influence the disease development [58], [59]. An another study reported that the

nucleus of somatic cells is covered by a perinuclear actin cap which controls the positioning of the nucleus in the cell and it can be disrupted due to laminopathic mutations [60], [61]. Alterations in the lamin A protein or its deficiency have been shown to disrupt the acto-myosin network of cells which also affects the overall integrity of cytoplasm [62], [63]. Lamins can thus be considered as a crucial link between the nuclear and cytoplasmic processes, and perturbations in those can affect the overall cell metabolism.

According to a recent report, the regulation of lamin A expression was found to be dependent on the localization of different tissues in the body [64]. Proteomic analyses done in this study, showed a correlation between the ratios of A-type to B-type lamins expressed in the tissues and their origin. A higher ratio of A-type to B-type lamins was seen for the tissues that are usually exposed to mechanical stress (for example, heart, muscle, cartilage). Contrastingly, fat tissue and brain tissues, which are not under mechanical stress, were found to contain a lesser amount of lamin A [64]. In all the tissue types, the amount of the B-type lamins remained unaltered but that of A-type lamins varied according to the stiffness of the extracellular matrix. On a hard substrate, the lamin A production was increased and the cells increased their rigidity. On the softer substrates on the other hand, lamin A expression was suppressed [64]. In the same report, the differentiation pattern of the mesenchymal stem cells was also shown to be dependent on the lamin A expression which was shown to be regulated via retinoic acid pathway. Moreover, these stem cells were able to differentiate into the cells of the fat tissue when lamin A was knocked down, while the same cells generated a bone phenotype upon upregulation of the lamin A expression. Increasing number of evidences thus show importance of lamin A in maintaining mechanical stability of the cell.

1.5.1 Nuclear mechanics

Mechanical properties of cells and nuclei have been recorded using various techniques like micropipette aspiration [65], [30], optical cell stretchers [66], microplate manipulation [67] and atomic force microscopy (AFM) [68], [69]. Depending on the technique, type of cells (adherent or in suspension) and the models used for

data analysis (Hertz model, Shell model etc.), conclusions based on the changes in mechanical properties can vary. Atomic force microscopy is a unique technique that allows measurements of the mechanical properties of living samples under near-physiological conditions. The atomic force microscope was invented by Binnig et al. in 1986 [70]. The precursor of the AFM, the scanning tunneling microscope, was invented by Binning and Rohrer in 1981 for which they were awarded a Nobel prize in physics later in 1986. The scanning tunneling microscope works on the principle of tunneling electron current, that is generated due to voltage difference, when a conductive tip is brought near to the sample surface. The AFM works on a principle where the tip can be brought in direct contact with the sample, to record sample topography or to obtain force curves, even when the tip or sample is non conductive. Therefore, AFM is widely used for cell imaging, to conduct live cell experiments to study processes like cell division, migration and also for measuring the elastic properties of the cells and nuclei [69], [71], [47].

Previous experiments have been done with *Xenopus* oocytes to study the mechanical properties of the isolated nuclei and alterations caused in them due to mutations in lamins [72]. The oocytes were used for ex vivo expression of the wild-type lamin A. An oocyte nucleus is ~500 µm in diameter and the chromatin is not attached to the lamina. These special features of oocyte nuclei allow for assessment of mechanical properties of the lamina layer without the influence of nucleoplasmic components. In the work done by Schäpe et al. [72], the overexpressed lamin A formed a thick lamina layer as was seen in the transmission electron micrographs. The thicker lamina was shown to be responsible for increased nuclear stiffness as judged by AFM. Taimen et al. [26] have reported that the progeria mutant lamin A E145K assembled in a defective manner in the in vitro assembly experiments. This hinted towards alterations in the lateral association of the lamin head-to-tail fibrils. A lamina made up of the lamin filaments that are assembled in a modified way, might influence the mechanical characteristics of the nuclei. AFM experiments were thus carried out on the nuclei isolated from the *Xenopus* oocytes overexpressing the E145K lamin A mutant (in comparison to those expressing wild-type lamin A) by Kaufmann et al. [47]. The AFM measurements on the isolated nuclei revealed significant differences in the lamina stiffness. The lamina layer of comparable

thickness, comprising of mutant lamin A E145K was found to be stiffer than that formed by the wild-type lamin A. This showed that the progeria mutation indeed alters the mechanical properties of the lamina. However, an amphibian oocyte nucleus is specialized experimental system (as oocytes are germ line cells) and is a heterologous system for analyzing effects of a human laminopahty mutation on nuclear mechanics. Further AFM experiments were therefore necessary to verify the effect of lamin A E145K mutation on the mechanical properties of the somatic cell nuclei i.e., from the cells of a progeria patient.

1.6 Aim of the thesis

The aim of this work was to determine the influence of E145K progeria mutation on mechanical properties of the dermal fibroblasts obtained from a progeria patient. Towards this, force measurement were recorded on adherent fibroblasts using an atomic force microscope (AFM). For assessment of nuclear mechanics, optimization of AFM data acquisition and analysis was required. Hence, pilot experiments were designed using HeLa cells, as the fibroblasts of progeria patient are difficult to maintain in culture for a longer time period. HeLa cells transiently transfected with the plasmids encoding wild-type or E145K lamin A were initially used for AFM experiments. AFM measurements were also obtained for non transfected and mock transfected controls. The force curves were obtained on the cells using sample indenters having different geometries (pyramidal tips and glass beads). In the next step, the effect of progeria mutation on the nuclear mechanics of dermal fibroblasts was analyzed. Additionally, the mechanical properties of two control cell samples, i.e, dermal fibroblasts of a young person and an old person were also determined. The fibroblasts were analyzed by fluorescence microscopy and transmission electron microscopy (TEM) to visualize the nuclear shape and to reveal details about the structure of the nuclear envelope respectively. Effect of the E145K progeria mutant on the nuclear mechanics was also measured by AFM using the isolated nuclei. Force curves were recorded by AFM indentation of nuclei isolated from dermal fibroblasts of the progeria patient, a young person and an old person. Isolated nuclei were further analyzed by TEM to analyze the nuclear envelope structure.

2

Materials and Methods

2.1 Cell culture techniques

2.1.1 HeLa cells

HeLa cells are the most widely studied type of cancer cells in cell biology and can be routinely maintained in cell culture laboratories. It is an immortal cell line as the cells can divide and grow indefinitely. HeLa cells are adherent epithelial cells which were originally isolated in 1951, from a biopsy tissue obtained from the cervix of a female adenocarcinoma patient named Henrietta Lacks. Since then, these cells have been used extensively where experiments with human cell samples are required. For this work, HeLa cell cultures were kindly provided by Prof. Dr. Andreas Dotzauer (Institut für Virologie, University of Bremen).

Culture maintenance

Cultures of HeLa cells were maintained in 25 cm^2 flasks (cat. no. 83.1810, Sarstedt, Germany), each containing 5 mL of Dulbecco's modified Eagle medium (DMEM, cat. no. FG 0435, Biochrom, Germany) containing 1% fetal calf serum (FCS, cat. no. S 0115, Biochrom, Germany), 1% penicillin − streptomycin (P/S); (1× P/S contains 100 Units penicillin, 100 µg/mL streptomycin, cat. no. P11-010, PAA, Austria). Cells were passaged twice a week depending on their confluency. For successive passaging of the cultures, cells were briefly washed with 5 mL of phosphate

buffered saline (PBS, 7.9 mM Na_2HPO_4, 1.5 mM KH_2PO_4, 7 mM KCl, 137 mM NaCl, pH 7.4) to remove the residual medium. Next, the cell layer was covered for a minute, with 1 mL of trypsin EDTA mixture (trypsin 0.05%, EDTA 0.02%, cat. no. L2153, Biochrom, Gemany) diluted in PBS, trypsin was removed and the flasks were incubated for 5 minutes at 37°C to allow cell detachment. 1 mL of DMEM supplemented with 10% FCS and 1% P/S (10% DMEM) was added to the flask and cells were resuspended under the flow of the media over the flask surface. Additionally, cells were detached by gentle tapping of the flasks to avoid excessive formation of air bubbles due to repeated pipetting. Cells were counted using the WBC (white blood cell) counting area of the Neubauer's chamber. The total number of cells counted in one WBC counting area multiplied by 10^4 gives the number of cells per mL. About $1/5^{th}$ of the total cells was seeded into a new 25 cm^2 flask. Generally 1-1.4 $\times$ 10^4 cells were seeded per cm^2 area. Cells were allowed to adhere to the flask overnight at 37°C. Medium was replaced with fresh DMEM supplemented with 1% FCS and 1% P/S (1% DMEM) the next day and cultures were maintained using 1% DMEM to avoid cell overgrowth. Flasks were screened daily for monitoring the sterility and health of the culture. For AFM experiments, cells were seeded on 1 cm wide sterile glass coverslips (Thermo Fischer scientific, Schwerte, Germany) kept in a cell culture dish having a 3.5 cm diameter (Nunc, Thermo Fischer Scientific). For AFM probing, the coverslips were removed under sterile conditions according to the experimental scheme.

Preparation of stocks

Cells were grown in 75 cm^2 flasks (cat. no. 658175, Greiner bio-one, Frickenhausen, Germany) to almost 100% confluency. They were washed with 3 mL of trypsin EDTA for two times, followed by detachment of the cells in 3 mL of trypsin EDTA at 37°C. Cells were resuspended by addition of 7 mL of 10% DMEM to the flask. Total 10 mL of cell suspension was transferred to a 15 mL tube and centrifuged at 1258 $\times$ g for 10 min at 4°C (Centrifuge 5810R, Eppendorf, Hamburg). The cell pellet was washed twice with 7 mL of 10% DMEM and a final resuspension was done in 4 mL of 10% dimethyl sulfoxide (DMSO) in 90% FCS. DMSO is used to prevent water crystallization during cryopreservation thus protecting the cells

from rupturing. FCS is used as a diluent for DMSO and it simultaneously provides nutrients to the cells while thawing. Cell count was noted and four aliquots of 1 mL, each containing ∼2-3 × 10^5 cells were distributed in sterile cryotubes (Nunc, Thermo Fischer Scientific). The cryotubes were initially maintained at -80°C for 2-3 days and then further maintained under liquid nitrogen at around -196°C. Cells from one tube were revived from the liquid nitrogen stock after 24 hours, to check their viability.

Cell transfection

Cells are generally transfected at ∼70-80% confluency to obtain a maximum transfection efficiency. For AFM experiments, HeLa cell samples were required over a total time period of four days, hence, a lesser initial number of cells was seeded. Typically, 1 × 10^5 cells were seeded on sterile coverslips kept in a cell culture plate having 3.5 cm diameter. After overnight incubation of cells at 37°C, one coverslip was removed from the plate prior to addition of the transfection reagent, as a non transfected control. The transfection mixture containing plasmid DNA and transfection reagent was incubated at room temperature (RT) for 20 minutes, before its addition to the plate containing cells. The transfection mixture consisted of approximately 2 µg of plasmid DNA, 5 µg of polyethyleneimine (PEI, cat no. 408727, Sigma, Hamburg, Germany) in 300 µL of serum free DMEM. The amount of plasmid DNA and PEI was calculated for respective plasmids using an online calculator program (http://www.cytographica.com/lab/PEItransfect.html, last access 24 November 2013). For preparation of the mock transfection mixture, an equivalent amount of sterile water was added to the PEI and DMEM, instead of the plasmid DNA.

According to the online calculator, the area of cell culture plate, the concentration and size (in bp) of the plasmid are taken into account for calculation of the relative amounts of DNA and PEI. The rationale behind the calculations is explained with an example given below.

A 6 kb plasmid with a concentration of 1 µg/µL is used for transfecting cells in a 3.5 cm diameter plate. A total of 0.5 pmol of plasmid DNA is required for transfecting cells in 3.5 cm plate. To calculate the equivalent volume (in µL) of

plasmid stock, first the molecular weight of the plasmid is calculated by multiplying the total number of basepairs by average molecular weight of a single basepair (for a double stranded DNA it is 650 g/mol).

According to the total number of basepairs, plasmid DNA has a molecular weight of 39,00,000 g/mol (i.e., (39,00,000 $\times$ 10^6) / (10^{12}) µg/pmol). Thus, a 0.5 pmol of DNA, in case of this example is equivalent to 1.95 µg of DNA. As the concentration of plasmid is 1 µg/µL, 2 µL will roughly yield the required amount of DNA.

For determining the amount of PEI (stock concentration 1 mg/mL) required to bind to 1.95 µg of DNA, the ratio of the nitrogen present in PEI to phosphorous present in the DNA is crucial. A nitrogen/phosphorous ratio of 20 is found to be best for obtaining high transfection efficiency, as suggested by the online calculator and by [73]. A microgram of dsDNA has 3 nmol of phosphorous, hence, 1.95 µg of DNA has 5.85 nmol of phosphorus. Thus multiplication of 5.85 nmol with 20 will give the total required amount of nitrogen in nmol, which is 117 nmol. One µL of PEI has 23.26 nmol of nitrogen. Therefore, 117 nmol divided by 23.26 nmol yields the amount of PEI (1 mg/mL) in µL that is needed, which is 5 µL. The volume of serum free media is $1/10^{th}$ of the total amount of media (total amount generally 2-3 mL) placed in the 3.5 cm plate. Thus transfection mixture consisting of 2 µL of plasmid DNA (1 µg/µL), 5 µL of PEI (1 mg/mL) in 300 µL of serum free DMEM should be added in case of this example, to the 3.5 cm diameter plate containing 2.7 mL of 1% DMEM.

After addition of the transfection mixture, the plates were incubated overnight at 37°C. Transfection was stopped by replacing the media with 2 mL of fresh 1% DMEM. For cotransfection, plasmids peGFP-C3 (1.664 µg/µL, Clontech laboratories) with pCS^{2+}-Hs-LA wild-type (960 ng/µL, [47]) or with pCS^{2+}-Hs-LA with E145K progeria mutation (960 ng/µL, [47]) were used.

Fixing and immunostaining

Cells were seeded on 1 cm wide glass coverslips for immunofluorescence microscopy. They were fixed using 3.9% formaldehyde (Sigma) in PBS for 20 minutes followed by 10 minutes incubation in 3.7% formaldehyde with 1% Triton X-100 (Sigma). Washing was done three times for 5 minutes each, using PBS. Further washing

steps were done with 50 mM NH_4Cl (Merck, Darmstadt, Germany) in PBS to block excess of aldehyde which could show autofluorescence and could inactivate the antibody. This was followed by incubation of the sample at RT with primary antibody for 30 minutes followed by the secondary antibody for 15 minutes in a humidified chamber. To detect proteins with a Flag octapeptide tag (DYKDDDDK), the mouse monoclonal antibody, M2 (stock 5 mg/mL, Sigma F3165), at a dilution of 1:1500 was used. For lamin B2 detection, mouse monoclonal antibody L7-8C6 [74] at a dilution of 1:200 was used. Detection of the primary antibody was done by 1:500 diluted Cy3-conjugated goat anti mouse IgG (H+L) polyclonal antibody (stock 1.4 mg/mL, Dianova 115-166-003). All antibodies were diluted using PBS. DNA staining was done with 4',6-diamidino-2-phenylindole (DAPI, 1 µg/mL in water, Sigma) for 2 minutes at RT. DAPI is a chemical that strongly binds to double stranded DNA molecules and upon excitation with UV rays, it fluoresces blue having a broad emission spectrum with the maximum at 460 nm. Cy3 is a fluorescent dye with the excitation maximum at 550 nm and emission maximum at the wavelength of 570 nm, rendering red fluorescence to the sample. The samples were mounted in Immunount (Thermo Fischer scientific) mounting medium and were stored at -20°C.

2.1.2 Human fibroblasts

Primary cultures of the dermal fibroblasts were obtained from the aging cell repository of the Coriell institute (Camden, New Jersey, USA). Cell samples were obtained from a four years old progeria patient (PP, cat. no. AG10677), a ten years old, healthy young person (YP, cat. no. AG08470) and a sixty one years old, healthy old person (OP, cat. no. AG02261).

Culture maintenance

Cells were maintained according to the instructions given by the cell repository. Briefly, cells were maintained in DMEM supplemented with 15% FCS and 1% P/S (15% DMEM). For further passaging, cells were detached by treatment with 1 mL of trypsin EDTA diluted in PBS for 5 minutes at 37°C. 4 mL of 15% DMEM was then added to the flask and cells were resuspended by gentle pipetting of the media over

the flask surface. Cell count was noted using Neubauer's chamber as described before. Quantity of the cells for seeding was determined according to protocol provided by the repository.

For AFM experiments, marked coverslips (CELLocate, Eppendorf, Hamburg) were used for seeding the fibroblasts, which allowed relocation of the cells under the phase contrast microscope, that were used for AFM data acquisition. As the same cells were processed for the immunofluorescence microscopy, analysis of the images of AFM investigated cells was possible.

Preparation of stocks

Cell stocks were stored under liquid nitrogen according to the steps described before in 2.1.1 cell storage section and the culture conditions were as mentioned by the protocol obtained from the cell repository.

Fixing and immunostaining

The dermal fibroblasts were fixed and immunostained as described in the section 2.1.1. Lamin A was detected using the lamin A specific mouse monoclonal antibody JOL2 (Anti-Lamin A + C antibody, ab40567, Abcam) at a dilution of 1:50 in PBS. The secondary antibody was a DyLight 488-conjugated goat anti mouse polyclonal antibody (stock 1 mg/mL, Thermo Fischer Scientific). DyLight 488 is a fluorescent dye with an excitation maximum at 493 nm and emission maximum at 512 nm thus imparting green fluorescence to the sample labelled with it. F-actin was labelled using phalloidin conjugated to rhodamine (cat. no. 00028, Biotium Inc., USA) which has an excitation maximum at 557 nm and emission maximum at 576 nm due to which it fluoresces red. The dilution of phalloidin was done using PBS according to instructions given in the user manual as one unit of phalloidin is used to stain the cells grown on an entire microscopic slide. Prior to the actin staining, a blocking step with 3% non fat dry milk (Sucofin) was performed for 60 minutes at 4°C. DNA was stained using DAPI as described before.

2.2 Sample preparation for AFM

2.2.1 Cells

The cells were grown on sterile glass coverslips kept in a cell culture dish. The coverslips were removed one by one under sterile conditions according to the day wise scheme used for AFM data acquisition. In case of the HeLa cell experiments performed using a pyramidal tip, cell samples were acquired on day 1, 2 and 3, for four different cell categories i.e., non transfected, mock transfected, lamin A wild-type expressing and lamin A E145K expressing HeLa cells. For AFM probing experiments done using glass beads as a sample indenter, cells were taken out at five different time points, namely, non transfected, four hours post transfection, day 1, day 2 and day 3 post transfection for either wild-type lamin A expressing cells or lamin A E145K expressing cells. In case of the dermal fibroblasts obtained from PP, OP and YP, the cells from each passage were analyzed on the next day after seeding of the cells.

A coverslip was transferred to a clean, 6 cm wide cell culture dish containing about 2.5 mL of 10% DMEM. This dish was fixed on a metal holder with help of vacuum grease taking care that the coverslip remained in the center of the dish. The metal holder along with the sample was kept on AFM stage with the help of two small magnets. The AFM head was lowered down slowly towards the sample till a meniscus was formed between the media and the cantilever holder. Care was taken that the meniscus formed without any air bubbles, as they can affect the measured deflection of the cantilever or even could destroy it. An atmosphere with 5% CO_2 was maintained around the cells by keeping them enclosed in a polymethylmethacrylate (PMMA) chamber. Temperature was not controlled, but it ranged between 23-27°C as indicated by the data acquisition software.

2.2.2 Preparation of polyacrylamide (PA) gels

Sterile glass coverslips were treated with 0.1N NaOH for 5 minutes. After removal of NaOH, coverslips were air dried for 15 minutes. All the further steps were performed under a fumehood. Each coverslip was then covered with 100 µL of (3-

aminopropyl)trimethoxysilane (3-APTMS, Sigma) for 5 minutes. Surface treatment with silane allows chemical cross-linking between the glass and the thin layer of PA gels casted on the coverslip. The coverslips were extensively washed with water to remove excess silane and then were dipped in water for about 10 minutes. Next, 0.5% glutaraldehyde (Serva, Heidelberg, Germany) diluted in PBS was placed on the coverslips for 30 minutes. After removal of the glutaraldehyde, PA gel mix (10% acrylamide, 0.13% bisacrylamide in water, Roth, Karlsruhe, Germany) containing the polymerizing agents - 0.5% ammonium persulphate (APS, stock 10% in water) and 0.05% tetramethylethylenediamine (TEMED, Sigma) was placed on the glass (25 µL for 1 cm wide coverslip, 250 µL for 3 cm wide coverslip). Another untreated clean coverslip was immediately placed on the drop of the PA gel mixture such that a thin, uniform layer of the gel was formed. Polymerization of the gel required 15-20 minutes. The top coverslip was carefully peeled off from the gel layer. Coverslips with PA gels were stored at 4°C immersed in PBS to avoid further drying until used for AFM experiments.

The collagen coating of the gels was done using the UV activable crosslinker, N-sulfosuccinimidyl-6-(4'-azido-2'-nitrophenylamino) hexanoate (Sulfo-SANPAH, Thermo Fischer scientific). The gels were briefly rinsed with sterile 150 mM NaCl in PBS. 100 µL of the 10 mM sulfo-SANPAH dissolved in 150 mM NaCl was placed on each coverslip. The coverslips were placed under UV lamp (Reproset, Amersham Pharmacia Biotech, USA) for 10 minutes at a distance of around 10 cm from the source. Sulfo-SANPAH was removed and UV exposure was repeated one more time. Gels were briefly washed with 150 mM NaCl, and 10 µL of human collagen type 1 (cat. no. 354243, BD Biosciences, 0.2 mg/mL diluted in 2 mM HCL) was placed on each coverslip. Incubation was done overnight in the dark at 4°C. The collagen coated PA gels were directly used for seeding of the cells the next day.

2.2.3 Isolation of nuclei

Nuclei were isolated from fibroblasts that were grown for 2 days in cell culture dishes having 3.5 cm diameter. Cells were incubated with 850 µL of a hypotonic solution of 0.56% KCl (Acros organics, Geel, Belgium) in water for 60 minutes at 37°C (see

Figure 2.1 A). To avoid protein degradation during this incubation period, 250 µL of protease inhibitor cocktail (Complete mini EDTA free, cat. no. 1836170, Roche, Germany) was added to the KCl solution in the plate. Incubation in hypotonic solution caused swelling of the cells as shown by arrows in the figure 2.1 B. The concentration of the protease inhibitor cocktail was used according to directions given in the product manual. After removal of the KCl, 1 mL of 0.05% NP-40 (Nonidet P-40, Sigma) in PBS, was added slowly from a side of the dish. Cells were incubated with the detergent for 5 minutes at RT (see Figure 2.1 C). Removal of detergent was done avoiding detachment of the cells, followed by resuspension of the cells in 1 mL of PBS. Repeated pipetting (using 1−1.2 mL capacity micropipette tip, nerbe plus, Winsen/Luhe, Germany) of the cells released nuclei from the cytoskeletal elements. The nuclei were centrifuged at 500 × g for 5 minutes at RT (Centrifuge 5415D, Eppendorf, Hamburg). Fresh PBS was added and the centrifugation step was repeated. The pellet fraction enriched in isolated nuclei (see arrowheads Figure 2.1 D) was resuspended in 1 mL of PBS. Nuclei were stored at 4°C until used for AFM experiments.

2.3 Microscopy

2.3.1 Conventional immunofluorescence microscopy

Lamins, chromatin and the actin network of cells were visualized using conventional immunofluorescence microscopy. The samples were examined under a Zeiss Axioplan fluorescence microscope (Zeiss, Germany) and images were taken using an Axiocam MRc5 camera (Zeiss, germany) with the software Axiovision 4.5. The excitation and emission of specific fluorescent dyes was done using three different filtersets - DAPI (Excitation BP 365, Beam splitter FT 395, Emission LP 397), Cy3/rhodamine - (Excitation BP 545/25, Beam splitter FT 570, Emission 605/70), DyLight 488/eGFP - (Excitation BP 485/20, Beam splitter FT 510, Emission 515-565).

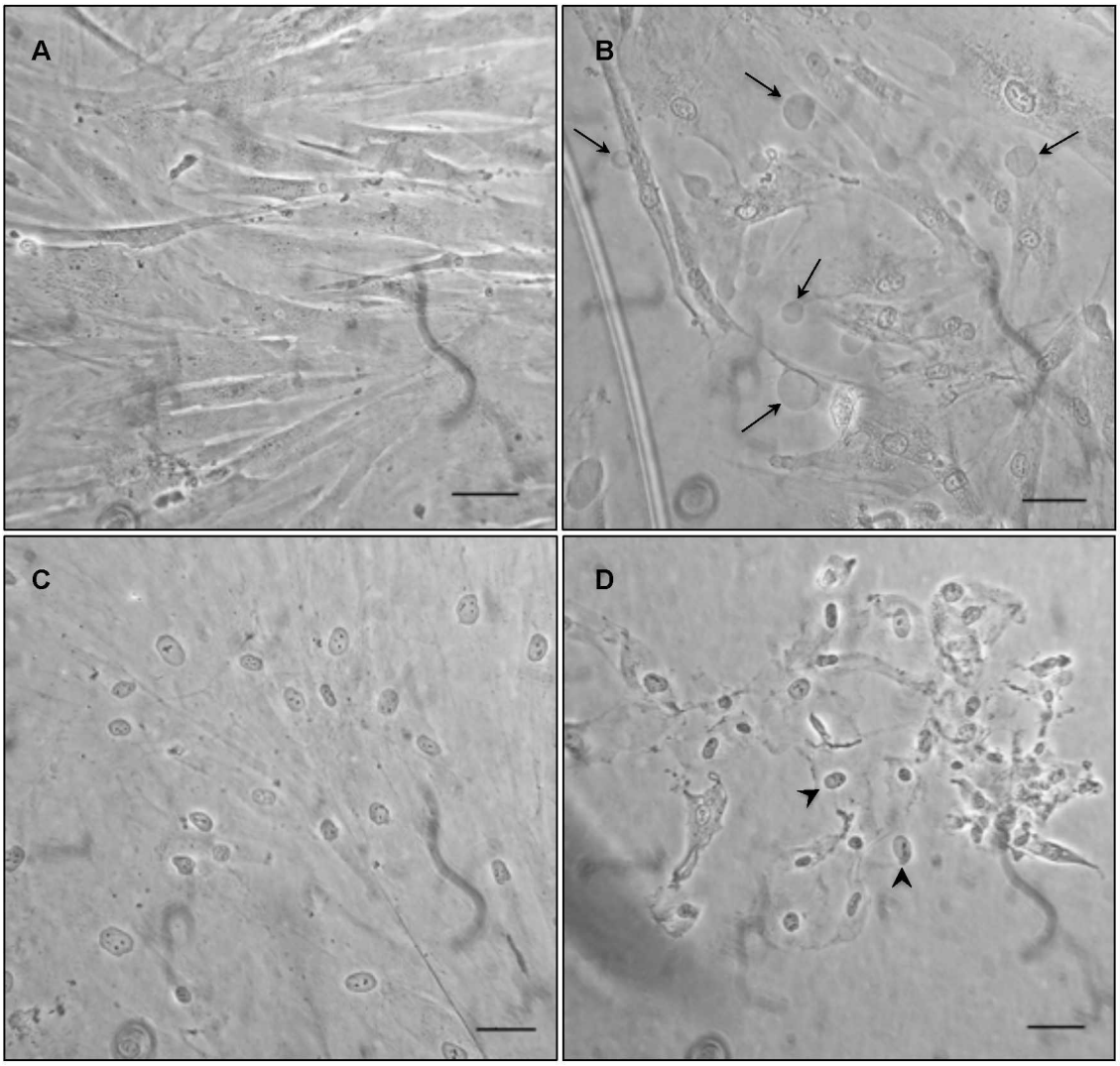

FIGURE 2.1 Isolation of nuclei from skin fibroblasts. To isolate nuclei from *(A)* the dermal fibroblasts, cells were incubated in a hypotonic solution of 0.56% KCl which causes swelling and bursting of cells due to osmotic shock. The swollen cytoplasmic regions are shown by arrows in *(B)*. This was followed by treatment with 0.05% NP-40 in PBS for 5 minutes for removal of surrounding membranes as shown in *(C)*. The nuclei were gently resuspended in PBS to release them from cytoplasmic remnants. Arrowheads in *(D)* show isolated nuclei suspended in PBS. Scale bar = 50 µm

2.3.2 Structured illumination microscopy

High resolution immunofluorescence images of the cells were obtained with the help of structured illumination of the sample using the ApoTome (Zeiss, Germany). ApoTome allows optical sectioning of the sample, simultaneously blocking the scattered, out of focus light by a striped grid as shown in Figure 2.2. The grid is situated in the plane of the diaphragm in the illumination pathway and its image is projected in the focal plane of the objective, thus allowing structured illumination of the sample. An optical-grade glass plate is placed next to the grid, which can be tilted at three defined angles relative to the sample. A composite image is generated by the software, form three separate images obtained at each tilt position of the grid. This composite image is an optical section, which has a sharp contrast. Multiple optical sections are obtained by moving the sample along the z direction, which gives a z-stack of optical sections of the sample. The images were obtained using the filtersets for DAPI, DyLight 488 and rhodamine. The ApoTome was used in combination with Zeiss Imager M2 (Zeiss, Germany). Black and white images were captured using a camera (Axiocam MRm, Zeiss, Germany) with the help of the corresponding software Axiovision 4.8 which was also used to generate corresponding false colored images of the sample.

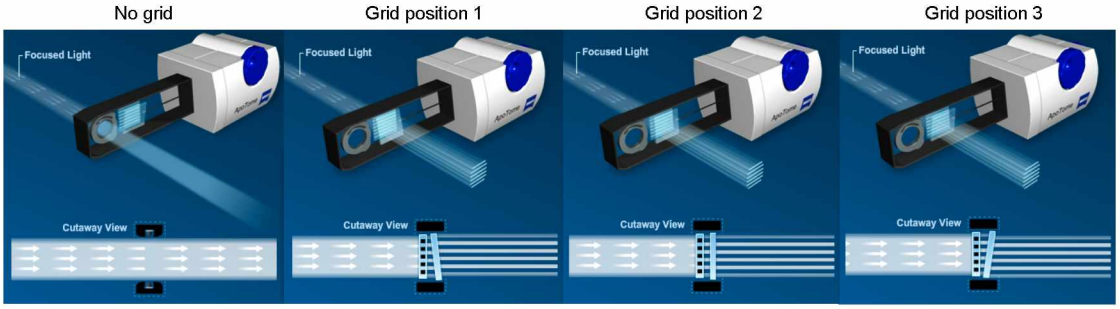

FIGURE 2.2 Principle of structured illumination by ApoTome. Optical sections were obtained using the ApoTome. At no grid position, incident light illuminates the sample over an entire area. Insertion of the grid and the plate placed next to the grid allow a structured illumination of the specimen. The plate is tilted in position 1, 2 and 3 to generate raw images which are combined together by the software to give an optical section of the sample. [Figures adapted from http://zeiss-campus.magnet.fsu.edu/tutorials/opticalsectioning/apotome/]

2.3.3 Transmission electron microscopy (TEM)

Fibroblasts grown in 6 cm wide plates were processed for TEM analysis. The medium was removed and cells were washed with PBS to remove residual medium. Cells were fixed using 2 mL of Karnovsky's fixative (2.5% glutaraldehyde, 2.5% formaldehyde in 0.1 M Na-cacodylate (Fluka, Hamburg, Germany) buffer, pH 7.4 adjusted by NaOH) for 30 minutes at RT. After removal of the fixative, 1 mL of 1% gelatin (Merck, Darmstadt, Germany) in PBS was added to the plate. Cells were scraped off from the culture dish and centrifuged at 500 $\times$ g for 5 minutes at RT. The cell pellet was dispersed in 2% agar (Sigma) dissolved in PBS and kept at 4°C for 5 minutes to allow solidification of the agar. The agar block was cut into small pieces of about maximum 1 mm length. The agar pieces were incubated in the dark, for 60 minutes at 4°C in 1% OsO_4 (Serva) diluted in PBS. This was followed by washing steps using double distilled water (ddH_2O), three times for 5 minutes each. The cells were contrasted using 1% uranyl acetate (Merck) in water at 4°C overnight in the dark. Uranyl acetate was removed by thorough washing with ddH_2O. This was followed by gradual dehydration of the sample at RT by treating them with successively increasing ethanol concentrations of 30%, 50%, 70%, 90% and 100%. The dehydration steps with 30% and 50% alcohol were carried out for 15 minutes including one change. Further dehydration steps with 70% and 90% alcohol were carried out for 20 minutes with three changes. The samples were treated with 100% alcohol twice for 15 minutes each and three more times for 20 minutes each using absolute 100% ethanol kept over a molecular sieve (Molekularsieb 0.3 nm, Perlform 2 mm, 105704, Merck). Subsequent to the dehydration, the cells were embedded in a medium hard resin, Epon 812. 5 mL of the resin mixture consisted of 3 volumes Epon A (6.2 mL glycidether, 10 mL DDSA hardner) and 7 volumes Epon B (15 mL glycidether, 13.35 mL NMA hardner) without the accelerator. The cells were initially incubated twice in a 1:1 mixture of 100% ethanol and the resin solution for 30 minutes each. This was followed by incubation of the cells in the 1:2 mixture of 100% ethanol and the resin for 90 minutes with one change. The samples were then immersed in the resin solution overnight in vacuum at 60°C. The next day, agar pieces containing the cells were transferred into agar forms containing the

resin with the accelerator DMP-30 (2,4,6-Tris-(dimethylaminomethyl)-phenol, Roth). Polymerization of the resin was done over 48 hours in vacuum at 60°C. The hardened resin blocks were trimmed and 60 nm ultrathin sections were taken using the ultra microtomes Ultracut R (Leica, Wetzlar, Germany) and Ultracut E (Reichert Jung, Leica, Wetzlar, Germany). The sections were placed on a copper grid and the grids were allowed to dry. The sections were analyzed using microscope EM 900 (Zeiss, Oberkochen, Germany) at 80 kV. Images were acquired using a CCD camera (TRS) with the corresponding software ImageSPviewer. The same software was used to measure the thickness of lamina. The measurements were done using the images acquired at primary magnification of 20,000× and 50,000× for total 10 nuclei from each cell type OP, PP and YP. Average lamina thickness was calculated from all the measurements obtained from one cell type.

A same protocol was followed for processing of the isolated nuclei for TEM analysis except for fixation procedure. As 1 mL of the nuclear suspension was obtained after isolation, 1 mL of double concentrated Karnovsky's fixative was added to fix the nuclei in suspension. Nuclei were centrifuged at 500 × g for 5 minutes at RT. The nuclear pellet was then embedded in 2% agar, all further steps were followed as described above.

2.3.4 Atomic force microscopy

The microscope

The atomic force microscope (AFM) was invented by Gerd Binnig and his co-workers in 1986 [70]. It is a multifaceted biophysical instrument that is not only used for determining the mechanical properties of materials but also for imaging the 3D topography of various biological as well as non biological samples at a high resolution in the range of few nanometers. The principle of the AFM is based on determining the forces (down to pN ranges) between the sample and an indenter mounted on a cantilever spring. AFM is also used to recognize different types of interacting forces, for example, van der Waals forces, adhesive and repulsive forces, electrostatic forces etc. One of the major advantages of AFM probing is, that, the samples can be analyzed under near-physiological conditions without prior fixation

or dehydration procedures that are generally required for analysis by fluorescence microscopy or electron microscopy. Hence, mechanical properties of living cells, which are electrically non-conductive, could be analyzed in this work even under aqueous environments.

The AFM (MFP 3D, Asylum Research, Santa Barbara, CA, USA) used in this study, consisted of an AFM stage on which the sample could be placed and positioned in the x- y direction, the AFM scanner and a z positioner for regulating the distance between the AFM probe and the sample (see Figure 2.3 A). The z positioner is made up of piezoelectric material which typically expands 0.1 nm upon application of electrical potential of 1V. In the set up used in this work, the sample was moved towards and away from the cantilever using the z positioner. Cell samples were viewed using an optical microscope (Zeiss Axiovert 135 TV, Zeiss) with a 20× LD achroplan objective lens (NA 0.40 Korr) used in combination with a 10× ocular lens. Additional magnification of the filed of view could be achieved using the 1.6× and 2.5× help lenses on the Bertrand lens wheel. The image output was visualized on a Philips video monitor. Corresponding images of cells and isolated nuclei were captured with the help of the iGrabber My gica digitizer. For vibration isolation, the whole setup was placed on a granite plate surrounded by a plywood box lined with corrugated acoustic foam sheets. The entire setup was held from the ceiling with the help of rubber cords.

Sample indenters

Force curves were acquired by indentation of the sample by a tip, which was mounted on a silicone nitride cantilever spring. A set of such cantilevers, named from B to F having different spring constants, are attached to a pyrex glass chip (MLCT, Veeco, Mannheim, Germany) as seen in the Figure 2.3 B. The biggest triangular cantilever (cantilever C), 310 nm in length, is the softest cantilever with a nominal spring constant of 0.01 N/m. This cantilever with a sharp pyramidal tip with its very end having an average diameter of 40 nm was used in most of the experiments. The backside of the cantilever is coated with reflective gold for allowing reflection of an incident laser beam. In some of the experiments, glass beads (7 µm diameter, SiO_2-R-7.0, Microparticles GmbH, Berlin) were used as a sample indenter, which

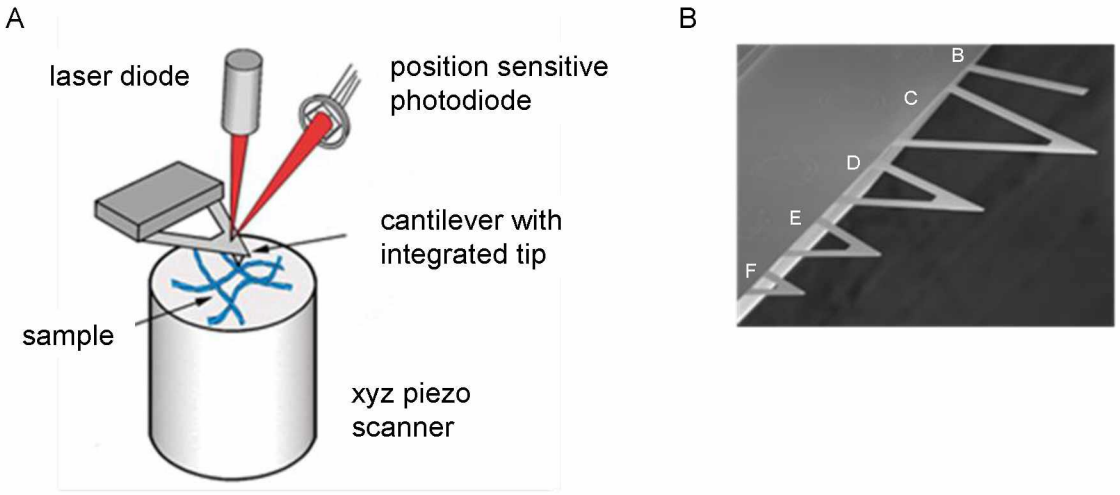

FIGURE 2.3 AFM assembly. *(A)* An AFM stage comprising of an xyz piezo scanner which holds the sample; the cantilever with an indenter and a photodiode laser sensor [75]. *(B)* Silicone nitride cantilevers mounted on a glass chip [76].

were glued on the cantilever C, using a two-part epoxy glue. The glass beads were dispersed on one half of a microscopic glass slide and a thin line of glue was placed over the other half region. The cantilever was mounted in the AFM assembly and the tip was dipped in the glue taking care that a minimal amount of glue is transferred near the pyramidal tip. The tip was then positioned over an isolated glass bead which could be picked up along with the tip upon bringing the tip in contact with the bead. It took about 24 hours for the glue to harden completely, which provided sufficient time for exact positioning of the glass bead behind the pyramidal tip with the help of the AFM assembly. This also allowed preparation of several cantilevers with glued glass beads in one batch. The size of the glass beads was selected such that they were of a bigger diameter than the length of the pyramidal tip (∼5-6 µm). This was necessary in order to avoid interference of the pyramidal tip during AFM probing of the cells with glass beads.

The spring constant of each cantilever was determined before every experiment using a **thermal tune method** which has been described in detail previously [75]. The average thermal energy (E) of each degree of freedom of a system is given by Eq. 2.1, that is derived according to the equipartition theorem of statistical

thermodynamics.

$$< E >= 0.5\ k_B\ T \tag{2.1}$$

(Where <> denotes time average, k_B is the Boltzmann's constant, T is absolute temperature)

Under the assumption that the cantilever shows mainly the bending vibrations (one degree of freedom), the energy at its resonant frequency is given by Eq. 2.2.

$$< E > \sim 0.5\ k_c\ < d^2 > \tag{2.2}$$

(Where <> denotes time average, k_c is the spring constant of cantilever, d is the mean squared displacement of tip)

Upon combining Eq. 2.1 and Eq. 2.2, the following equation is obtained which gives an approximate value of the force constant of the cantilever.

$$k_c = \frac{k_B T}{< d^2 >} \tag{2.3}$$

However, the cantilever has more than one degrees of freedom which can be detected by AFM. Hence, to obtain a more accurate value of the spring constant, a power spectral density (PSD) map, which shows the deflection signal of the cantilever due to its random motion in the air, (recorded as its thermal noise) as a function of the frequency, was plotted. The intensity of the frequency was calculated as square of the vibration amplitude. Figure 2.4 shows an example of a typical power spectral density map. At the resonating frequency, the intensity of vibration is highest as shown by the highest red colored peak in the image. The following peaks represent the intensities of the vibration in air at higher harmonics. As observed, these peaks are not sharp but have a certain peak width. In addition, the basal noise in the system results into overestimation of the vibration amplitude. The interference by basal noise, however, could be minimized by acquisition of at least 100 thermal cycles to generate the PSD map. A Lorentzian fit (shown as the blue curve in Figure 2.4)

based on the principle of simple harmonics, was thus fitted to the highest peak to calculate the d^2 which lead to an accurate determination of the spring constant of the cantilever by the software.

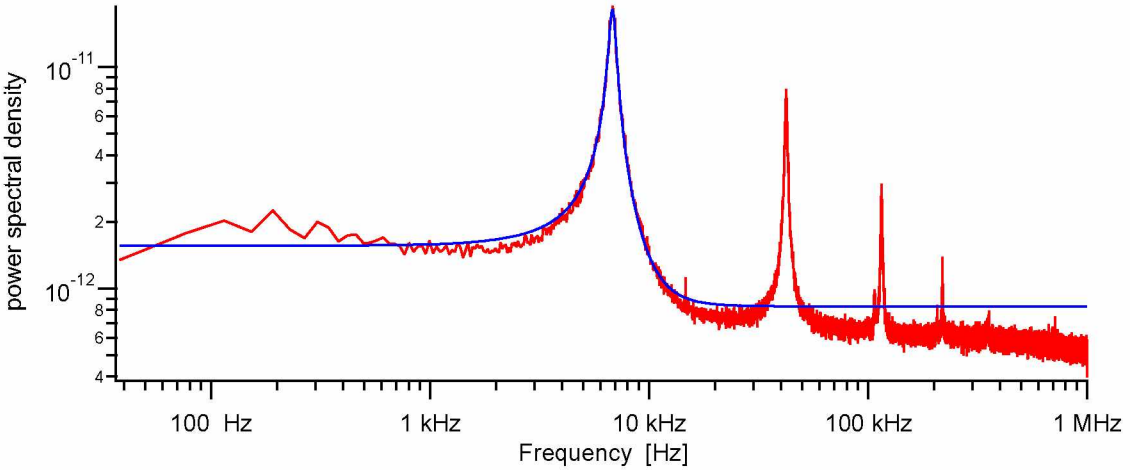

FIGURE 2.4 A thermal spectrum of a vibrating cantilever spring in air. The power spectral density is represented as square of the amplitude of vibration versus the vibration frequencies of the cantilever at different harmonics. The model curve *(blue)* is fitted to the peak at a resonant frequency *(red)* to calculate an accurate spring constant of the cantilever.

The sensitivity of the cantilever deflection was calibrated by obtaining series of force curves on a glass slide (see 2.3.4 **Data acquisition**). As glass is a comparatively hard material, the change in the deflection is directly proportional to the change in the z height. The resultant force curve thus has a slope of 1. An inverse of the calibration factor derived from the slope value is further used to calculate inverse optical lever sensitivity (InvOLS). With the help of the InvOLS value, the deflection of in terms of volts is converted to units of nm. Thus, the measurement of deflection in nm per volt signal obtained from the laser detector is used to calibrate the deflection sensitivity. The deflection sensitivities of cantilever were calibrated in air and in liquid, as the refraction pattern of the laser changes in aqueous surroundings.

Data acquisition

When the tip comes in contact with the sample, the resultant change in cantilever deflection is recorded with the help of light sensor levers. A laser beam, incident on

the cantilever surface, is reflected to a balanced photodiode. As the probe comes in contact with the sample, the path of the reflected light changes which is recorded by the position sensitive photodiode. In this way, the mechanical properties of the sample can be deduced from the changes occurring in cantilever deflection, that are monitored by the AFM. A schematic diagram representing this process in shown in Figure 2.5.

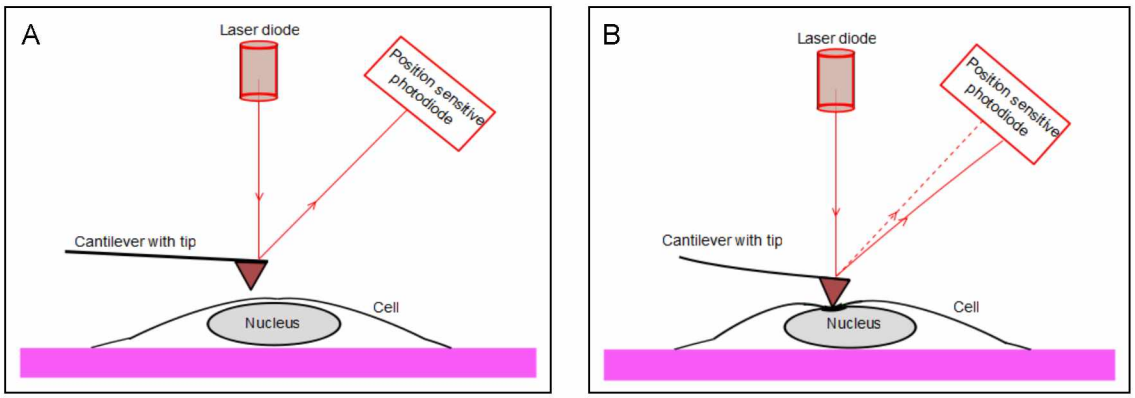

FIGURE 2.5 Schematic representation of AFM probing of a cell. *(A)* The AFM probe not in contact with the sample, resulting in no change in the deflection of the laser beam. *(B)* The cantilever deflection changes as the probe touches the sample, which is recorded by the position sensitive photodiode.

Force curves were obtained on various cell samples using the AFM in a contact mode with a preset constant deflection limit. In contact mode, the underlying sample is brought in contact with the indenter causing a deflection of the cantilever. Simultaneously the sample can get indented as a certain amount of force is exerted on it. The amount of force generated on the sample is limited by a predefined cantilever deflection limit to avoid sample destruction while obtaining the force curves. As the deflection reaches the set limit, the feedback controller monitors the movement of the z positioner via voltage manipulation. The stage can thus be moved in z direction to bring the sample either in or out of contact with the tip. In this work, the cantilever deflection limit was set to 200 nm for AFM data acquisition of living cells, while the same was set to 30 nm in case of AFM probing of isolated nuclei.

A typical set of force curves is shown in Figure 2.6 obtained on a glass surface. The approach curve (red) is the change in the deflection as a function of change in z height when the sample approaches the tip and makes contact with it. The

retract curve (blue) is the change in deflection corresponding to the movement of the tip away from the sample. In both curves, a part of the curve numbered 1, shows constant deflection of cantilever when the sample is not in contact with the tip. The part numbered 2 represents the gradual change in deflection as the tip touches the sample. Only in case of the retract curve, the region marked by an open black circle, numbered 3, represents adhesion forces that are generated during the tip sample separation.

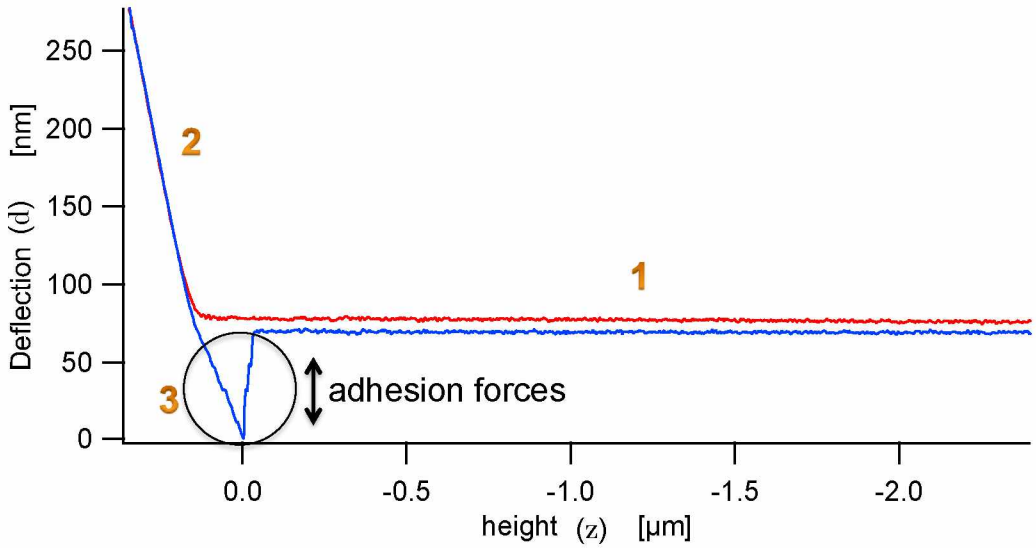

FIGURE 2.6 Set of force curves recorded on a stiff surface. A pair of approach *(red)* and the retract *(blue)* curves obtained upon AFM probing of a glass slide. Curves show different parts, 1 representing the constant deflection of the cantilever when the tip is not in contact with the sample; 2 showing increase in the cantilever deflection upon establishment of contact between tip and the sample; 3 only in case of retract curve which shows fluctuation in deflection due to adhesion forces while retraction of the tip from the sample.

Arrays of force curves i.e., force volumes were acquired over 50 × 50 µm^2 area on the sample in a rasterized manner at a scanning speed of 0.99 Hz with a z scan range of 10-12 µm. AFM probing of the HeLa cells with a pyramidal tip was done with an x-y resolution of 1.25 µm, while that using glass beads was done at a resolution of 2.5 µm. In case of the fibroblasts, the resolution was also kept as 2.5 µm. In Figure 2.7, a phase contrast image of a cell and the corresponding force volume

obtained over the marked region of the cell is shown. The force volume represents the elastic moduli of the sample, where white colour represents the stiffest part and black represents the softest region. The mechanical properties of the sample were determined from these force curves which were analyzed according to specific models described for calculation of the Young's modulus of elasticity, a measure of stiffness.

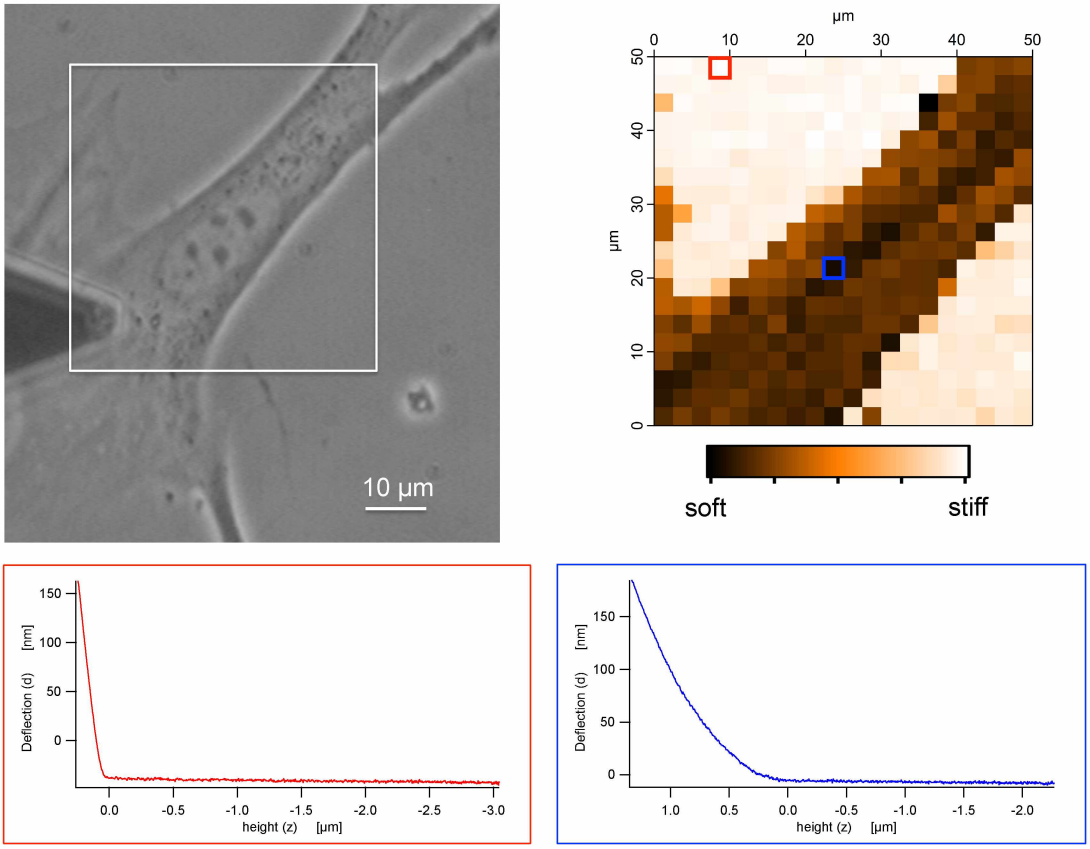

FIGURE 2.7 A force volume generated by AFM probing of a cell. The figure shows a phase contrast image of a fibroblast *(left)* from which a force volume *(right)* was obtained. The area marked by an open white square represents the region of the cell on which the force curves were recorded. An open red square and an open blue square respectively show the representative regions on the coverslip and on the cell. Corresponding force curves on these regions are shown in red and blue boxes.

Data Analysis

AFM data analysis was done by a home built software written in Igor (Wavemetrics, Lake Oswego, USA) [75] with some preset parameters. The spring constant of the

cantilever (k_c) was 0.01 N/m for the data obtained with HeLa cells. The dimensions of the pyramidal tip were as follows: The half opening angle of the pyramidal tip was 40° with a radius of curvature of 40 nm at the very end of the pyramidal tip. In case of glass beads the opening angle of the tip was not taken into account but the tip radius was 3.5 µm. For fibroblasts, the k_c was taken as 0.015 N/m, while the rest of the parameters for the pyramidal tips remained the same. Data analysis was limited in the range of low loading forces, i.e. between 50 to 100 nm deflection limits. In case of the isolated nuclei, data analysis was restricted in the range of even lower loading forces, between 2 to 10 nm deflection limits. The mechanical properties of cells were represented in terms of Young's modulus (E, also called elastic modulus). Often, the logarithm of E was calculated for a clearer representation of the data. Cells are assumed as linear elastic material for the kind of AFM experiments done in this work, as low loading forces result into small reversible deformation of the sample allowing it to be considered as linear-elastic in nature.

According to the Hooke's law, a force (F) needed to extend or compress a spring by some distance (d) is proportional to that distance. The materials which are considered to be linear-elastic obey this law. Hence the force exerted by the AFM tip on the cells can be stated by Eq. 2.4

$$F = k_c \, d \tag{2.4}$$

(Where, F is the loading force, k_c represents the spring constant of the cantilever, d is the deflection of the cantilever)

Thus, the accuracy with which the amount of loading force is determined, depends on the on the accuracy of the spring constant value and the quality of calibrating the deflection signal. In principle, a company provided spring constant value of 0.01 N/m could be used; but due to variation in the thickness of the silicon wafer from which the cantilevers are made, the exact spring constant values can differ from cantilever to cantilever. Thus the thermal tune method (see section 2.3.4 **sample indenters**) was used for measurement of the spring constant of each cantilever

before every experiment.

In Figure 2.8, examples of different types of force curves are shown that can be obtained in a force volume generated on a cell. To calculate the elastic moduli of the samples, a model curve (blue) is fitted to the obtained AFM data (described later in detail under **Hertz model**). The figure shows examples of elastic moduli values obtained for a stiff substrate (for example glass, 10^4 - 10^7 kPa), for cell cytoplasm (42 kPa) and for the nucleus (3.5 kPa). The linear deflection curve on a stiff substrate is shown as a black dotted line, where the deflection and distance from the sample is directly proportional. The indentation (δ) of the sample is given by the difference between the z-position value of the black dotted line at the contact point and the measured deflection (d). This relation is represented in Eq. 2.5.

$$\delta = z - d \tag{2.5}$$

Hertz model

Heinrich Hertz had originally proposed a model in 1882 to calculate local elastic deformations of two filled half-spherical surfaces touching under load [77]. In the simplified version of the Hertz model (one sphere touching a flat surface) the Young's modulus (E) of the surface can be calculated using Eq. 2.6.

$$E = \frac{3}{4} \frac{F(1-\nu^2)}{\sqrt{R\delta^3}} \tag{2.6}$$

(Where E is the Young's modulus of elasticity, F denotes the loading force, ν is the Poisson's ratio (0.5), R is the tip radius, δ is the indentation)

This model was applied for analyzing the AFM data that were obtained by probing of the cells using a glass bead, as the cell and the glass bead, both, can be considered as spherical bodies. Hence, to calculate the Young's modulus of elasticity of the cells, Eq. 2.6 was used. Figure 2.9 shows an example of a force curve analyzed using the Hertz model. The upper panel shows a force curve which represents change

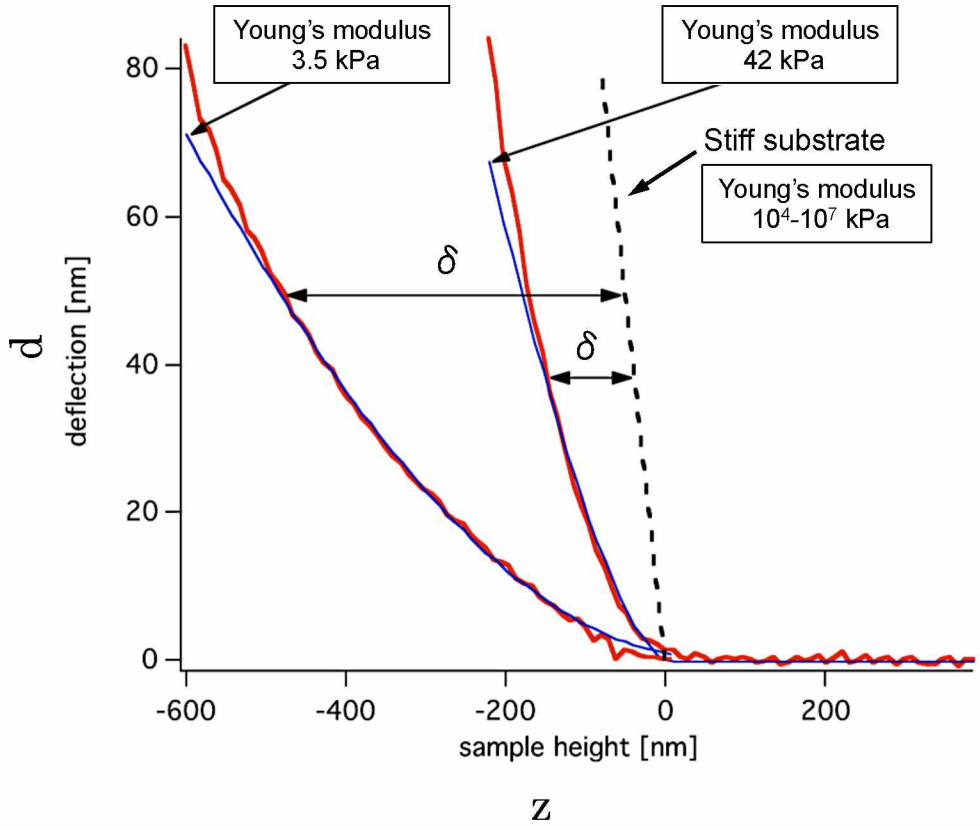

FIGURE 2.8 Typical force curves obtained on samples of different stiffnesses. The force curves are shown in red to which the model curve according to Hertz-Sneddon theory *(blue)* is fitted to calculate the elastic moduli values. The elastic modulus of glass (10^4 - 10^7 kPa), that of the cell cytoplasm (42 kPa) and that of the nucleus (3.5 kPa) is shown. The black dotted line represents the linear curve for a stiff substrate. The indentation (δ) of the sample is given by a difference between the z sample height at contact point and the measured deflection (d). Image adapted from [75].

in deflection (d) of the cantilever as function of the sample movement in z direction. For calculation of the force (F), Eq. 2.4 was used. Next, Eq. 2.5 was used to determine the indentation (δ) of the sample. For this, an exact determination of the contact point (z_0) between the sample and the tip was done, after fitting the Hertzian model curve (blue) to the experimental data (red) as shown in the upper panel of the Figure 2.9. The dotted green horizontal lines show the range (50 - 100 nm in this case) of the cantilever deflection that was considered for the data analysis. Hence the loading forces corresponding to this deflection range were taken into consideration by the software, for further calculations. The two vertical lines in shades of red show initial and final estimates of z_0 from the experimental data. Two more vertical lines in shades of blue are initial and final estimates of the z_0 according to the Hertzian fit. The final contact point shown by a green vertical line was determined by the software after taking into consideration all the previous four contact point values.

The lower panel in Figure 2.9 shows the loading force (deflection range denoted by dotted horizontal green lines) as a function of sample indentation. In this way the values for F and δ could be determined from the recorded force curves. As the indenter was a glass sphere, the tip radius (R) was 3.5 µm. As an incompressible material like water has a Poisson's ratio (measure of compressibility) of 0.5, and the cells contain about 70% water, the (ν) for cells was also assumed to be 0.5.

Modification of the Hertzian model by Sneddon

Sneddons modification of the Hertzian model is applied for a conical tip that is used for AFM probing of the cell sample instead of a spherical tip. This modification for calculation of the elastic modulus of a material was suggested by Ian N. Sneddon in 1965 [78]. As the indenter tip geometry changes from a sphere to a cone or a pyramid, the half opening angle of the tip (α) plays a key role in determining the elastic modulus of the sample in addition to the average radius of the pyramidal tip. The modified equation is called the Hertz-Sneddon equation which is stated in Eq. 2.7. Hence, all the force curves obtained by AFM probing of different cell samples

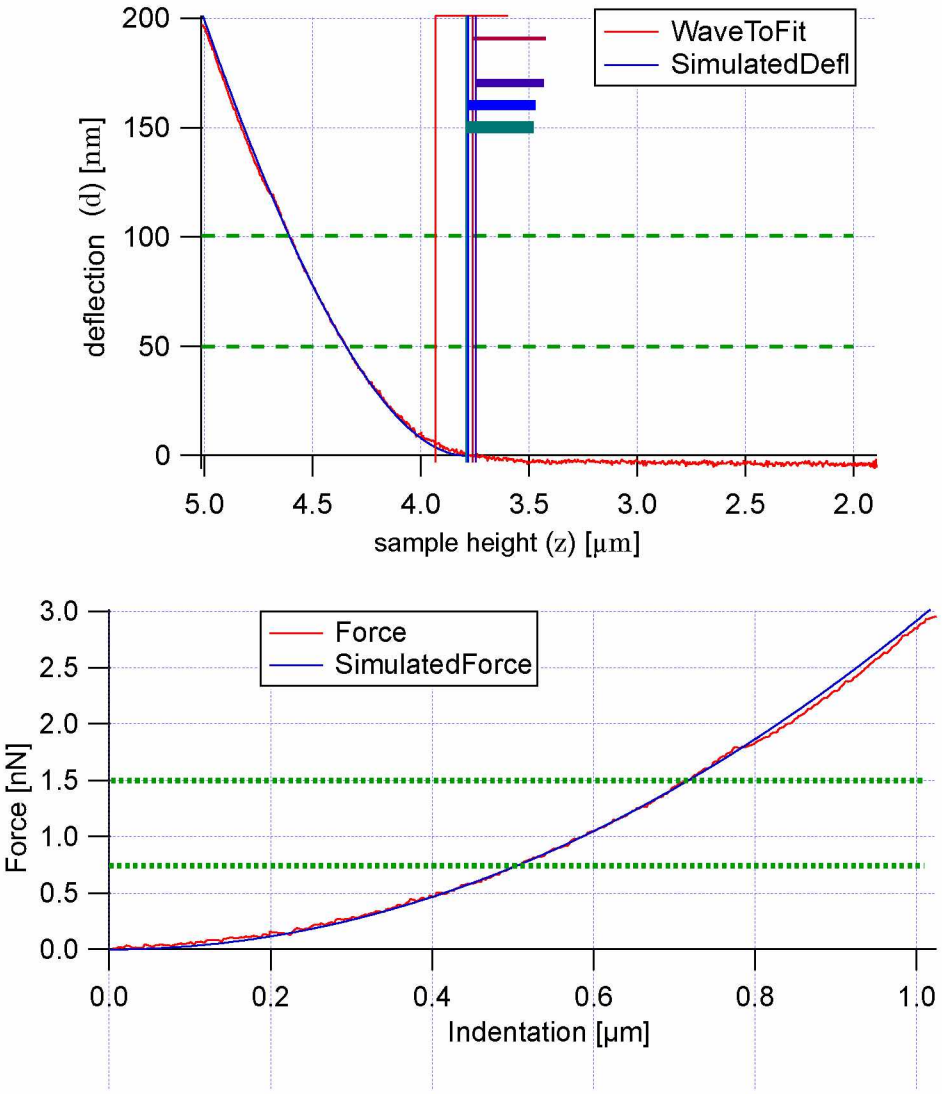

FIGURE 2.9 AFM data analysis done according to the Hertz model. The AFM data were analyzed by fitting a Hertzian model curve *(blue)* to the experimental data *(red)*. The upper panel shows a deflection curve as a function of the z height. The red and blue vertical lines are initial estimates for the contact point between the tip and the sample. The green vertical line is the final contact point considered for further calculations. The horizontal dotted green lines indicate the deflection range selected for data analysis. The lower panel shows the loading force as a function of sample indentation. Horizontal dotted green lines indicate the deflection range used for data analysis.

with pyramidal tips were analyzed according to the Hertz-Sneddon model [78].

$$E = \frac{\pi}{2} \frac{F(1-\nu^2)}{\delta^2 \tan \alpha} \tag{2.7}$$

(Where E represents the Young's modulus of elasticity, F is the loading force, ν is the Poisson's ratio (0.5), α denotes the half opening angle of the tip, δ is the sample indentation)

Shell model

The elastic shell model is applied for analysis of samples that are made up of a thin elastic shell which primarily determines the mechanical properties of that sample and the content of the sample does not contribute to the resultant stiffness. Bacterial surfaces and *Xenopus* oocyte nuclei have been demonstrated as typical examples where application of this model has been described in detail [79], [72], [47]. According to the shell model, the elastic shell shows a linear mechanical response to the indentation by a point force, as the sample and the cantilever spring are considered as two linear springs in series. Thus, from the slope of a linear force curve, the spring constant of the sample can be calculated by Eq. 2.8 and Eq. 2.9.

$$s = \frac{d}{z} \tag{2.8}$$

$$k_n = k_c \frac{s}{1-s} \tag{2.9}$$

(Where d is the deflection, z is the z height of the sample, k_n is the spring constant of the nucleus, k_c is the spring constant of the cantilever, s denotes the slope of the curve)

The AFM data obtained by probing of isolated nuclei by a pyramidal tip were analyzed according to the shell model. A part of the force curves obtained on the nuclei showed a clear linear correlation between change in the deflection as a function

of the z height. Thus the data analysis for calculation of the spring constant of the nucleus, i.e., nuclear stiffness, was restricted only to the linear region of the curves. This was achieved by limiting the analysis in the deflection range corresponding to the linear region (2-10 nm in this case). In Figure 2.10, few examples of the force maps and representative force curves from the areas marked with open red boxes, that were obtained on the isolated nuclei, are shown. The slope from the region of the curve that is marked between solid black arrows, was used for calculation of the nuclear stiffness. Moreover, the nuclei were devoid of membranes due to detergent treatment carried out during isolation procedure as revealed by TEM analysis. In addition, a heavy extraction of nuclear contents was also evident. Hence an elastic response of the lamina layer could be directly assessed by this method.

Selection of nuclear and cytoplasmic regions of a cell

To assess the mechanical properties of the nuclear region of the cells, the corresponding Log E values could be selected roughly, on the basis of the sample height z recorded while obtaining force curves. As the sample is moved towards the tip, the z distance travelled to make contact with the edge of the cell is larger than the z distance required to reach the top of the cell (where the nucleus is situated). In Figure 2.11, an example of such a type of analysis is shown. Panel A shows a false colored map of the z height recorded during one AFM reading on a cell. The color scale represents the z distance travelled for recording force curves ranging from 1 µm (top of the cell) - 5 µm (coverslip). The panel B shows a graph where Log E values calculated from the force volume shown in A, are plotted as a function of z sample height. Each red datapoint in the graph represents Log E value obtained by analysis of each force curve in the force volume. The cluster marked by a black bracket belongs to the nuclear region of the cell while the one within the range marked by blue bracket is the cytoplasmic region. The z height range selection was done with the aid of phase contrast images of the cells acquired during AFM experiments.

In this way, from each force map, the z height points corresponding only to the nuclear region (top of the cell to periphery of the nucleus) were selected and an average of the Log E from only these data points was calculated. The stiffness of

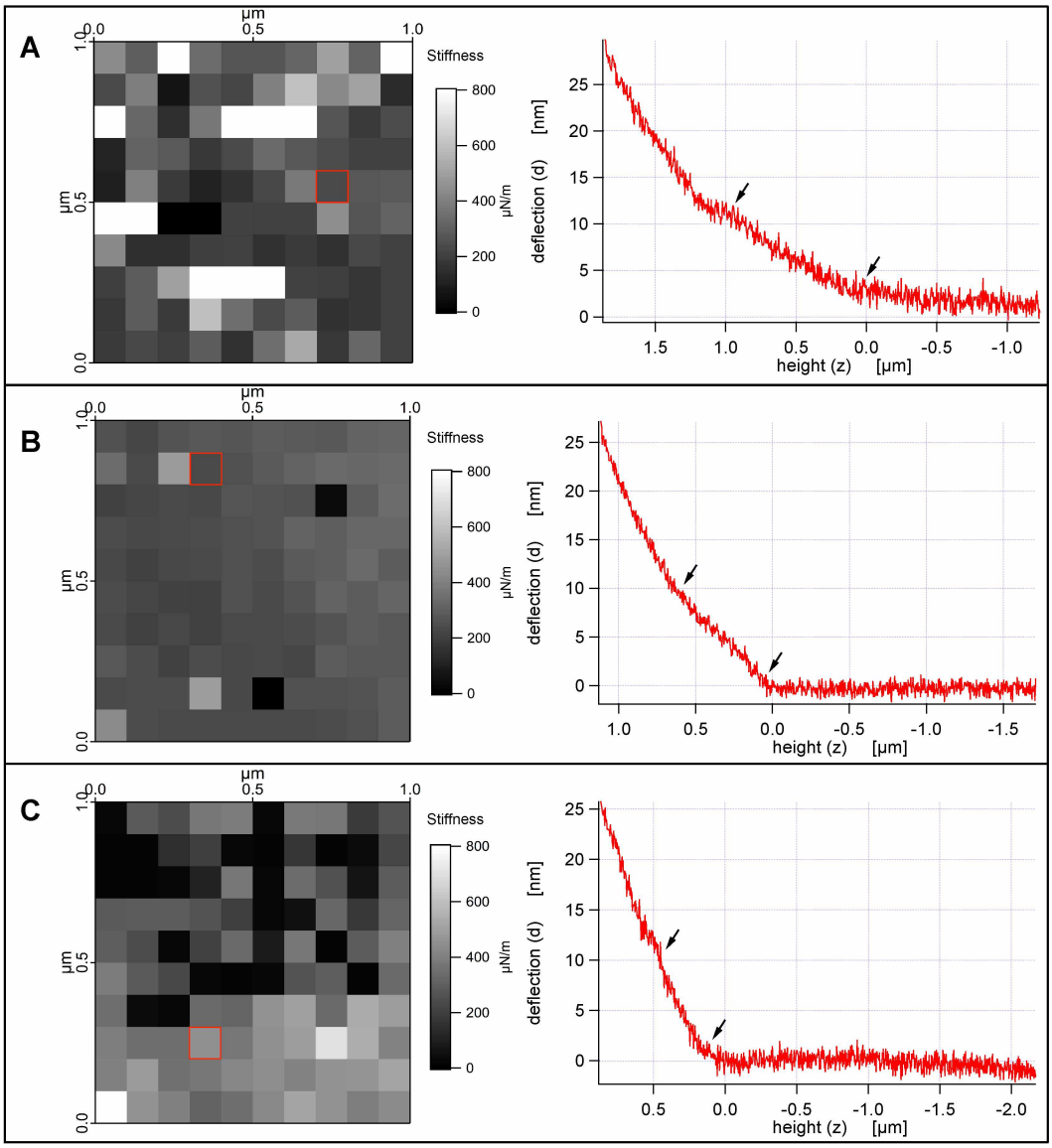

FIGURE 2.10 Typical force curves obtained from isolated nuclei probed with a cantilever with a pyramidal tip. On the left side, panels *(A, B and C)* show force maps obtained on the surface of three different isolated nuclei. The force curves shown on the right hand side were obtained in areas marked with open red squares on the respective force maps in each panel. Nuclear stiffness was calculated using slope of the linear part of the curves marked between the arrows.

the nuclear region of each cell is thus represented by the average Log E values of selected data points.

For analyzing the stiffnesses of the cytoplasmic region of the cells, an approximate z height range was chosen from the base of the cell till the periphery of the nucleus, excluding data of the nuclear region and the substrate. The average Log E of these selected data points represents the stiffness of cytoplasmic region of each cell. The experimental data for each force map of each experiment done with dermal fibroblasts is given in Appendix A.6.

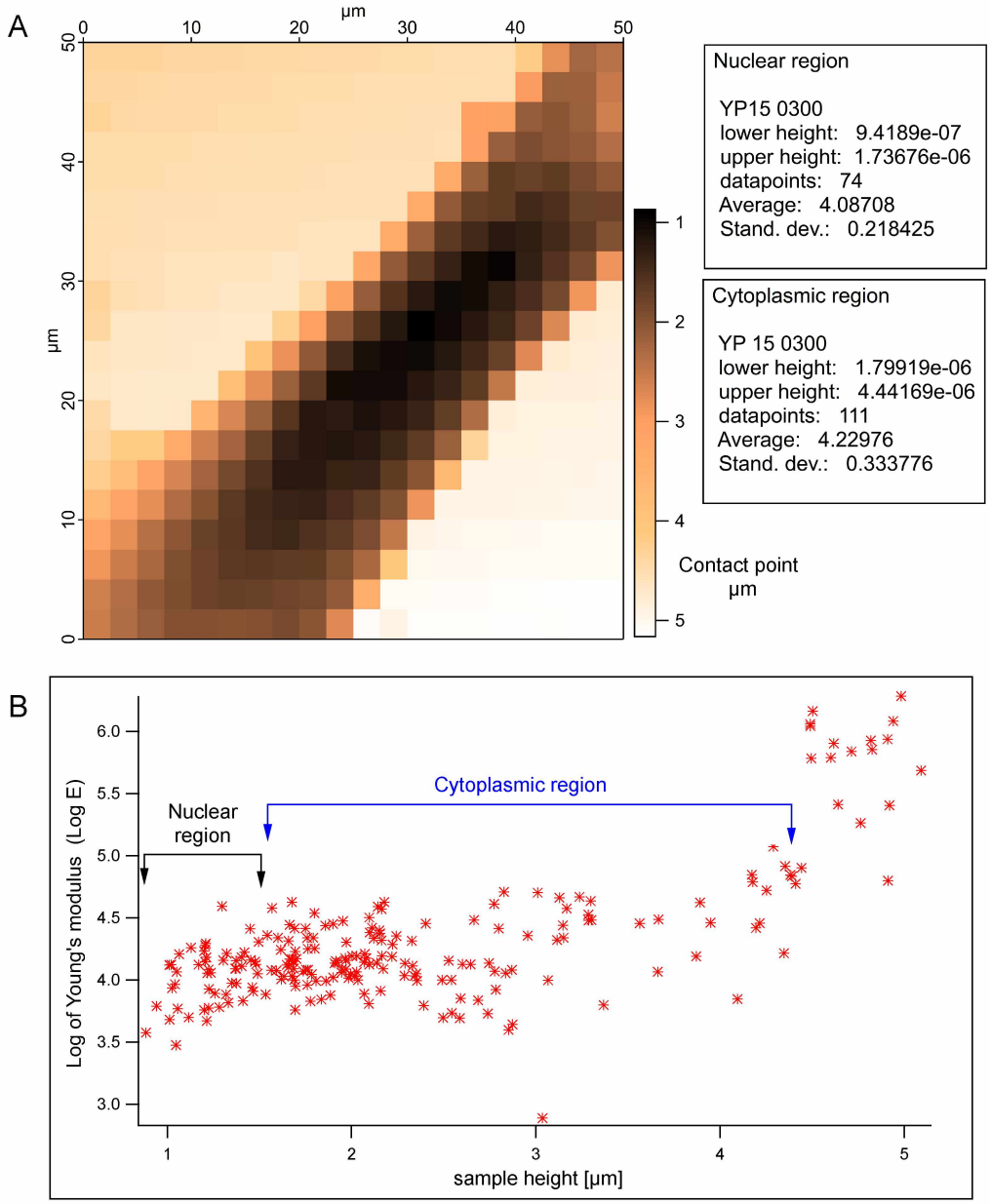

FIGURE 2.11 Selection of nuclear and cytoplasmic regions of a cell on basis of z height. *(A)* A z height map obtained by AFM probing of a cell. The color scale shows the z height ranging from 1 *(black)* to 5 *(white)* correspondding to top of the cell and the coverslip respectively. *(B)* A graph of all the Log E values calculated from the force volume in *(A)*, as a function of the z sample height. Set of points indicated by a black bracket represent the nuclear region, while the blue bracket indicates points belonging to the cytoplasmic region of a cell.

3

Results

Hutchinson-Gilford progeria syndrome (HGPS) is a rare premature aging disorder. In 80% of the cases, it is caused due to a silent point mutation in the *LMNA* gene which results into occurrence of a mutated lamin A protein, LAΔ50/progerin [80]. Progerin is a truncated version of pre-lamin A which retains its farnesyl moiety and disturbs proper functioning of the nuclear processes in a cell. In the past decade, additional reports about mutations in *LMNA* causing progeroid syndromes have been reported. Eriksson et al. in 2003, reported an HGPS mutation in the lamin A protein where a lysine residue replaces the glutamate residue at the position 145 in coil 1B of the lamin A [23]. The lamin A E145K mutant was shown to assemble in a defective manner in in vitro lamin filament assembly experiments in contrast to the wild-type lamin A [26]. To study the possible effect of alterations in the lamin filament assembly on the mechanical properties of the nuclear lamina, *Xenopus* oocyte nuclei were used to obtain force curves with the atomic force microscope [47]. As the cells of a progeria patient are exclusive samples and it is difficult to maintain them under in vitro culture conditions for a longer time, initial AFM experiments were carried out using *Xenopus* oocyte system. *Xenopus* oocyte nuclei are large ($\sim$500 µm diameter) in size and do not contain peripheral chromatin attached to the lamina, make them convenient for handling and allows better understanding of lamina structure. The work done by Kaufmann et al. [47], indicated that ex vivo expression of lamin A E145K causes alterations in the mechanical properties of the lamina. Laminae of comparable thickness made up of mutant lamin A E145K

were stiffer than those comprising of wild-type lamin A. Although the nucleus of the *Xenopus* oocyte is a heterologous system to study effects of a human laminopathy mutation, these results clearly show that alterations in mechanical properties of the nuclear lamina occur due to the progeria mutation [47].

Nonetheless, further AFM experiments on cells obtained from a progeria patient with the lamin A E145K mutation were necessary. As these somatic cells are not heterologous samples, experiments with them would reveal in vivo changes occurring in the elastic properties of the lamina formed by mutant lamin A proteins in combination with other lamin proteins. AFM data acquisition from different cell types including platelets, fibroblasts, *Xenopus* oocyte nuclei has been well established [81],[82],[72], but further optimization was required to estimate the elastic moduli on relevant regions of the adherent cells grown on coverslips. As the nuclear region of a cell was the target, establishment of a method for selective analysis of data confined to the nuclear region was required to obtain the corresponding elastic moduli values.

Dermal fibroblasts of a progeria patient with the lamin A E145K mutation are available from a cell repository where they were isolated from skin biopsy sample of the patient. Taimen et al. (2009) showed that these cells develop post mitotic nuclear lobulations and show alterations in localization of the telomeres and centromeres. These alterations disturb overall cell function. This implies that the diseased cells are under stress and might not grow and divide as efficiently as healthy cells. It has been documented that the effects caused by mutated lamin A worsen the health of the cells rapidly with successive passage numbers, causing a reduction in their proliferative capacity [26]. Maintaining the cells in culture over a longer period of time was thus not possible. Hence, the initial experiments were carried out with HeLa cells which can be maintained easily in culture. These cells were transfected with the respective plasmids to express either wild-type lamin A or the E145K mutant.

3.1 Expression of wild-type and mutant lamin A E145K in HeLa cells

HeLa cells were transiently transfected with plasmids encoding either wild-type or E145K mutant lamin A along with a second plasmid encoding eGFP. The resultant lamin proteins were not tagged and therefore, expression of eGFP was used as an indication for a successful transfection of cells with both the plasmids. The success of cotransfection resulting in protein coexpression was tested in a prior experiment, in which, Flag tagged *Xenopus* lamin A and eGFP were expressed after cotransfection of the respective plasmids. Cell samples were fixed and stained using the monoclonal antibody M2 to detect the Flag tagged protein followed by a polyclonal antibody conjugated with the fluorophore Cy3. Cy3 fluorophore is excited at around 550 nm and emits light at the wavelength of around 570 nm. In contrast, eGFP has its excitation maximum at 488 nm and an emission maximum at 507 nm. A considerable difference between the emission maxima of both Cy3 and eGFP thus allowed detection of lamins and visualization of eGFP in the same sample. In about 99% of the cells, that showed presence of eGFP, Flag tagged lamin A was present as well (see Appendix A.1). This test showed that eGFP fluorescence is a reliable indicator for the lamin coexpression, and can be used to select the cells for AFM data acquisition. HeLa cells expressing mutant lamin A E145K develop nuclear lobulations by 72 hours post transfection [26]. Hence, the experiments done in this work were carried out for a time period of three days post transfection.

Figure 3.1 shows indirect immunofluorescence microscopy images of HeLa cells that were cotransfected with plasmids coding for eGFP and, either wild-type lamin A or the E145K mutant. Cells were fixed and immunostained on day one and day three post transfection. The transfected cells fluorescing in green can be identified in the GFP panel. The nuclei are identified by staining of the DNA with DAPI as shown in the DNA panel. The comparison of the GFP and DNA panels indicates that the transfection efficiency is not 100%. The transfection efficiency for HeLa cells was shown to be ~40-50% [83]. The cells expressing eGFP can also be considered to coexpress either wild-type or E145K mutant lamin A. The nuclear shape of these cells was visualized by immunostaining of the endogenous lamin B2 as shown in

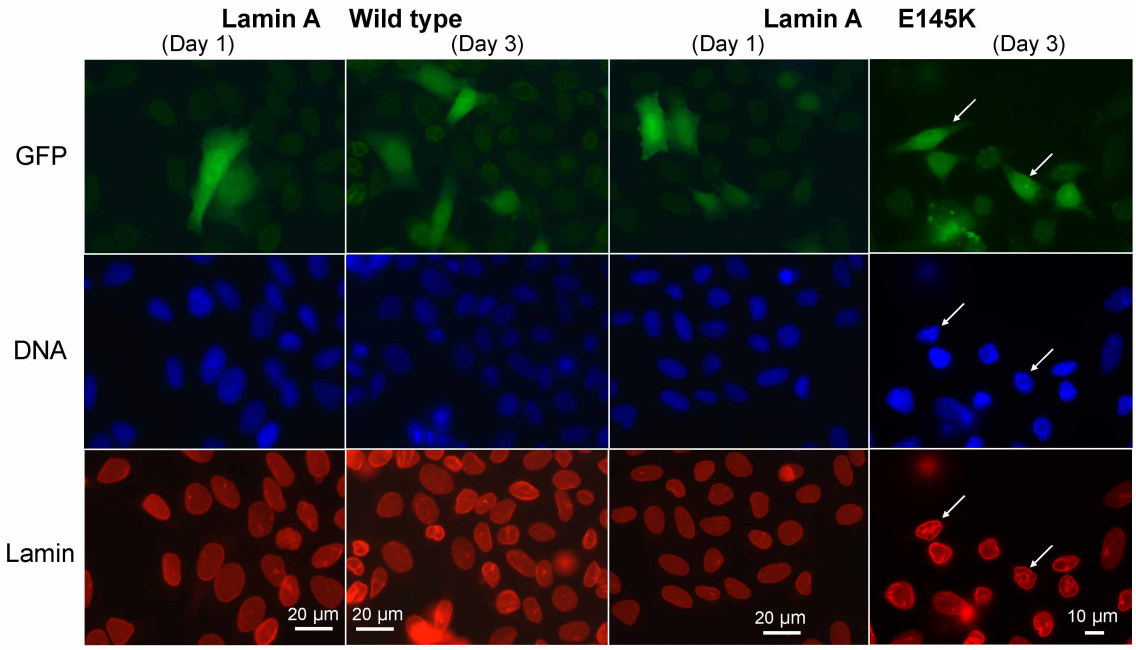

FIGURE 3.1 HeLa cells expressing eGFP and lamin A. HeLa cells were cotransfected with plasmids encoding eGFP and wild-type (WT) lamin A or lamin A E145K mutant. Cells were fixed and stained for indirect immunofluorescence microscopy after 24 h *(Day 1)* and 72 h *(Day 3)* post transfection. The panels show transiently transfected cells expressing eGFP *(green)*, DNA stained with DAPI *(blue)* and endogenous lamin B2 detected using a monoclonal anti-B2 (L7-8C6) primary antibody followed by Cy3-conjugated polyclonal secondary antibody *(red)*. The expression of mutant lamin A E145K leads to lobulations in the nuclei by day 3 *(arrows)* while lamin A WT expression does not affect nuclear shape over the same time period. Note that images for lamin A E145K day 3 category are single optical sections obtained using an ApoTome while the other images are obtained by conventional fluorescence microscope.

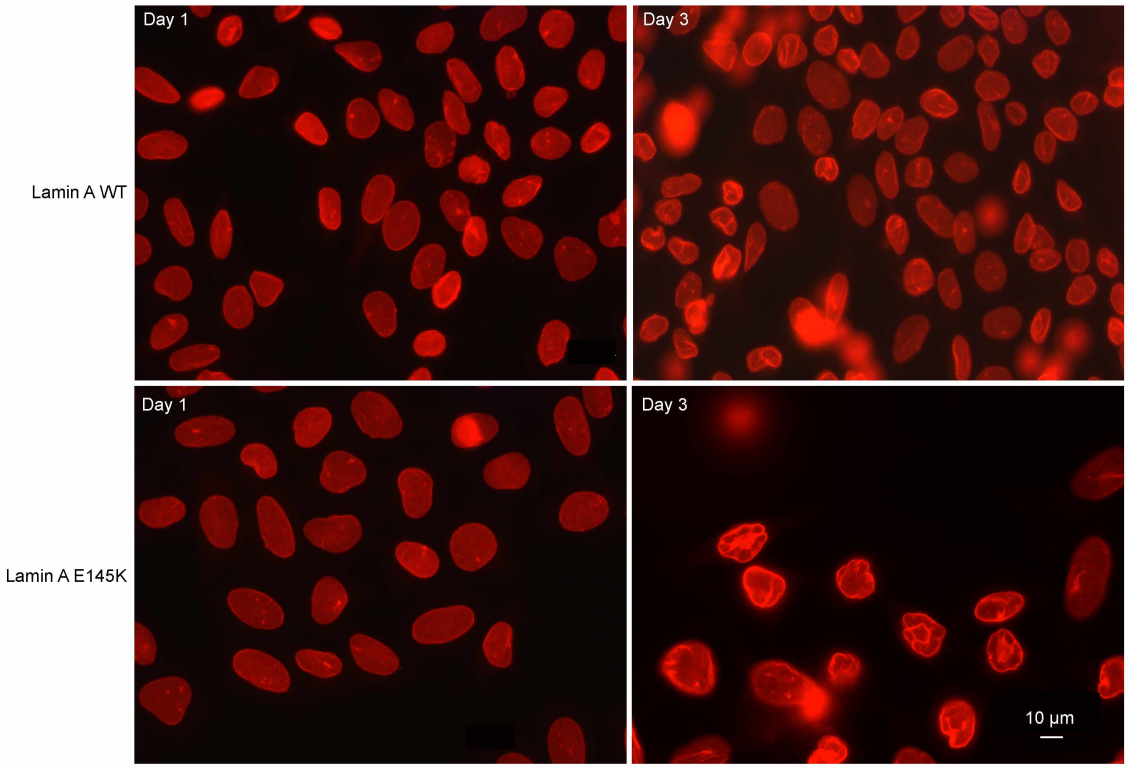

FIGURE 3.2 Lamin B2 detection for visualizing the nuclear shape. HeLa cells were cotransfected with plasmids encoding eGFP and lamin A WT or lamin A E145K. Cells were fixed and stained for indirect immunofluorescence microscopy after 24 h *(Day 1)* and 72 h *(Day 3)* post transfection. The panels show the endogenous lamin B2 detected using a monoclonal anti-B2 (L7-8C6) primary antibody followed by Cy3-conjugated polyclonal secondary antibody. Nuclear lobulations are caused due to the expression of mutant lamin A E145K by day 3, while the nuclear shape does not change due to lamin A WT expression over the same time period. Note that image for lamin A E145K day 3 category is a single optical section obtained from ApoTome while the other images are obtained by a conventional fluorescence microscope.

the lamin panel. The presence of a smooth nuclear boundary indicates a normal nuclear morphology on day one in case of both the lamin A variants. For recognition of the nuclear shape, detection of the ectopically expressed lamin A would have been an obvious choice. However, this staining would not distinguish between the endogenous lamin A and the ectopically expressed lamin A, as both are of human origin. Moreover, lamin A is not only confined to the nuclear envelope but is also present in the nucleoplasm. Lamin B2, on the other hand, is exclusively present at the nuclear periphery [84], [85]. Thus, immunostaining of lamin B2 was done to clearly recognize the nuclear shape of the transfected cells. Lamin B2 was detected using the monoclonal antibody L7-8C6 and a Cy3-conjugated secondary antibody. Day three samples of the cells expressing the mutant lamin A E145K show lobulated nuclei with nuclear envelope invaginations, some of which, are indicated by arrows in Figure 3.1. In contrast, nuclei of the same sample are normally shaped on day one. The details of nuclear lobulations can be seen in the Figure 3.2, where, only lamin B2 staining of the same cells from Figure 3.1 is shown in a bigger panel. Cells expressing lamin A wild-type maintain a normal nuclear morphology even on day three. The development of nuclear lobulations also confirms a successful protein expression from the cotransfected plasmid although the presence of the ectopically expressed lamins could not be shown directly. The results of indirect immunofluorescence microscopy thus confirmed the observations reported by Taimen and co-workers about changes in nuclear shape due to expression of the mutant lamin A E145K [26].

3.2 Atomic force microscopy of HeLa cells

Atomic force microscopy is a novel biophysical technique wherein force curves generated as a result of the indentation of a sample are used to interpret information about the mechanical properties of the sample. Estimation of elastic moduli of the probed samples is done by analyzing the data according to appropriate models depending on the sample properties (for details see section 2.3.4). Cells grown on various substrates have been used previously in such experiments. Adherent cells can spread well on hard substrates where they form flat monolayers. Due to spreading, the cell height is low as the cytoplasm spreads over a large area generally

leaving the nucleus protruding in height in the center of the cell. As a very thin layer of cytoplasm covers the nucleus on top (for TEM analysis of fibroblasts, see Appendix A.4), AFM probing of such a region could be used to assess the mechanical properties of the underlying nucleus. With such an approach the elastic moduli of nuclei could be obtained without isolating them from the cells. To avoid the nuclear isolation procedure, which, generally involves a harsh treatment of cells, AFM probing of intact cells grown on glass coverslips was done. HeLa cells were subjected to AFM readings taken with the help of a triangular cantilever spring with a spring constant k_c of 0.010 N/m having a pyramidal tip at its end. The pyramidal tips with which the cells are probed have an average diameter of 40 nm at its very end. While obtaining force curves, the cells were maintained in an atmosphere containing 5% CO_2. The temperature was not regulated but the overall temperature of the system generally remained in the range of 23-27°C as indicated by the data acquisition software. Transfected HeLa cells were identified by eGFP fluorescence and only those cells were used for recording AFM measurements. In addition non transfected and mock transfected cells were used as controls.

3.2.1 AFM probing by a pyramidal tip

For each experiment, the cells were grown on glass coverslips which were placed in separate cell culture dishes (one dish for each day) for transient transfection experiments and were further maintained over a time span of three days. For each experiment, a common stock of transfection mix was prepared and added to individual plates to minimize pipetting differences. As controls, non transfected and mock transfected cells were used. Mock transfected cells were used to consider a putative effect of the transfection reagent on the cell mechanics. AFM readings were obtained 24, 48 and 72 h post transfection.

Force curves were generated over an area of 50 × 50 µm^2 consisting of 40 lines, each containing 40 points. The resultant array of force curves, called a force map or a force volume, has a resolution of 1.25 µm. Each force map therefore consisted of 1600 force curves covering some region of the substrate and the nuclear region of the cell. Three independent experiments were carried out on each category of

cells to obtain large amount of AFM data (Generally 5-6 force maps per day per experiment). As the total number of force curves analyzed for each day and cell category was very large, the data of the three experiments are considered together to compare the elastic moduli of different cell categories.

Data analysis was restricted to the nuclear region of the cells as the effect of the lamin A E145K mutation on nuclear mechanics was under question. From each force curve, the Young's modulus of elasticity (E) was calculated using the Hertz-Sneddon model (for details, see section 2.3.4). As the number of force curves obtained per force map was high, the average of the logarithm of the Young's moduli values (Log E) was calculated. The graph in Figure 3.3 shows the data obtained from four different HeLa cell categories. The y axis shows the resultant Log E average values acquired for non transfected, lamin A wild-type expressing, lamin A E145K expressing, and mock transfected HeLa cells according to the days when AFM readings were obtained. The days are color coded as indicated in the figure legend. Each asterisk in the graph represents an average Log E value obtained from each force map. The average and median of these Log E average values are indicated by a solid dash and a solid diamond, respectively. Within each experiment, the same cantilever was used over the whole time period of three days to acquire AFM data.

Non transfected HeLa cells show no significant change in their elastic moduli over three days. The overall data distribution shows little variation as the Log E median value is around 3.3 for all the three days. Cells expressing wild-type lamin A show an increase in stiffness on day three as compared to day one and two indicating that excess of wild-type lamin A increases the stiffness of the nuclear region. In contrast to that, the cells expressing mutant lamin A E145K show a significant decrease in stiffness on day one from which they recover by day two and three as indicated by Log E values which are similar to those shown by non transfected samples. The mock transfected samples maintain the same elastic moduli over the three days' time period. The overall elastic moduli of mock transfected samples are lower than that of non transfected samples. This indicates that the transfection reagent might have some effect on cellular mechanics. A statistically significant difference is observed between the stiffness of lamin A wild-type expressing versus lamin A E145K expressing cells ($p \leq 0.005$) only in case of the day one samples.

The statistical test used for comparing the Log E values of all the data sets was the Mann-Whitney U test. This test is used to compare datasets that show a non-Gausian data distribution with different numbers of total data points. Consideration of the averages of such samples for comparison would be unfair as the average value is influenced by the total number of readings and range of their distribution. Hence, generally the median of the samples is considered instead of the average for a fair comparison and calculation of the resultant p values.

Although significant differences are observed between the elastic moduli of wild-type lamin A and mutant lamin A E145K expressing cells on day one, no clear trend of further changes in the elastic moduli is seen. Furthermore, neither a comparison between the corresponding days of four cell categories, nor a comparison of days within a single cell category gave clear idea about changes in the mechanical properties of the transfected HeLa cells. This might be attributed to variations occurring in the transfection and culture conditions. The outcome of these experiments gives some hints towards changes in the mechanics of cells/nuclei, but the data are not truly conclusive. Hence, further experiments were designed with a modified experimental setup.

3.2.2 AFM probing with a glass bead

In the modified approach, the cells were allowed to grow on glass coverslips which were placed together in one cell culture dish to rule out variations in the transfection and culture conditions over the time span of three days. The transfection of HeLa cells with the plasmids encoding eGFP and wild-type lamin A or with those encoding eGFP and mutant lamin A was done in parallel. In these experiments, instead of a pyramidal tip, a glass bead with a diameter of 7 µm was used to indent the cells. This modification was necessary to determine if the AFM probing of the cells using a tip with a changed geometry results into a similar trend of changes in elastic moduli. As the glass bead has a different geometry than a pyramidal tip, a larger surface area comes in contact with the underlying sample which influences the resultant indentation and the amount of loading force exerted on the sample. Change in the tip geometry thus allowed verification of the reproducibility of the results that

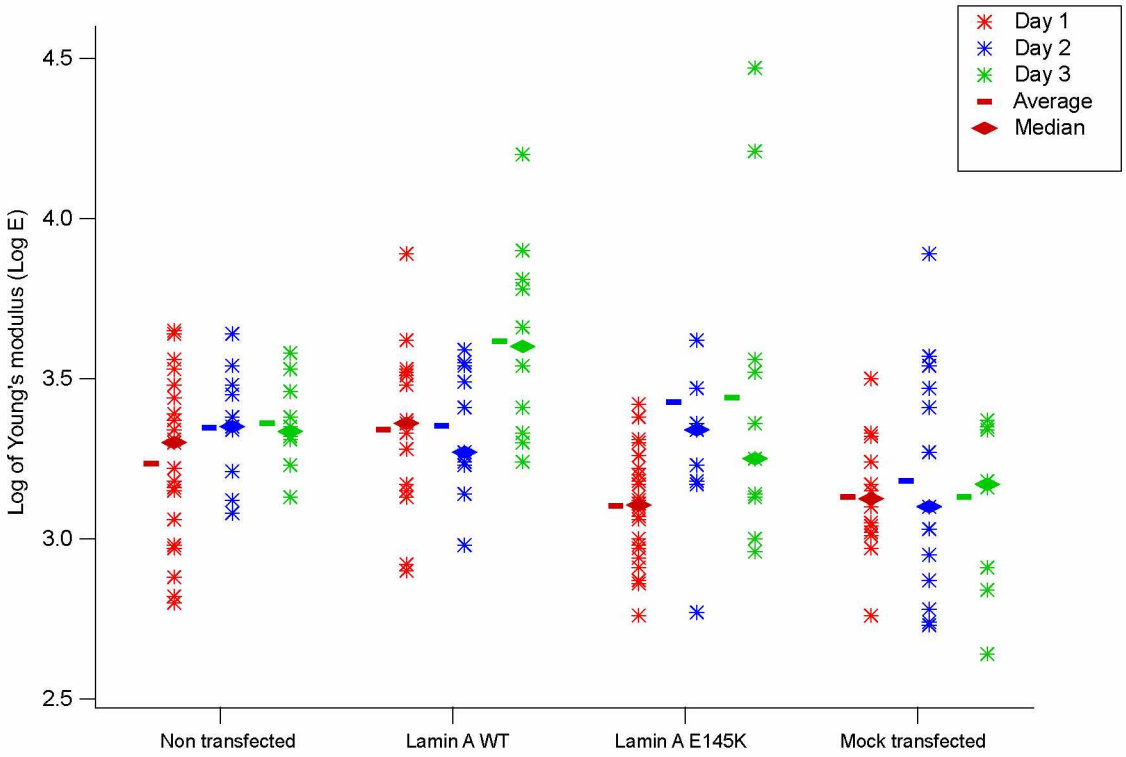

FIGURE 3.3 Elastic moduli of HeLa cells probed by a cantilever with a pyramidal tip. HeLa cells expressing either wild-type or E145K mutant lamin A, were probed by a cantilever ($k_c = 0.010\ N/m$) with a pyramidal tip. The AFM readings were obtained over a time period of three days; day 1 *(red asterisk)*, day 2 *(blue asterisk)* and day 3 *(green asterisk)*. The graph represents averaged values of Log Young's moduli (Log E) plotted for non transfected, lamin A WT expressing, lamin A E145K expressing and mock transfected HeLa cells. Solid dashes indicate the average and solid diamonds represent the median of all datapoints of each cell category. The graph shows data from three independent experiments which are represented here together.

were previously obtained using a pyramidal tip (see Figure 3.3). The glass beads were glued with the help of the AFM assembly to the same type of cantilevers that were used in the previous experiments. The glass bead was positioned exactly behind the pyramidal tip using a minimal amount of glue to avoid contamination of the cantilever with the glue. To obtain AFM data from non transfected cells, the coverslips were taken out prior to the addition of the transfection mix. A second coverslip was analyzed four hours post transfection. In previous experiments, it was shown that HeLa cells did not express eGFP four hours post transfection [83]. Hence, this time point was taken into account to check if the transfection reagent alone caused alterations in mechanical properties of the cells. Further samples were analyzed according to the previous regime, i.e., on day one, two and three after transfection.

AFM data were acquired from three independent experiments using HeLa cells that were expressing eGFP together with either wild-type lamin A or mutant lamin A E145K. Each force volume over an area of 50 $\times$ 50 µm^2 consisted of 20 lines containing 20 indentation points each. The force volumes were analyzed using the Hertz model. This model was originally proposed to estimate the elastic moduli of two filled half spheres pressing against each other. The cells can be considered as filled spherical bodies and as the indenter used in this experiment is a spherical glass bead, application of Hertz model is justified (for details see section 2.3.4). To estimate the elastic properties of the nuclear region of a particular cell, the average of all the Young's moduli values (E) was calculated from each force volume, consisting of around 150-200 force curves representing the nuclear region of a cell. For ease of representation the logarithm of the average Young's moduli values (Log E) was calculated. Hence, each data point in Figure 3.4 represents the Log E value from an individual nuclear region of the cell sample mentioned on the x axis at time points indicated by the color code in the legend. The graph also shows the average of all Log E average values of a particular time point indicated by solid dashes. The medians of all Log E average values are shown by solid diamonds. The data shown here were compiled from three independent experiments. There is no remarkable difference between the Log E medians of data sets of non transfected cells and cells analyzed four hours post transfection for both, the wild-type and mutant lamin A E145K cell

categories. On day one, the lamin A wild-type expressing cells show an increase in the elastic moduli of the nuclear region, while, in case of the cells expressing mutant lamin A E145K, the median of Log E values has decreased ($p \leq 0.005$). This indicates that the expression of mutant lamin A causes a reduction in the stiffness of nuclear area compared to a mild stiffening caused by expression of wild-type lamin A. The elastic moduli of lamin A wild-type expressing cells do not deviate much on the following two days and in case of the lamin A E145K expressing cells, there is slight increase in stiffness on day two followed by slight decrease in stiffness by day three. Post transfection day wise comparison of elastic moduli within each sample set shows only minimal variations which were shown to be non significant by statistical tests. The overall stiffness of cells expressing wild-type lamin A seems to be higher than that of the corresponding non transfected cells and four hours post transfection cell samples. In case of cells expressing mutant lamin A E145K, an overall reduction in the elastic moduli values can be observed in comparison to corresponding controls but these differences were also proven to be statistically insignificant.

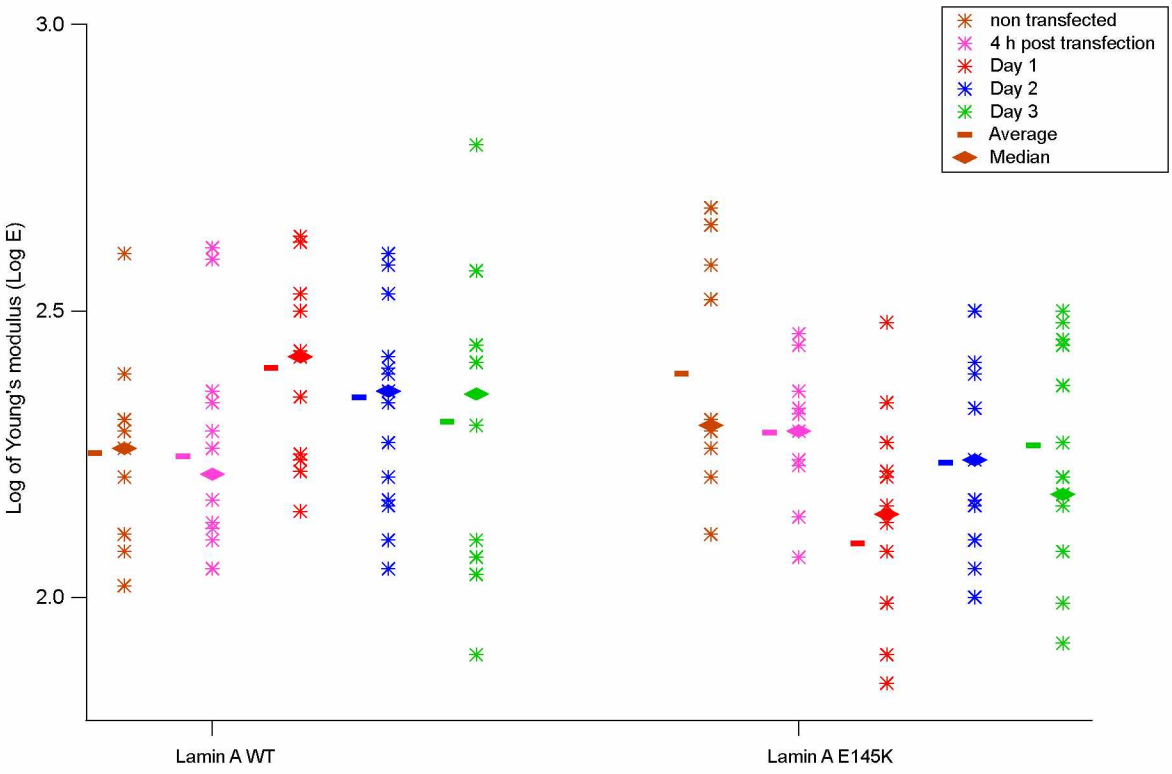

FIGURE 3.4 Elasticity of HeLa cells probed with the glass bead as a modified tip. The graph shows elastic properties of HeLa cells in terms of average Log Young's modulus of cells expressing either wild-type or E145K mutant lamin A using a glass bead of 7 µm diameter as a sample indenter. The glass bead was glued on a cantilever ($k_c = 0.010\ N/m$) with the help of the AFM. The data acquisition was carried out on following time points: non transfected *(orange)*, four hours post transfection *(pink)*, day 1 *(red)*, day 2 *(blue)* and day 3 *(green)*. Data acquired from three independent experiments are represented here together.

3.3 Atomic force microscopy of dermal fibroblasts

While the pilot experiments done with HeLa cells helped to optimize the methods used to obtain and analyze force curves, the outcome of those experiments showed minor differences in mechanical properties of the cells and these differences were statistically not significant as described in the sections 3.2.1 and 3.2.2. In the further experiments, dermal fibroblasts obtained from a progeria patient (PP) were used for AFM probing. The primary fibroblasts derived from the skin tissue of a progeria patient carrying the mutation E145K in lamin A, serves as a good model system to assess the dependence of cellular mechanical properties on premature aging. These cells were obtained from the Coriell cell repository. The cells (cat. no. AG10677) were taken from a four years old male HGPS patient carrying the heterozygous mutation 433 G>A (causing the amino acid residue change from E to K) in the *LMNA* gene. Additionally two dermal fibroblast samples were used as controls. One was from a 10 years old healthy female candidate (YP, cat. no. AG08470) while the other one was from 61 years old healthy male candidate (OP, cat. no. AG02261). These controls were necessary to compare the mechanical properties of progeria patient's cells with the healthy cells originating from a young person and an old person.

3.3.1 AFM analysis of the nuclear region

The fibroblasts grown on glass coverslips were subjected to AFM measurements using a cantilever with a spring constant k_c of 0.015 N/m having a pyramidal tip. The AFM probing of HeLa cells with glass beads and pyramidal tips revealed the same trend of changes in the elastic properties of the cells. As gluing of the glass beads to the cantilevers was an additional step which could introduce further variations, experiments with dermal fibroblasts were performed using cantilevers with a pyramidal tip. The AFM data were obtained from all three samples for a variable number of successive passages, as the cell samples were received from the repository at different initial passage numbers. As the fibroblasts have the tendency

to spread over a large area, the force maps were generated over an area of 50 × 50 µm^2 consisting of 20 lines each containing 20 measurement points. The force curves were recorded such that either the entire cell or a part of the cell with the nuclear region and the surrounding cytoplasmic region was covered. This implies that the cell would be indented at maximum 400 points and as a result a corresponding number of force curves would be generated. The force curves were analyzed using the Hertz-Sneddon model (as described in section 2.3.4 **Data analysis**). The stiffness of a cell is represented here as the Log of Young's modulus of elasticity (Log E). In one reading consisting of several force curves, the average of all Log E values is considered as indicative of the stiffness of the corresponding cell. Each datapoint in Figure 3.5 A represents the average value obtained over the nuclear region of a single cell plotted against the passage number of that cell. The color code, namely, OP (red), PP (green) or YP (blue), indicates the donor of the sample. Determination of the nuclear region of the cells was done on the basis of the sample height (z) recorded during AFM probing. From each force volume, the z height values from top of the cell till the nuclear periphery were taken into consideration for corresponding Log E average calculation (for details see section 2.3.4 **Selection of nuclear and cytoplasmic regions of a cell**).

Figure 3.5 A shows that the stiffness of the nuclear region of OP cells is independent of increasing passage numbers. Cells of the old person were received from the repository in passage number 12, thus, for this sample the AFM readings could be obtained for passage number 14 to 19. In case of YP, the cells were obtained at passage number 6, hence AFM data were recorded from passage number 7 to 15. The PP samples arrived in passage 8 and thus passages 9-13 could be analyzed. In case of YP and PP there is a slight increase in the elastic moduli of the nuclear region as the passage number increases but this difference is statistically not significant. A few PP cell samples in passage 12 are almost 10-15 fold stiffer but are considered as outliers as the rest of the data clusters at a cumulatively lower Log E value as shown in Figure 3.5 B. In this graph, the data presented in Figure 3.5 A are displayed groupwise without considering respective passage numbers. The histograms in Figure 3.5 C, D and E show the data distribution and give the frequencies of the Log E values in that particular data set. The data set for OP shows a bimodal distribution

with the first peak around a Log E value of 3.4 and the second one at around 3.8. The data obtained from cells of the old person and the progeria patient show higher variation than that of the young person. In case of the progeria patient's cells, a prominent peak around Log E of 3.5 is seen with the data distributed over the range of 3 to 5.3. The nuclear regions of YP cells show a left skewed distribution with a single peak around a Log E value of 4.0. The peak values for OP and PP are smaller than that of the YP, indicating that the stiffness of the nuclear region of the OP and the PP samples is lower than that of the YP, but statistical tests indicated that these differences are of low significance in case of OP ($p \leq 0.05$) and insignificant for PP (for details see Appendix B).

3.3.2 AFM analysis of the cytoplasmic region

It is known that the nuclear lamina and the cell cytoskeleton are connected (especially the actin filaments) via the LINC complex proteins [56],[86]. A lamina, that is comprised of mutant lamin A E145K in addition to other lamins, might show alterations in its binding to LINC complex proteins, eventually affecting the interaction with the cytoskeleton. Disturbances in this interaction might also result in changes in the mechanical properties of the cytoplasmic region of the affected cells.

Hence, the same set of force volumes that were analyzed to calculate the elastic moduli of the nuclear regions of OP, PP and YP cell samples, were reanalyzed to estimate the stiffness of the cytoplasmic regions. This was done by selective analysis of the data points of the cytoplasmic region of the cell excluding the nuclear region. This selection could be done on basis of sample height (z) as mentioned before. The force curves were analyzed as described before and the averages of Log E values were calculated. Figure 3.6 A shows the corresponding data plotted against passage numbers of the respective cell samples. The elastic properties of cytoplasmic region of the cells do not change with increasing passage numbers. When the same set of Log E values is plotted groupwise, an upward shift of the YP data set is observed compared to the PP data set (see Figure 3.6 B). Statistical analysis indicates a difference between the elasticities of the cytoplasmic regions of PP and YP, with a

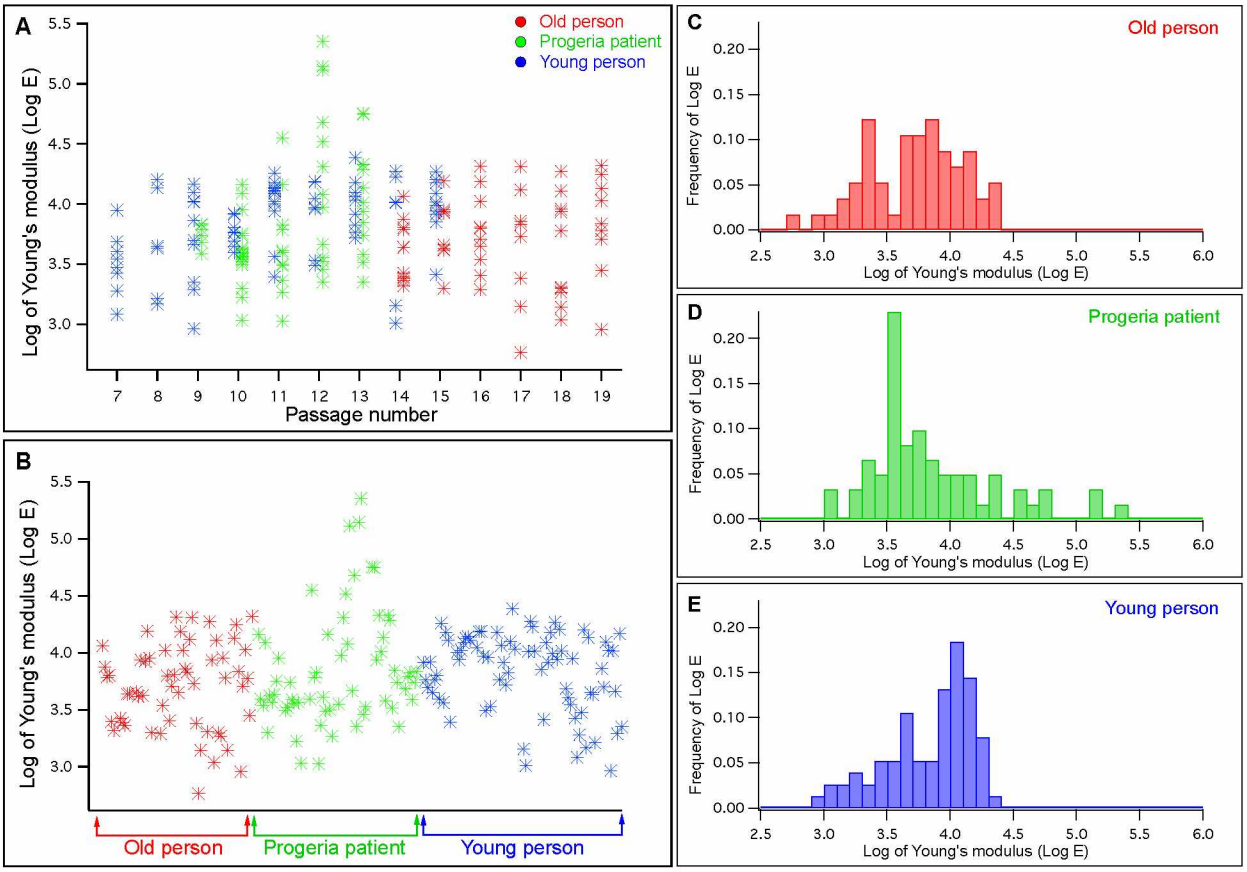

FIGURE 3.5 Elasticity of the nuclear region of human dermal fibroblasts. AFM data of dermal fibroblasts obtained from a healthy old person *(red)*, a progeria patient *(green)* and a healthy young person *(blue)*. The cells were probed using a cantilever ($k_c = 0.015\ N/m$) with a pyramidal tip. *(A)* The graph shows averages of Log Young's moduli plotted against cell passage number. *(B)* The same data points in *(A)* are grouped together irrespective of cell passage numbers. *(C, D, E)* The histograms representing the frequency of Log E averages for cells obtained from respective donors.

low significance ($p \leq 0.05$). The difference can be deduced from the peaks at around Log E of 3.7 and 4.3 in the histograms of the respective samples (see Figure 3.6 D and 3.6 E respectively). The histograms show a higher degree of variation for the PP Log E values in comparison to the YP data distribution. The data obtained from OP samples in Figure 3.6 C shows two groups, similar to the trend seen for the elastic moduli of the nuclear region of the same cell samples (see Figure 3.5 C). In Figure 3.6 C, a broader peak appears at the Log E range of 3.5 to 4 and a sharper one between 4 to 4.5.

These observations show that the mechanical properties of the cytoplasmic part of young dermal fibroblasts differ from that of prematurely aged cells. Although there is not a remarkable difference in the elasticities of OP and PP cells, it should be noted that the data distribution patterns of these samples differ a lot. The OP cells show histograms with a bimodal pattern which hints that the dermal fibroblasts of the healthy old donor consist of two subpopulations. The PP cells on the contrary show a single peak but with a high variation in the distribution of the overall data.

The AFM probing of intact cells thus revealed differences in the mechanical properties of different regions of the cells. But the trends observed for the changes in elastic properties of the nuclear regions do not differ from that of the cytoplasmic regions. This indicates that the AFM probing of the intact cells followed by a restricted analysis of the nuclear region might not reveal elastic properties of the nuclei. It might be possible that the indentation of the nuclei was masked due to presence of cytoskeletal elements. It is known that in addition to the actin stress fibers spanning the entire cell, a perinuclear actin cap surrounds the nucleus of adherent cells which renders exact positioning of the nucleus within the cell [60]. As the mutant lamin A E145K predominantly localizes in the nuclear lamina [47], [26], and the interaction between nuclear lamins and cytoskeletal proteins might be altered due to the progeria mutation, this type of AFM analysis might have measured the changed elastic response of the underlying cytoskeleton and the cytoplasmic contents, and therefore the mechanics of the nuclear surface might not have been analyzed by these kinds of experiments.

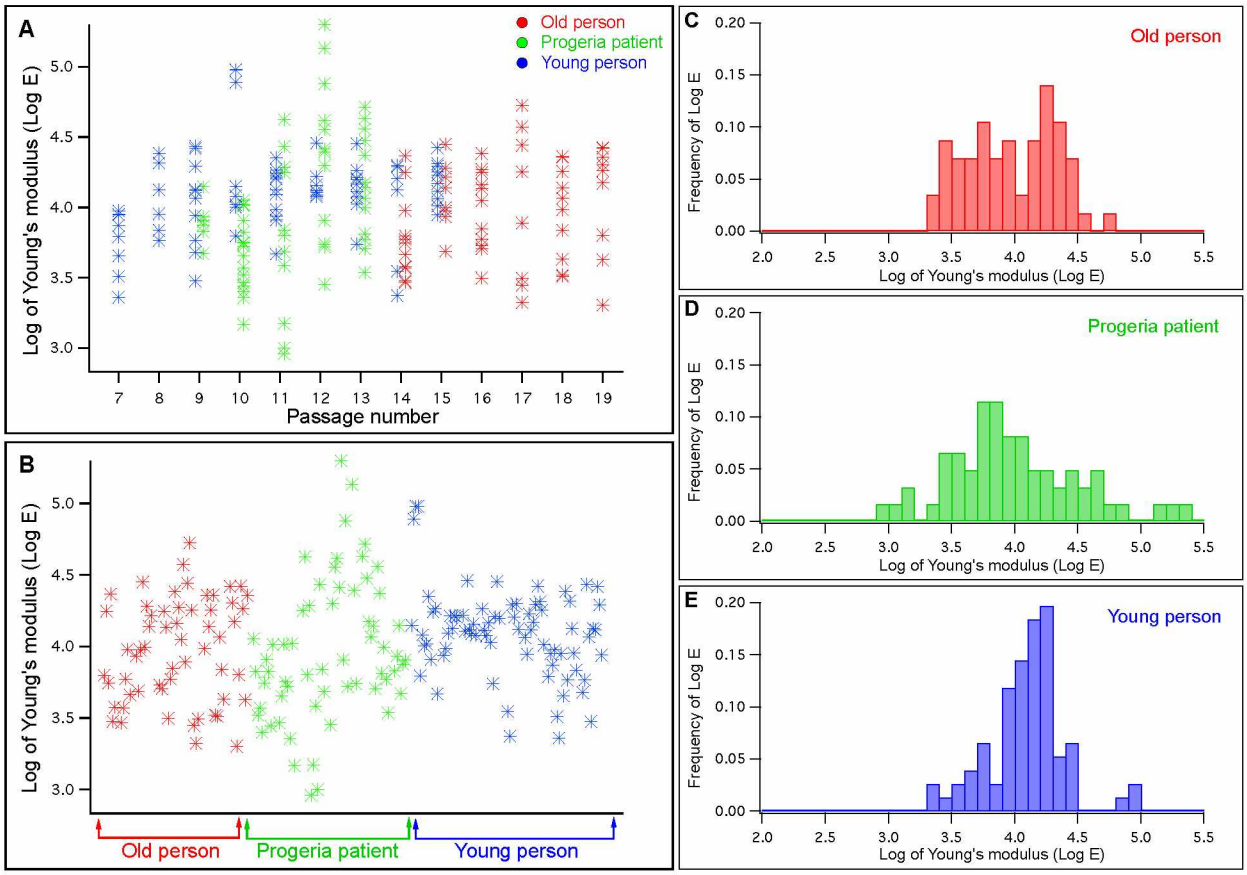

FIGURE 3.6 Mechanical properties of the cytoplasmic region of human dermal fibroblasts. *(A)* Elastic moduli of the cytoplasmic region of fibroblasts are represented as Log E average values plotted against the cell passage number. *(B)* All data points in *(A)* are grouped together according to different cell samples. *(C, D, E)* Histograms showing distribution of the Log E averages for each category of cell sample which is indicated as Old person *(red)*, Progeria patient *(green)* and Young person *(blue)*.

3.4 Visualizing the effect of progeria mutation on dermal fibroblasts

3.4.1 Indirect immunofluorescence microscopy

Dermal fibroblasts from each passage of OP, PP and YP were fixed and processed as described in section 2.1.2). Briefly, cells were fixed with formaldehyde which stabilizes proteins and retains an intact cellular structure. Permeabilization of fixed cells was done using 0.1% Triton X-100. Detection of lamin A was done by indirect immunostaining using the monoclonal antibody JOL2 specific for lamin A, and a polyclonal secondary antibody conjugated with the fluorophore DyLight 488. As shown in the lamin A panel of Figure 3.7, the majority of lamin A is detected at the periphery of the nuclei. The fluorescence of the surrounding cytoplasmic region is caused by channel bleeding of the red fluorescing F-actin which is stained by rhodamine conjugated phalloidin. Phalloidin selectively binds to F-actin, thus allowing recognition of the stress fibre network of a cell. The actin filaments can be readily noted in the actin panel of Figure 3.7. The nuclei were identified by DAPI staining of the chromatin as shown in the DNA panel. Cells from the progeria patient (PP) often show an irregular nuclear shape as it was previously shown by Taimen et al. [26]. Multiple lobulations of the nucleus give it a typical flower-shaped appearance, which is absent in the two control cell samples obtained from an old (OP) and a young person (YP). An altered appearance of chromatin in PP cell nuclei might be due to the irregular nuclear shape. The long intact stress fibers which form the F-actin network are particularly prominent in the YP cells. The actin network of OP cells is similar to that of YP cells. Mild disruptions or occurrence of actin aggregates might be attributed to aging.

In case of the PP cell sample, a reduction in number of the long thick parallel running actin filaments is seen (see Figure 3.8). The filaments are comparatively shorter in length, and the well structured appearance of the actin network is lost. The cells show a higher proportion of actin aggregates as observed for the old person. A reduction in the stress fibers spanning the entire cell could be attributed to alterations in the interaction between cytoplasmic actin and nucleoskeletal elements

probably caused by a defectively assembled lamina comprising of lamin A E145K. This possibility however needs further verification by additional experiments in which other cytoskeletal and nucleoskeletal interaction partners especially LINC complex proteins are analyzed. A faulty lamina assembly caused by lamin A E145K might lead to disturbances in the actin network. The images in the merge panel of the Figure 3.7 are composites of the respective individual images. The signals caused by channel bleeding can be seen in yellow while the lamin signal is shown in cyan. As staining of the different cells samples was done separately, variations in the signal intensities are obtained.

3.4.2 Transmission electron microscopy

Dermal fibroblasts of a progeria patient along with two control samples, one of a young person and other of an old person, were processed for transmission electron microscopy. Transmission electron microscopy (TEM) allows visualization of the sample with a nanometer resolution. The sample is treated with compounds containing heavy metals such as osmium tetroxide and uranyl acetate to obtain an enhanced contrast in the TEM images. Osmium tetroxide acts as a fixative as it reacts with unsaturated lipids of the cell and nuclear membranes resulting in deposition of osmium ions on them. The cationic stain, uranyl acetate can bind to membrane lipids due to affinity of its cationic counterparts to the membrane phospholipids [87]. Both of the elements are heavy metals which impart a higher electron density to the material to which they bind and as a result it appears as electron dense region in the TEM micrographs. In addition uranyl acetate stabilizes the cellular proteins thus protecting the sample from further deterioration during dehydration procedure. The treated cell samples are embedded in an epoxy resin and 50-60 nm ultrathin sections are obtained.

In the Figure 3.9 transmission electron micrographs of the cells obtained from an old person are shown. The nuclei show a normal morphology with smooth nuclear boundaries. Presence of heterochromatin is indicated by arrowheads. The lamina layer is marked by solid red dashes with white boundaries beneath the nuclear membranes which are marked by a solid white bracket. The insets contain images of the entire cells where the magnified area of the panels A and B is marked by open

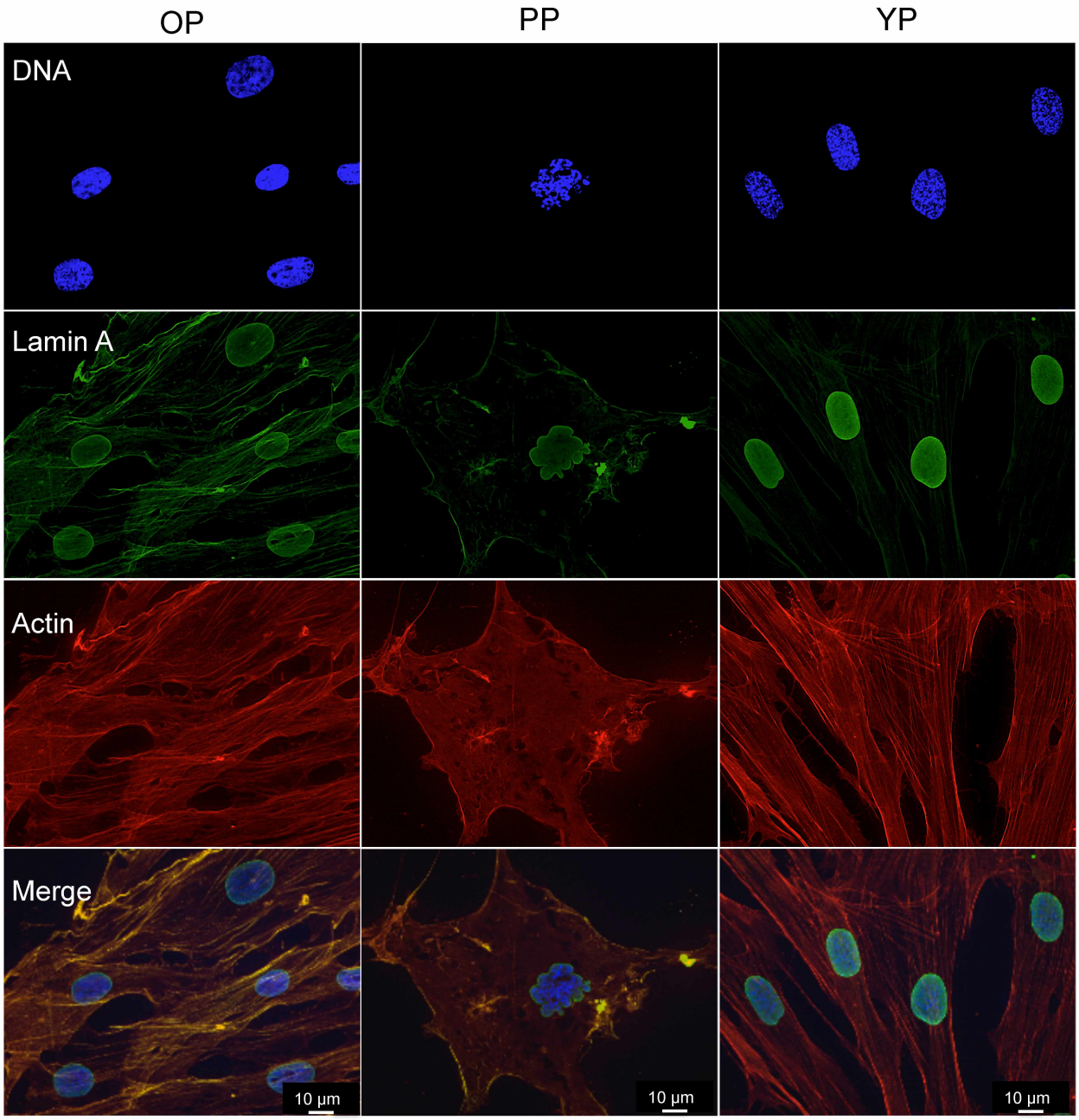

FIGURE 3.7 Lamin A E145K mutation affects the cytoskeleton of dermal fibroblasts. Immunofluorescence microscopy of dermal fibroblasts obtained from OP, PP and YP was done to visualize lamin A, DNA and F-actin network. JOL2, an anti-lamin A monoclonal antibody followed by a DyLight 488 coupled polyclonal antibody was used to detect endogenous lamin A. DAPI staining revealed chromatin and F-actin was visualized by direct staining with rhodamine-phalloidin. Nuclear lobulations due to mutant lamin A E145K are seen in case of the PP cell sample. OP and YP cells were used as controls. Merged images are shown in the panels on the bottom. Scale bars = 10 µm.

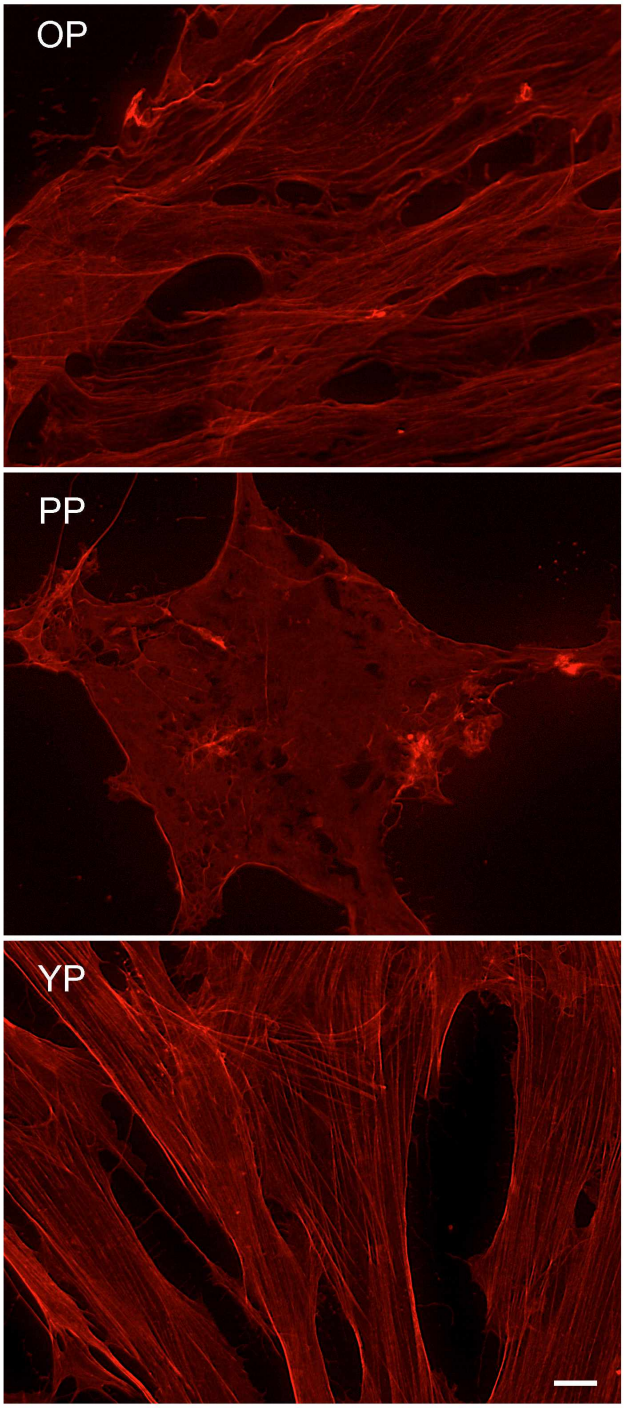

FIGURE 3.8 Actin cytoskeleton of dermal fibroblasts. Immunofluorescence microscopy of dermal fibroblasts obtained from OP, PP and YP was done to visualize F-actin network by a direct staining with rhodamine-phalloidin. Cells of progeria patient show disrupted actin filament network. Scale bar = 10 µm.

white squares. Figure 3.10 shows micrographs of cells of the progeria patient. Cells of the progeria patient have lobulated nuclei unlike the nuclei of the cells obtained from YP and OP (see Figures 3.9 and 3.11 for comparison). Panels A and D in Figure 3.10 show the images of cells taken at a primary magnification of 7000×, where, the shape of the entire nucleus (N) is visible. The panels B and E in the same figure, respectively, show enlarged areas from panels A and D, taken at a primary magnification of 20,000×. In panels C and F, 50,000× primarily magnified images of the regions marked with open white squares in B and E, are shown. The width of the nuclear lamina layer is marked by solid red dashes with white border, beneath the nuclear membranes (NE), while the arrowheads point to the chromatin. The chromatin has a highly contrasted appearance due to the uranyl acetate staining while the lamina appears as a comparatively less contrasted homogenous layer. The thickness of lamina is quite consistent along the inner side of NE. Invaginations or protrusions of the nuclear membrane seem to form due to presence of mutant lamin A E145K as the nuclei of YP and OP do not show such nuclear phenotypes. Moreover, it can be observed that these folded regions contain only the lamina, whereas, no heterochromatin is present in these areas. The nature and extent of lobulation differs from cell to cell. In the Figure 3.10 C, a secluded cytoplasmic region surrounded by nucleoplasmic content and a membrane lined with the lamina is seen. A cytoplasmic region captured between the two nuclear lobules which when cut in transverse direction would appear exactly as seen in the figure. The micrographs of YP cells, in Figure 3.11 show two different cells, both, with normal nuclear morphology. The electron dense dots depicting peripheral chromatin show a typical pattern of distribution with regular intervals beneath the lamina layer which is indicated by solid red dashes with white borders, in both the panels A and B of Figure 3.11. Nuclear pore complexes are shown by black arrows which intercept the nuclear membrane at several points with discontinuation of the lamin layer occurring only at the pore complex region. The TEM analysis of the intact cells thus revealed structural details about the nuclear envelope of the cells obtained from the progeria patient and from healthy persons.

The TEM micrographs of intact cells were also analyzed with a double-blind approach (with the help from Dr. Annette Peter, AG Stick, Institut für Zellbiologie,

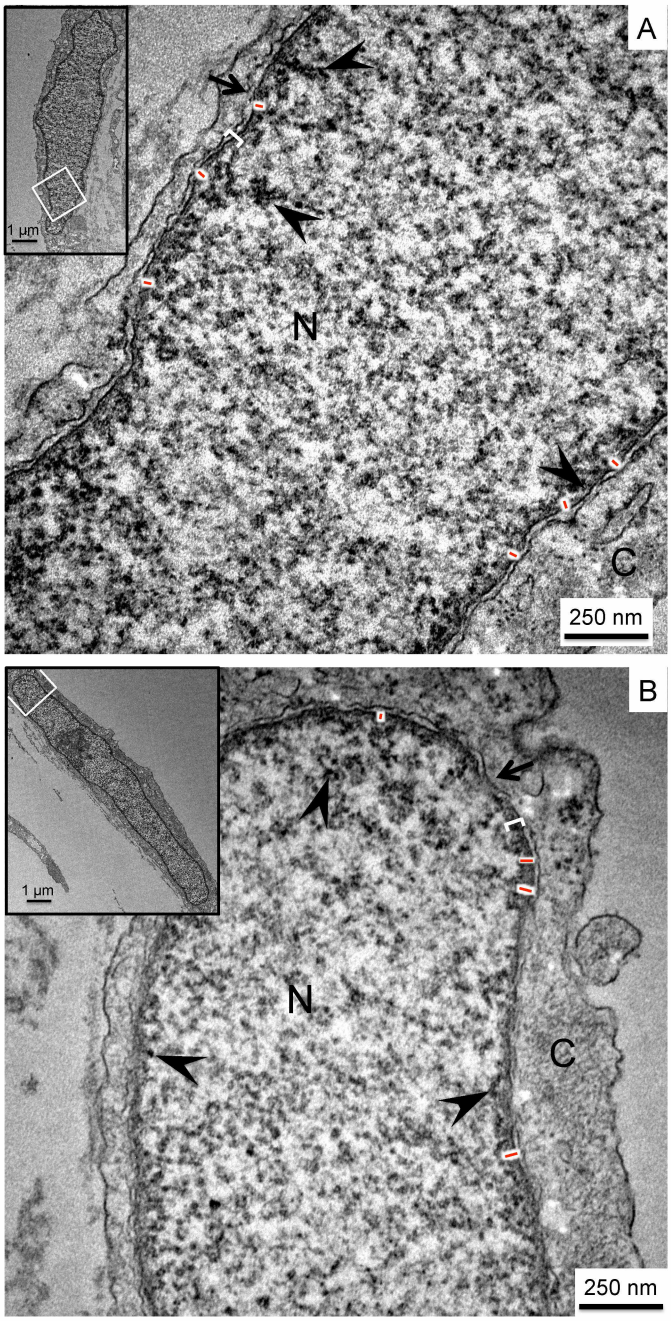

FIGURE 3.9 TEM analysis of dermal fibroblasts obtained from an old person. Dermal fibroblasts were fixed with Karnovsky's fixative and were further processed for transmission electron microscopy. Panels *(A)* and *(B)* show cells of the OP sample at 50,000× primary magnification. Corresponding insets show the images of the entire nuclei inside the cells. The white squares mark the magnified part of the cell. Arrowheads indicate the chromatin and the arrows point to the nuclear pore complex region. The thickness of the lamina layer is marked by solid red dashes with white borders. Solid white brackets indicate the region of nuclear envelope. N = nucleus, C = cytoplasm.

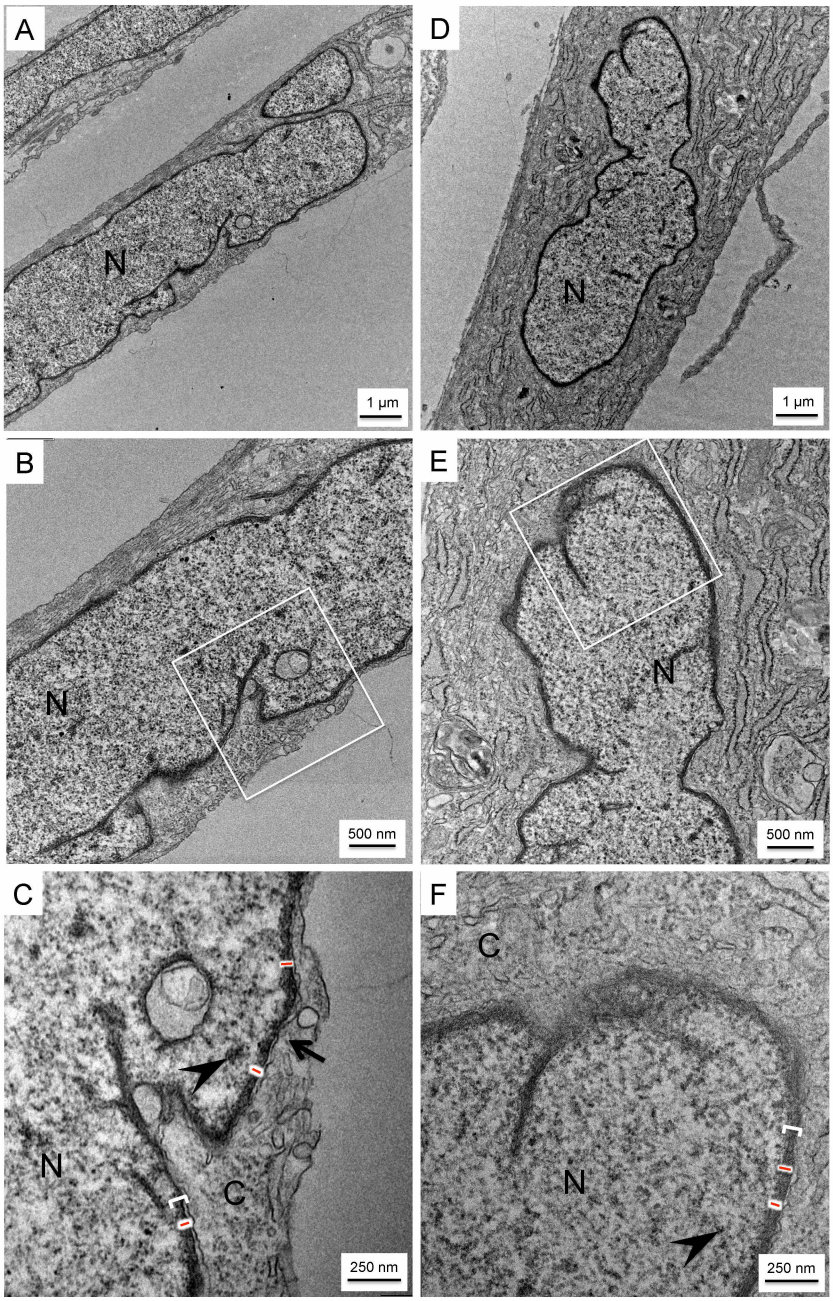

FIGURE 3.10 TEM analysis of dermal fibroblasts obtained from the progeria patient. Dermal fibroblasts were fixed and processed for transmission electron microscopy as mentioned in the section 2.3.3. Panels *(A)* and *(D)* show two typical cells from the progeria patient with severe nuclear lobulations, details of which are shown in panels *(B, C)* and *(E, F)* respectively. The magnified images are from the area marked within open white squares in panels *(A)* and *(D)*. The chromatin is indicated by arrowheads while the width of lamina is shown by solid red dashes with white borders. Position of nuclear pore complex is indicated by solid black arrow. The width of the nuclear envelope (NE) is shown by solid white brackets. N = nucleus, C = cytoplasm.

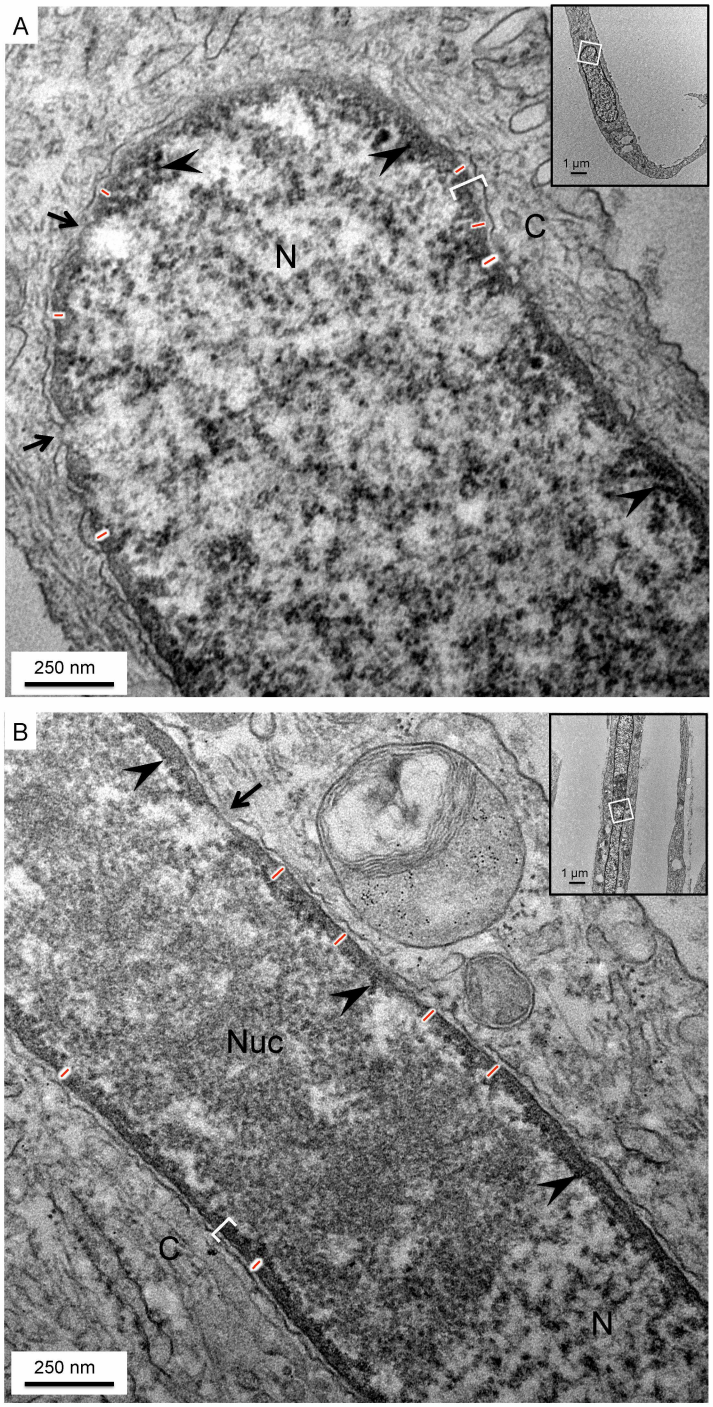

FIGURE 3.11 TEM analysis of dermal fibroblasts obtained from a young person. Dermal fibroblasts were processed for transmission electron microscopy. Panels *(A)* and *(B)* show the cells with normal nuclear morphology obtained from a young healthy person. The insets show entire cells at primary magnification of 7000×. The region of the cells marked with open white squares is primarily 50,000× magnified to create the panels A and B. Refer to description of figure 3.10 for a detailed legend. Nuc = nucleolus.

University of Bremen) to estimate the average thickness of the lamina layer of each cell type (see Figure 3.12). The measurements were obtained from maximum ten nuclei of OP, PP and YP cell samples each. Approximately 300 measurements were noted per nucleus. The average lamina thickness of the nuclei belonging to the cells of the OP sample is 22.9 nm (± 3.3 nm). Lamina of cells obtained from the progeria patient is 19.1 nm (± 2.8 nm) thick while that of the cells from the YP sample is 22 nm (± 2.2 nm) thick. The graph in the Figure 3.12 shows average thickness values *(solid diamonds)* of each nucleus with the error bars showing the standard deviation in the thickness corresponding to each nucleus. Statistical comparison between the lamina thicknesses of OP, PP and YP was done using a modified t test.

For each cell category, upto 10 different nuclei were measured at many regions along the nuclear envelope. Hence, for each category several samples (nuclei) were measured several times (replicate measurements). These replicate measurements are statistically not independent, thus it was not appropriate to pool all measurements of one cell type in one group and test the differences between cell types via a simple t-test. As each lamina thickness measurement in a single nucleus is not an independent value, the degrees of freedom used for comparison were considered according to the number of nuclei (max. 10) and not according to the number of total measurements (max. 3,500) done for one cell category.

As the lamina thickness was measured for individual nuclei, the variation in the measurements belonging to a single nucleus can be considered as an error in the measurement (depicted as error bars in Figure 3.12). For comparing thicknesses of several nuclei, a simple t-test would only consider the standard deviation (sdv) between measurements of different nuclei, but would not take into consideration the error bars shown in the graph (variation of thicknesses within each nucleus). Therefore, a modification was done in the t-test, where the average thickness, the degrees of freedom, and the total error (the sdv between different nuclei (between averages of each nucleus) and the error in the measurements for individual nucleus) were taken into account.

The comparison of the thicknesses of the OP, PP and YP lamina layers shows that the lamina thickness of PP nuclei is slightly reduced possibly due to the presence of E145K progeria mutation. However, the differences in these thickness values are

not statistically highly significant (for details see Appendix B). The nuclei of PP cells can be further subcategorized into two groups, PPa (nucleus no. 1,3,4,5) and PPb (nucleus no. 2,6,7,8), depending on their lamina thickness, but differences in lamina thickness of PPa and PPb are also not highly significant.

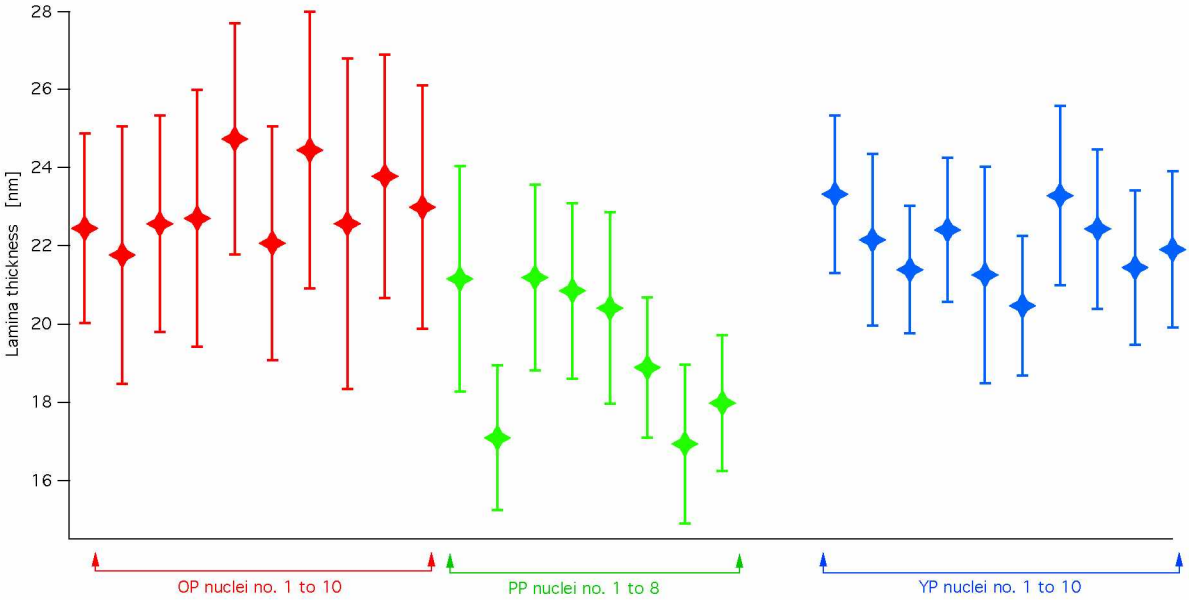

FIGURE 3.12 Lamina thicknesses measured using TEM micrographs. Dermal fibroblasts were processed for transmission electron microscopy. Lamina thickness measurements were done using a double-blind process. The y axis shows thickness measurements obtained from the nuclei of OP *(red)*, PP *(green)* and YP *(blue)* cell samples shown on the x axis. The solid diamonds represent the average thickness of each nucleus, with error bars showing the standard deviation in thickness for each nucleus. No significant differences are seen between the lamina thicknesses of the three cell categories.

3.5 Modification of the actin cytoskeleton

The AFM data obtained using intact cells revealed minor changes in the elastic properties of HeLa cells. The elastic properties of dermal fibroblasts from a progeria patient showed more obvious differences in comparison to those of the healthy donors. The force curves were generated by indentation of cells by either using a pyramidal or a spherical indenter. Optimized cantilever deflection parameters were used to obtain the force curves to avoid rupturing of the intact cell structure. However, the

force curves obtained did not reveal if the expression of the progeria mutant affects mechanical properties of the nuclei or if the observed change in elastic properties is a response due to alterations in the cytoplasm, as actin normally forms an extensive network of filaments around the nucleus. Attempts were made to grow the cells under conditions in which minimal amounts of actin stress fibers are generated (softer cell substrate) or under which actin filaments are disrupted (cytochalasin treatment).

3.5.1 Change of substrate

Cultured cells are routinely grown on hard surfaces such as glass coverslips or on plastic cell culture dishes. The stiff substrate supports the cell attachment and spreading. The cells produce more stress fibers and are thus firmly attached to the surface. In a modified approach, HeLa cells were grown on soft polyacrylamide (PA) gels coated with type I collagen. Collagen is naturally found in the extracellular matrix surrounding the cells in vivo. The collagen coating of PA gels was achieved by cross linking the collagen molecules to the PA gels via N-sulfosuccinimidyl-6-(4'-azido-2'-nitrophenylamino) hexanoate (Sulfo-SANPAH). This chemical cross linker is activated by UV and thus can be used to link specific substrates like collagen to non adherent surfaces like PA gels. The cells were seeded on PA gels coated with collagen and cotransfection experiments were carried out as described under section 3.2.2. The samples for AFM analyses were obtained as mentioned in the same section and force maps were generated using the same type of cantilever with a pyramidal tip. However, these experiments could not be repeated due to various technical problems. The cells adhered well onto the collagen coated PA gels and were successfully grown on them but they either died or showed presence of contaminants at random time points post cotransfection. Neither a consistency in the occurrence of the contaminations nor a specific survival pattern of cotransfected cells could be determined. Thus, only limited amount of AFM data could be obtained. Analysis of the data obtained for the nuclear regions of these cells was done as explained before (see section 3.2.2). The calculated Log E values are represented in a graph in the Figure 3.13. The pattern of changes in elastic moduli of cells expressing

either wild-type lamin A or mutant lamin A E145K resembles the results obtained in previous experiments with HeLa cells. The transfection reagent seems to change the elastic properties of the cells to some extent. Judging the changes occurring in the elastic properties of cells grown on softer substrates based on these observations is difficult, as the number of AFM data is inadequate to draw statistically relevant conclusions.

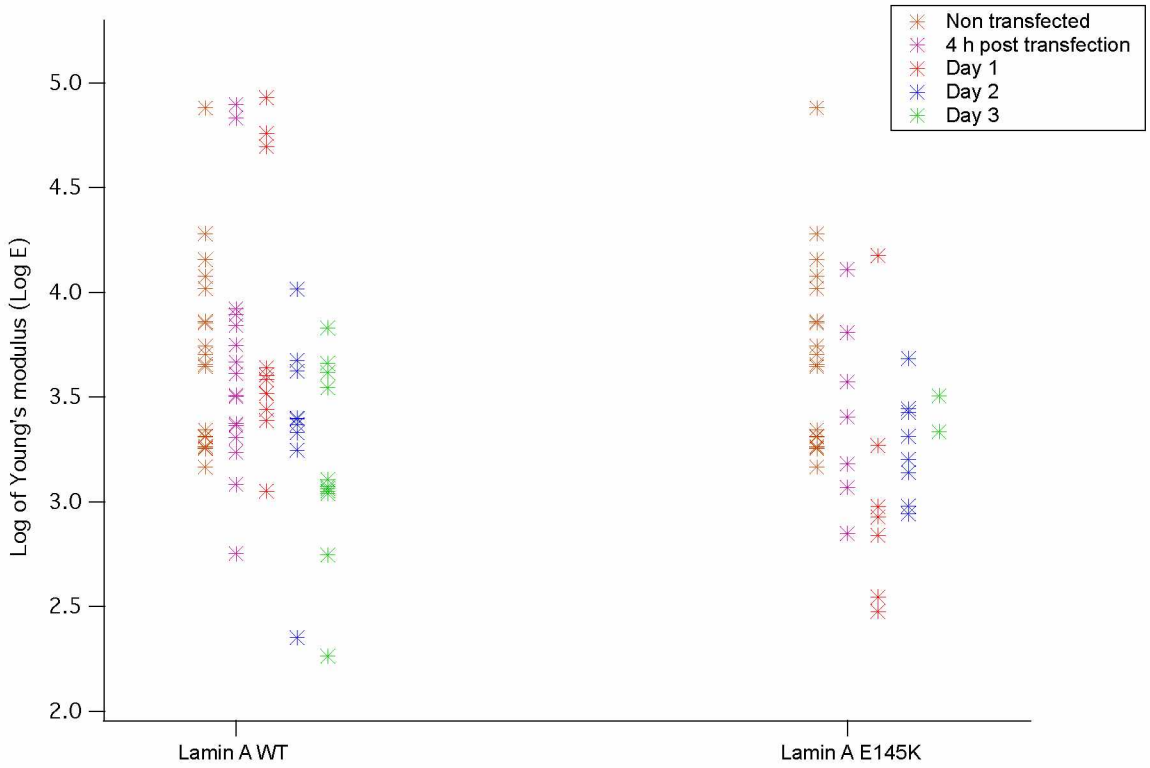

FIGURE 3.13 Elastic moduli of HeLa cells grown on PA gels. The graph represents Log E median values obtained for transiently transfected HeLa cells grown on collagen coated PA gels. Cells expressing either wild-type lamin A or the mutant lamin A E145K were probed using a cantilever ($k_c = 0.010\ N/m$) with a pyramidal tip. Analysis of the data to calculate the Young's modulus of elasticity (E) was done as described before. Due to lack of enough data, statistically relevant conclusions cannot be drawn.

3.5.2 Treatment of cells with cytochalasin B

Cytochalasin B is a toxin widely used in cell culture experiments to inhibit actin filament formation. It is a compound isolated from the fungus *Drechslera dematioidea* which is a known plant pathogen. The drug caps the growing ends of the actin filaments thereby inhibiting their further elongation [88] and thus selectively disrupts the actin cytoskeleton of cells. In this work, HeLa cells were grown on glass coverslips and were subjected to AFM probing to obtain data from normal, untreated cells. Then, to the same cell sample, cytochalasin B was added to a final concentration of 2 µM. Cytochalasin treatment was stopped after 15 minutes by replacing the medium with fresh 10% DMEM. Only a limited number of readings could be recorded for cytochalasin B treated cells as the cells soon started to detach from the glass substrate. This was a technically challenging problem as the floating cells had a tendency to adhere to the cantilever and rendered it unusable for obtaining further readings. Figure 3.14 shows a graph where the acquired readings were analyzed to obtain Log E values for cytochalasin B treated and corresponding untreated HeLa cell samples. The Log E values obtained for cells treated with cytochalasin B are lower than those obtained for untreated HeLa cells meaning that the cytoplasmic actin network adds to the mechanical stiffness of the nuclei. The disruption of actin network is evident from the fluorescence micrographs which are shown in Figure 3.14. The treatment with cytochalasin B disturbs the actin stress fiber network which results into formation of small actin aggregates in cytoplasm as can be inferred from the fluorescence images. In principle, a disruption of actin network allowed direct probing of the nucleus by the pyramidal tip of the cantilever. It was not possible to draw significant conclusions from this single experiment, as an insufficient amount of data could be obtained due to the fast detachment of treated cells from the substrate. A cantilever contaminated with cells would generate errors in the resulting force curves which in turn would hamper calculation of the elastic moduli of the sample and thus additional experiments were not carried out using this approach.

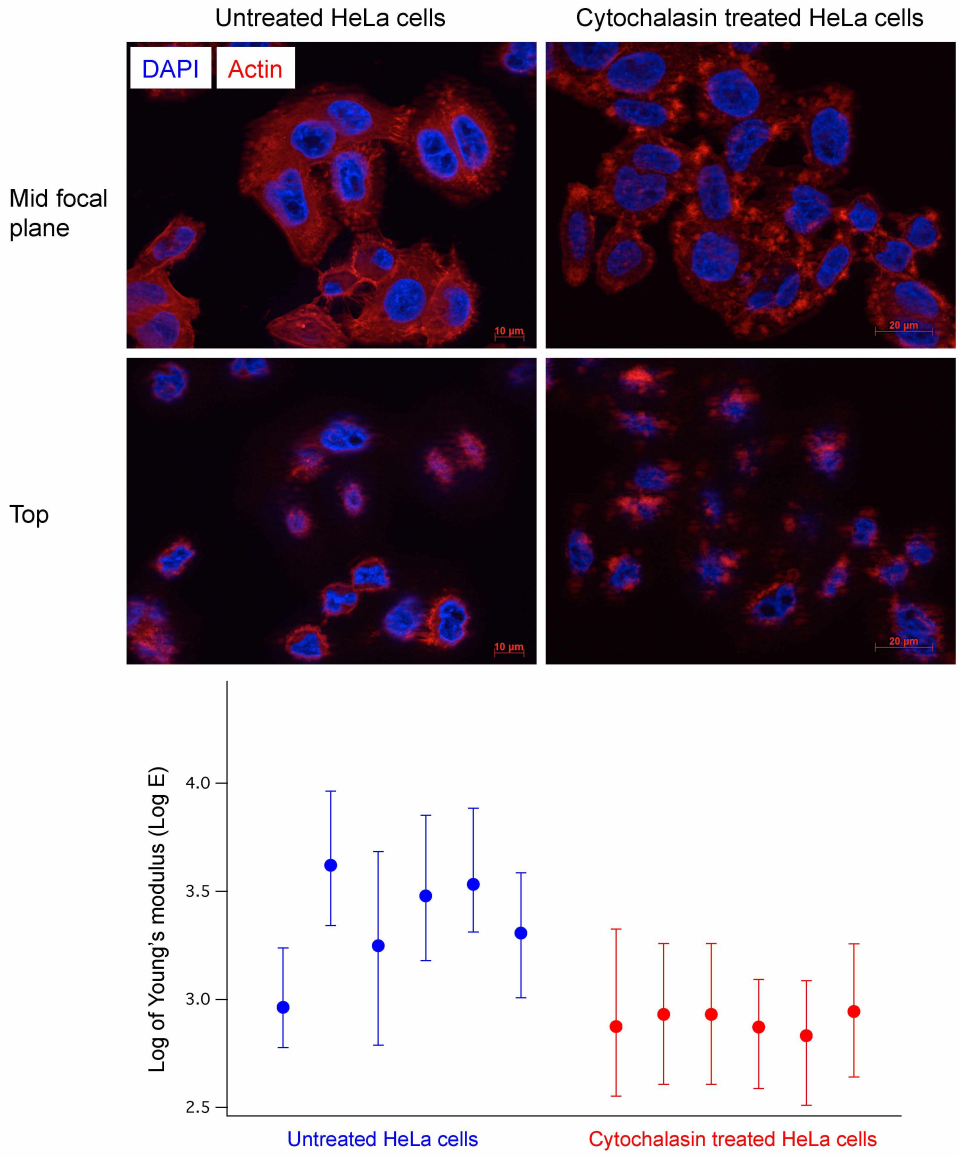

FIGURE 3.14 Cytochalasin B treatment of HeLa cells. Actin microfilament network in HeLa cells grown on glass coverslips was disrupted by incubation of the cells with 2 µM cytochalasin B for 15 minutes. Cells were fixed and stained for immunofluorescence microscopy using DAPI for detecting chromatin *(blue)* and rhodamine-phalloidin for F-actin visualization *(red)*. The optical sections obtained by ApoTome show intact network of F-actin in untreated cells versus the disrupted F-actin network in cytochalasin B treated cells indicated by presence of several aggregates in the cytoplasm. Prior to fixing and immunostaining of the cells, force curves were recorded on the living cells before and after cytochalasin B treatment. Elastic moduli and corresponding Log E values were determined as described before. Significant conclusions cannot be drawn due to presence of limited data obtained for cytochalasin B treated cells. Error bars indicate $25th$ and $75th$ percentiles of the data.

3.6 Mechanics of nuclei isolated from dermal fibroblasts

Several attempts were done to measure the stiffness of nuclei without disturbing the intact cellular structure. Using this approach, some differences in elastic moduli were obtained but it was unclear if the measured mechanical responses are an answer of the indentation of the nuclei surrounded by cytoplasm or originated from the cytoskeletal elements covering the nucleus. Further trials were then carried out to record the mechanical properties of nuclei still residing in the cells, but in a surrounding of a disrupted cytoskeleton or with a less amount of stress fibers around the nucleus. These attempts were unsuccessful due to various technical problems. To specifically determine the nuclear stiffness, isolation of the nuclei from dermal fibroblasts was thus inevitable.

For the isolation of nuclei, cells were first incubated in a hypotonic solution which caused severe swelling of cells especially on the peripheral regions due to changes in the osmotic pressure (see Figure 2.1). This was followed by a treatment with a detergent to remove the membranes. Gentle resuspension of cells separated the nuclei from the cytosolic components as judged by phase contrast microscopy of the nuclear suspension. The nuclei were allowed to settle on a clean plastic cell culture dish and were then used for recording force curves by AFM. Only clean nuclei to which no cell debris was attached were used for measurements. Nuclei were indented to a very small extent by using low loading forces. Force maps were generated over an area of 1 μm^2. Multiple readings were recorded over the surface of a single nucleus, to fairly estimate the elastic moduli of entire nucleus. A sole reading over an area of only 1 μm^2 on a nucleus with an average diameter of 15 µm would not include the changes in stiffness caused by local variations on the entire nuclear surface. For example, nuclei isolated from cells of a progeria patient, which retained their lobulated shape even after isolation (for images, see Appendix A.5), might show differences in their mechanical properties between a plain nuclear region and a region where two lobules meet. At least 10 nuclei from each passage of cells from OP, PP or YP were used to obtain force maps. The resultant shape of the force curves was different than the curves obtained using entire cells. The force curves

generated on isolated nuclei are comprised of a linear region and a curved region (see Figure 2.10). According to the elastic shell model used to calculate the stiffness of a thin elastic shell indented by a point force, a linear correlation is seen between the sample indentation and the corresponding change in deflection. Hence data analysis was restricted to the linear part of the force curves as an isolated nucleus is considered as a thin elastic shell. The stiffness of the nucleus is expressed in terms of its spring constant k_n.

Figure 3.15 A shows a graph where the Log k_n values of different nuclei belonging to cell samples obtained from either OP, PP or YP are plotted on the y axis against corresponding passage numbers of the samples on the x axis. The Log k_n values are negative because the spring constant values obtained for isolated nuclei lie in the range of several µN/m. This indicates that the nuclei in general appear as a very soft material when probed with a cantilever with a pyramid shaped tip. The stiffness of nuclei does not change with successive passage numbers. The same data corresponding to the individual groups of cells are shown in panel B, which shows that the nuclei of dermal fibroblasts from the progeria patient are stiffer than those of the young healthy person. The comparison between stiffnesses can be visualized better in the histograms shown in panels C, D and E. The frequencies of Log k_n values are plotted for the respective samples. As mentioned before, the spring constant values of nuclei are very low and hence negative Log k_n values are obtained. A higher variation in the data is seen for stiffness values of OP nuclei as the peak is much flatter and broader than that shown for the Log k_n values obtained for nuclei from the young person. The nuclei isolated from PP cells show a Log k_n peak at around -3.2 while the peak for YP is at around -3.7. Note that a change from value of -4 to -3 indicates a 10 fold increase in stiffness. The increase in the stiffness of nuclei obtained from the progeria patient is attributed to presence of mutant lamin A E145K in the nuclear lamina. This difference is statistically highly significant ($p = 0$). The nuclei of OP cells are also stiffer than those from the YP cells ($p \leq 0.0005$). The treatment of the cells with a detergent resulted into removal of cell membranes which was evident even under the light microscope as the cells became more translucent and nuclei were more clearly visible in detergent treated samples. But if this treatment also removed nuclear membranes or not,

had to be confirmed as the nuclei maintained their shape after isolation from the cells and during AFM experiments. It is known that unlike membranes, lamins cannot be extracted from filaments by detergent treatment [89], [90]. Thus the possibility that, in absence of membranes only the lamina keeps these nuclei intact, needed a verification. The samples of isolated nuclei were processed for analysis by transmission electron microscopy to visualize the structure of the nuclear envelope in detail.

3.6.1 Transmission electron microscopy of isolated nuclei

TEM analysis could be carried out only for nuclei isolated from YP, as the number of nuclei that could be isolated from the cells of PP and OP was not sufficient considering the sample losses that occur at each step of isolation and processing for TEM analysis. This analysis was also done to demonstrate the efficiency of removal of cytosolic fractions which might adhere to the nuclei and thus affect the AFM data acquisition. Figure 3.16 displays the TEM micrographs of the nuclei (N) isolated from YP cells from passage numbers 15, 18 and 19. The isolation procedure was carried out at three different times with different cell samples to confirm the reproducibility of the isolation procedure. As shown in the figure, nuclei almost free of cytosolic remnants, were obtained in all three isolation experiments. The isolated nuclei exhibit some irregularities in their shapes which can be attributed to the handling of the samples during sample preparation for TEM analysis. The samples although priorly fixed, are subjected to treatment with chemicals followed by subsequent dehydration steps done using increasing percentages of alcohol. The detergent treatment in the isolation procedure extracts the nuclear contents and hence, only residual amounts of nucleoplasmic components remain inside the nuclei. Figure 3.17 shows an image of the periphery of an isolated nucleus at a primary magnification of 30,000×. The corresponding entire nucleus is shown in the inset on the upper left side in which the area marked by an open white square is shown in the magnified image. Inside the nucleus (N), arrowheads indicate the chromatin which has a highly contrasted dotted appearance. The red brackets mark the lamina layer forming the boundary of nucleus.The lamina layer is less contrasted in comparison to

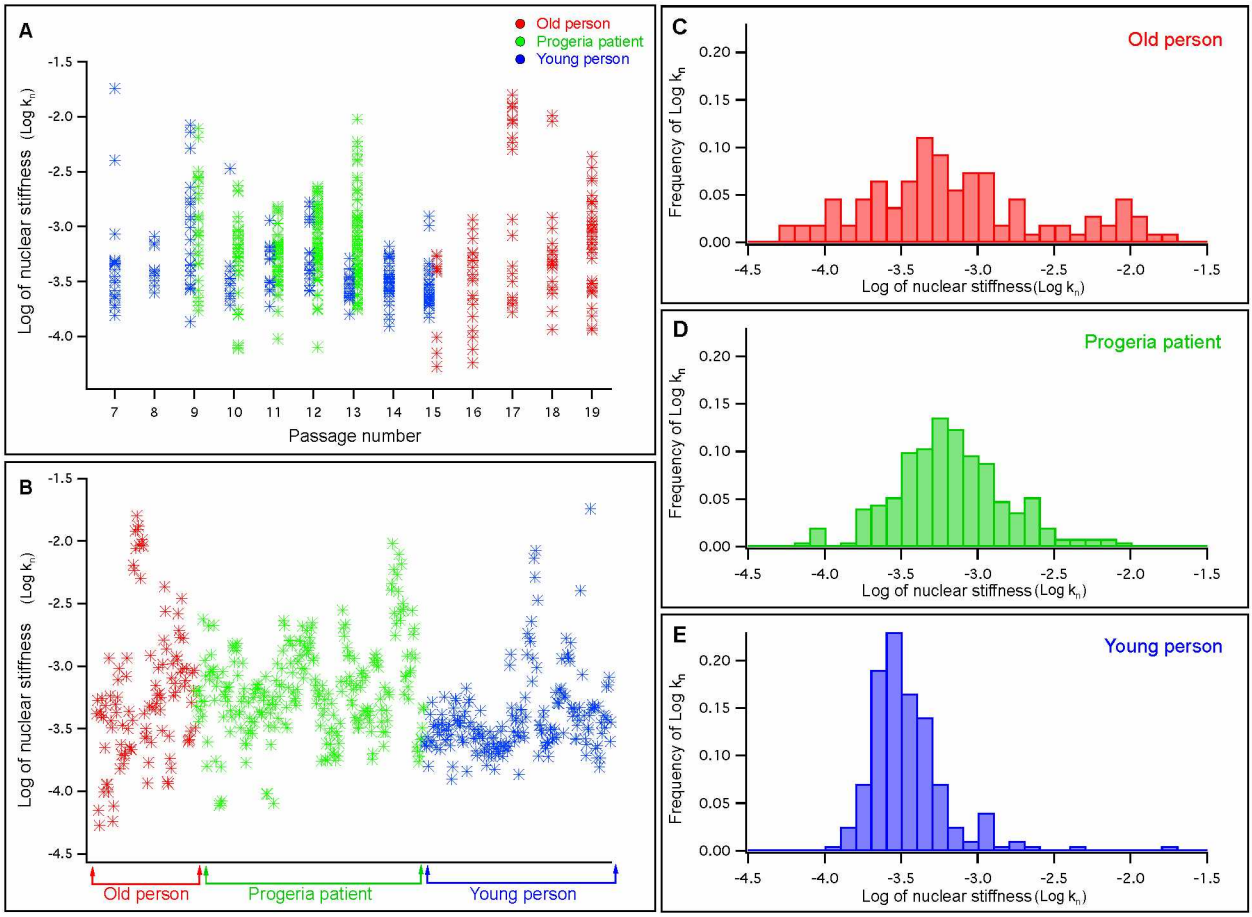

FIGURE 3.15 Stiffness of the nuclei isolated from human dermal fibroblasts. The mechanical properties of isolated nuclei were assessed using a cantilever ($k_c = 0.015$ N/m) with a pyramidal tip. The force maps were obtained using very small loading forces. Stiffness (k_n) was calculated according to the shell model as the isolated nucleus is considered as a thin elastic shell. At least ten nuclei were examined for every passage of each cell sample. Multiple readings were obtained on different regions of individual nuclei. This was done in order to fairly estimate the stiffness of entire nuclear surface rather than relying on sole set of force curves obtained on a single point. *(A)* Each point in the graph depicts the median of Log k_n value obtained for each force volume. The samples are indicated with the same color code as indicated before. *(B)* The same data points are represented in a group irrespective of cell passage numbers. *(C, D, E)* The histograms show frequency and data distribution of Log k_n of nuclei isolated from cells belonging to respective donors.

the black colored chromatin. Absence of nuclear membranes is strikingly noticeable but the remnants of a nuclear pore complex can be seen as indicated by an arrow. The nuclei seem to maintain their integrity upon removal of membranes because of the presence of the lamina. This implies that the AFM force curves that were obtained from isolated nuclei are an elastic response of the lamina layer. As the contents of nuclei seem to be heavily removed, the isolated nucleus truly behaves as a thin elastic shell and hence analysis of the corresponding AFM data by the elastic shell model is clearly justified.

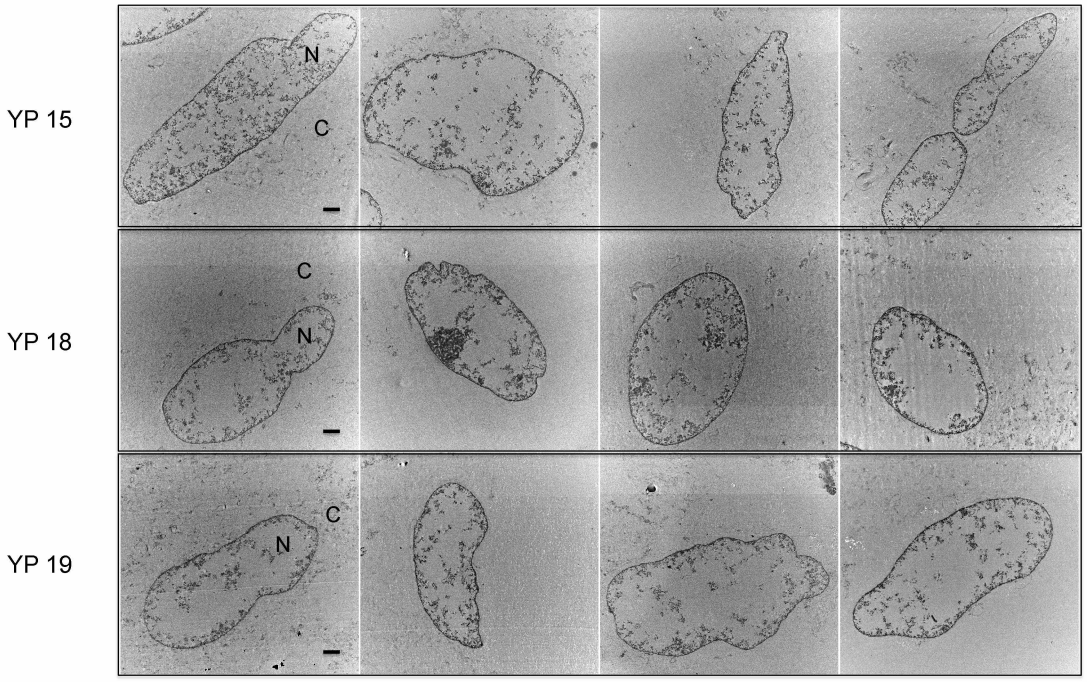

FIGURE 3.16 TEM analysis of nuclei isolated from dermal fibroblasts. The nuclei of dermal fibroblasts were isolated using a hypotonic solution and a detergent. They were fixed in suspension using Karnovsky's fixative prior to embedding in 2% agar. Small pieces of agar containing the nuclei were subjected to subsequent dehydration steps followed by embedding in epoxy resin. Sections of 60 nm thickness were used to obtain high resolution images of nuclei to demonstrate the efficiency of the isolation procedure. Three independent isolation and embedding procedures were carried out using the cells from three different passages of a young person as indicated on the left. Irregularities in the nuclear shape are seen because of extensive handling and exposure to various chemicals used during sample preparation for TEM. N = nucleus, C = cytoplasmic side, Scale bars = 1 µm.

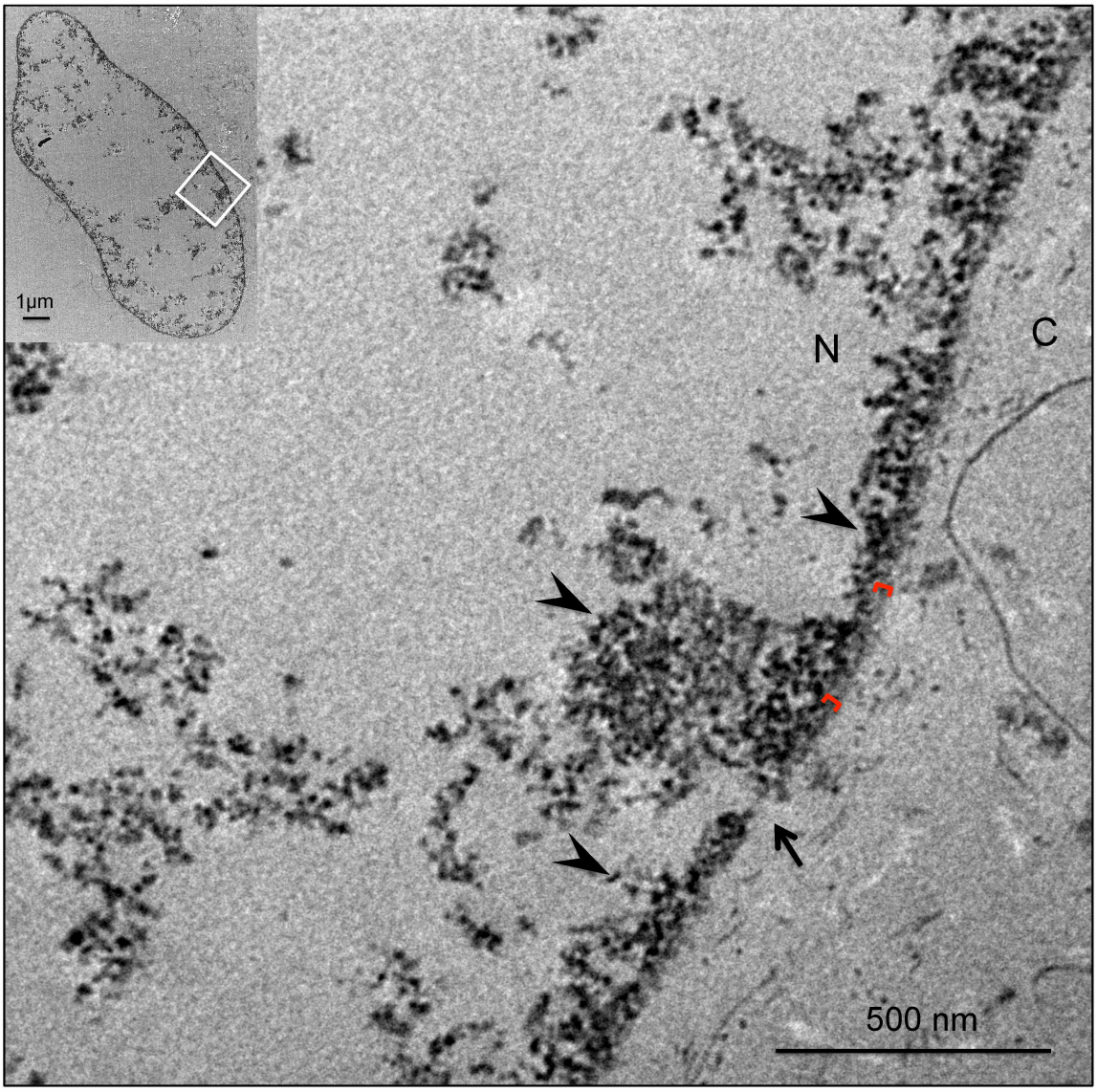

FIGURE 3.17 Transmission electron micrograph of the nuclear periphery of an isolated nucleus. Nuclei isolated from dermal fibroblasts were processed for TEM analysis. A micrograph obtained at the primary magnification of 30,000× reveals absence of nuclear membranes due to detergent treatment done during isolation procedure. The nuclear lamina is intact (*red brackets*) but heavy extraction of nucleoplasmic contents is evident. Chromatin can be recognized mainly along the inner face of the nuclear periphery as highly contrasted dotted structure (*arrowheads*) in comparison to the less contrasted, grey layer of lamina. Remnants of a nuclear pore complex are marked by an arrow. The inset shows the isolated nucleus from which the enlarged area (*open white square*) is shown in this figure. N = nucleus, C = cytoplasmic side.

4

Discussion

Atomic force microscopy has been developed over the past two decades as a diagnostic as well as an analytical tool, to study mechanical properties of various types of cells like human fibroblasts, platelets, myocytes, endothelial cells and cancer cells. It allows judgement of the local mechanical properties of individual cells and fluctuations caused in them, due to various physiological, mechanical or chemical stimuli [69], [71], [68]. The mechanical properties of cells can be determined by recording arrays of force curves i.e. force maps, which are generated by indentation of living cells under near-physiological conditions. Cell membranes and organelles including the nucleus, undergo continuous modifications during cell migration, proliferation and even in diseased conditions which alter their biomechanical properties. Although aging is not a disease, it is a complex process where the mechanical properties of cells undergo alterations. Aging is a natural phenomenon encountered by every human being where changes in physical appearance are readily seen due to the changes occurring at cellular and molecular levels. In a recent AFM study, reported by Zahn et al. (2011), the stiffness of skin fibroblasts was found to be dependent on the donor's age [91]. Probing of the cells obtained from healthy donors of different age groups revealed a significant decrease in the cellular stiffness as a function of the increasing age. The mechanics of the cells were also found to be dependent on the amount of total actin in the cell [91]. In another study, laser-based optical stretchers were used to determine viscoelastic properties of dermal fibroblasts grown in suspension [92]. This study reported observations contradictory to those shown by Zahn et al.

(2011). The stiffness of cells was shown to increase with an increase in the age. Such a discrepancy could be due to differences in the techniques or due to assumptions used for estimation of elastic moduli. The apparent stiffness of cells is also dependent on the morphology of the cells as the cytoskeletal protein composition of cells grown in suspension [92] differs dramatically from those grown on hard substrates [91].

Besides natural aging, there exist a few premature aging disorders like the Hutchinson-Gilford proegria syndrome (HGPS), atypical Werner's syndrome and restrictive dermopathy. These diseases are either hereditary or arise due to de novo mutations in the *LMNA* gene. HGPS is one of the premature aging disorders, which in most of the cases is caused by generation of a cryptic splice site in the *LMNA* gene, which leads to an alternative splicing of the lamin A mRNA. As a result, a lamin A protein, shorter by 50 amino acid residues, is generated which permanently retains its farnesyl moiety [10]. This mutant is called LAΔ50 or progerin. Accumulation of progerin at the nuclear periphery is shown to be the primary cause of disease development. The fibroblasts obtained from HGPS patients exhibit nuclei having abnormal shapes with severe lobulations [25]. Presence of progerin in the cell samples of healthy individuals (age group: newborn child to 97 years old) has been observed by McClintock and coworkers [93]. They showed that although the progerin mRNA transcripts were present at low levels in all the samples, age dependent increase in the accumulation of progerin was observed indicating an important role of progerin in natural cellular aging [93].

Out of several known mutations causing progeroid syndromes, the lamin A mutation E145K was shown to cause HGPS [23]. Introduction of the corresponding progeria mutation Q159K in the *Caenorhabditis elegans* lamin (Ce-lamin), was shown to severely affect hypodermal tissue in the nematodes. Ce-lamin is a B-type lamin encoded by the single lamin gene *lmn-1* of the nematode. So far, it is the only lamin for which in vitro 10 nm thick filament assembly has been shown under specifically buffered conditions [50], [94]. Attempts for assembling Ce-lamin Q159K mutant in vitro, revealed that this mutant lamin forms filaments and paracrystals which differ in appearance from those formed by wild-type Ce-lamin. The "striped" appearance of mutant Ce-lamin filaments is attributed to defects caused in the lateral interaction of head to tail fibrils made up of Ce-lamin Q159K mutant [95]. Dermal fibroblasts

obtained from the progeria patient bearing lamin A E145K show abnormally shaped nuclei with severely disturbed chromatin organization. These cells also showed less proliferative capacity and increased senescence [26]. In addition, the ability of this mutant human lamin A to form filaments and further assembly into the lamin meshwork was assessed in vitro. The wild-type lamin A assembled into well structured paracrystalline arrays while the dimers of the E145K mutant lamin A formed fibrous strands which assembled into globular structures indicating defects in lateral association of lamin filaments [26]. A defectively assembled meshwork of lamin A, thus, might affect interactions between A- and B-type lamin filaments which, in turn, could change the mechanical properties of the lamina. Micropipette aspiration experiments carried out using *Xenopus* oocyte nuclei have shown that the oocyte lamina acts as a molecular shock absorber [30]. This indicates that the lamin meshwork underlying the nuclear membranes is responsible for maintaining the integrity of the nuclei, and alterations in the lamina layer might affect their mechanical stability.

The mechanical properties of the *Xenopus* oocyte nuclei have been well studied using atomic force microscopy [72], [47]. A large size of the oocyte nucleus allows easy handling and manipulation of the isolated nuclei. As the endogenous lamin LIII, the B-type lamin of oocyte nuclei, forms very thin lamina layer and as the chromatin is not attached to it, mechanical contribution of overexpressed lamins can be assessed by probing the isolated nuclei by AFM. The stiffness of the oocyte nuclei was shown to increase due to the overexpressed wild-type lamin A, which formed very thick lamina layer beneath the oocyte nuclear membranes [72]. As reported by Kaufmann et al., ex vivo expression of the lamin A E145K resulted into changes in the mechanics of the *Xenopus* oocyte nuclei as revealed by AFM probing. The nuclear lamina was visualized in transmission electron micrographs. Although the wild-type and the E145K mutant lamin A, both, could form thick lamin layers, the filaments made up of lamin A E145K created a stiffer lamina of same thickness in comparison to that formed by wild-type lamin A [47].

Although the results of Kaufmann et al. [47] clearly showed that mechanical properties of the nuclear lamina are altered due to the progeria mutation, similar experiments with human cells were necessary [47]. The fact that the amphibian

oocytes are non somatic cells with their nuclei being a specialized system, makes them a heterologous sample to study effects of a human laminopathic mutation. Properties of dermal fibroblasts obtained from a progeria patient were thus analyzed in this work. The elastic properties of the cells were determined with the help of the atomic force microscopy. As the primary fibroblasts of the progeria patient can not be maintained in culture over a long time period due to their reduced proliferative capacity, pilot experiments were carried out using HeLa cells to optimize AFM data acquisition and analysis methods. Acquisition of AFM data was done using cantilever having a pyramidal tip. Intact cells grown on glass coverslips were used for recording the force curves. As the mechanical properties of the nuclei were of interest, data analysis of HeLa cells was restricted to the nuclear regions on the basis of sample height recorded in the force curves.

4.1 Determination of the nuclear stiffness using adherent cells

The wild-type or mutant lamin A E145K were ectopically expressed by transiently transfected HeLa cells. As these ectopically expressed lamins were untagged, coexpression of eGFP was used as an indicator of successful expression of lamin A and only those cells were used for recording the AFM data. The success of protein coexpression from two separate plasmids was verified beforehand using plasmids encoding Flag tagged *Xenopus* lamin A and eGFP (see Appendix A.1). Previous attempts to express a GFP tagged mutant lamin A in the HeLa cells made by Taimen et al. (2009) were unsuccessful as the development of the disease phenotype could not be seen upon expression of the GFP tagged lamin A E145K. This could be attributed to the large size of the eGFP tag (~27 kDa) which might interfere in the dimerization and further assembly processes of lamins [26]. Hence, GFP tagged human lamin A proteins were not used in this work. Use of an untagged lamin A also allowed determination of the mechanical properties of the lamina layer that was formed without any influence of the protein tag sequence on filament assembly. The force curves were analyzed using the Hertz-Sneddon model [71] and Young's

modulus of elasticity (E) was calculated as a measure of stiffness. Logarithm of elastic moduli (Log E) is used for comparison of different datasets in all the graphs shown in results section.

The mechanical properties of non transfected and mock transfected HeLa cells do not change over the time span of the experimental period. The mock transfected cells show a minor decrease in the overall elastic moduli, which could be because of presence of the transfection reagent, but this difference is statistically not significant. A similar trend is seen also with the samples assessed four hours post transfection in case of the AFM probing of HeLa cells done by a tip with a different geometry (glass bead). The changes observed in the elastic moduli of transfected cells, thus, can be considered to occur due to the ectopically expressed wild-type or mutant lamin A proteins.

The stiffnesses of the nuclear regions of the cells expressing wild-type lamin A versus the cells expressing the mutant lamin A E145K differ significantly only on day one. The elastic moduli for both the cell samples on day 2 and 3 do not show significant changes. A similar trend of changes in the elastic moduli values is observed when the cells were probed with a glass bead. The elastic moduli of the nuclear region of the HeLa cells range from 0.6-7 kPa (Log E range 2.7 to 3.8) when the AFM probing is done by a pyramid shaped indenter. The corresponding elastic moduli appear to be reduced by a factor of 10 (range 50-500 Pa, i.e., corresponding Log E range 1.7 to 2.7) when cells expressing wild-type or mutant lamin A are probed using a glass bead with a diameter of 7 µm. Differences in apparent elastic moduli are seen due to the variation in the tip geometry. A glass bead has a relatively larger surface area that comes in contact with the underlying cell sample in comparison with the area of a pyramidal tip which can be considered as a point force. The amount of force exerted by a point force is larger than the same generated by a tip with relatively larger surface area as the force is distributed over a larger region of the same sample. Hence, the indentation by a point force estimates stiffer mechanical responses of the cells in comparison to the glass beads. The AFM indenters having different geometries, however, revealed similar trends in the day wise changes in the elastic properties of HeLa cells expressing either wild-type or mutant lamin A. To use the glass bead as an indenter, an additional step of gluing it to the cantilever with

a pyramidal tip was required. As the gluing procedure introduces amount of glue on the cantilever as an additional variable, all further AFM readings were obtained using commercially available cantilevers with pyramidal tips. The nuclear region of cells was determined from the force volumes obtained on the cells with the aid of phase contrast images obtained while probing the cells. From the total recorded height of the cell, a rough height range for nuclear region could be estimated which was often a distance in the range of 500 nm - 1 µm below the top most point of the cell. The analysis of transmission electron micrographs of ultrathin sections of cells obtained from the progeria patient (PP), the young person (YP) and the old person (OP) corroborate the estimates done for position of nucleus beneath the cell cytoplasm (for details see Appendix A.4).

The AFM data were recorded for a variable number of successive passages as the cells were obtained at different starting passage numbers from the repository. The elastic moduli of the nuclear regions of OP (total 6 passages), YP (total 9 passages) and PP (total 5 passages) cells do not show any dependence on the increasing passage numbers. Consideration of the Log E values from several passages of one cell sample is thus justified for the comparison of elastic moduli values between the three cell samples. The comparison of all the elastic moduli values reveals that the nuclear regions of the cells of OP and PP are softer than those of the cells obtained from YP, although this difference in the elastic moduli has low statistical significance. To verify if AFM probing of intact cells indeed measures the elastic response from underlying nucleus or not, analysis of only the cytoplasmic areas of cells excluding the nuclear region was done. To this end, the same set of force volumes obtained from the dermal fibroblast samples were reanalyzed.

The comparison of the elastic moduli of the cytoplasmic regions of three different dermal fibroblast samples obtained from OP, PP and YP reveals differences with a low statistical significance. The cells of a young person have cytoplasmic elements with stiffer mechanical properties than those of an old person or a progeria patient. However, these age dependent changes in the cytoplasmic elastic moduli are remarkably similar to the trend seen in case of the elastic moduli of the nuclear regions of the corresponding samples. Some of the studies, however, have shown the nuclei exhibit different mechanical properties than the corresponding viscous cytoplasmic

components. Compression of intact endothelial cells between glass microplates has revealed that cytoplasm shows elastic moduli in the range of 500 Pa, while the nuclei have their elastic moduli in the range of 5-8 KPa [67]. In contrast, AFM studies using cardiomyocytes and adherent endothelial cells of bovine pulmonary artery have revealed that the nuclear region of these cells is softer compared to the stiffer peripheral region [96], [97]. Such contradictory observations arise due to differences in the cell morphology and techniques used for estimation of the elastic moduli. Microplates were used for compression of rounded cells which have different cytoskeletal composition than that of the adherent cells. In addition, changes in the size and shape of the indenters and underlying cell samples, also demand for different set of assumptions about material properties and appropriate use of theoretical models (for example, Hertz model, Elastic shell model, Finite element model etc.) used to analyze the data.

In this work, the shape of the fibroblast nuclei was visualized by detection of lamin A using indirect immunofluorescence microscopy. Lamin A was found to be localized mostly in the peripheral regions beneath the nuclear membrane along with the presence of a nucleoplasmic fraction. Such a distribution pattern of lamin A within the nucleus has been reported previously [84], [85]. The nuclei of PP cells show typical flower shaped appearance instead of a smooth oval/round shape. Such an alteration in the nuclear appearance has been previously reported by Taimen and coworkers [26], where severe lobulations in the nuclei were shown to arise post mitotically. Mutant lamin A E145K creates defects in the filament assembly and this progeria mutation is known to heavily affect the chromatin distribution [26]. Several laminopathic mutations affect the interactions between lamins and INM proteins which in turn interact with their cytoplasmic interaction partners (for review see [57]). LINC complex proteins are shown to connect the lamins on nucleoplasmic side [56] and with actomyosin network on the cytoplasmic side [98]. Mutations in the *LMNA* gene that are responsible for causing various types of laminopathies have been shown to disrupt the interaction between LINC complex proteins like nesprin-2 and lamin A [58]. A myopathic mutation in lamin A has been recently reported to disrupt the interaction between cytoskeletal and nucleoskeletal components [59].

Besides AFM probing of intact cells, the structural status of the cytoplasmic

microfilament network of the dermal fibroblasts was assessed by direct immunofluorescence staining of the F-actin. The actin filament network in the PP cells is moderately disrupted while that from OP cells is mildly affected. In contrast, the F-actin network in YP cells is well organized with several parallel stress fibers spanning the entire cell. The disruption of the actin cytoskeleton could be attributed to alterations caused by the mutation E145K in lamin A protein. As shown by Taimen et al. [26], the lamin A E145K dimers assembled laterally to form a fibrous meshwork which lead to formation of irregular paracrystal arrays in vitro. Assuming the occurrence of such a faulty assembly of lamins in vivo, the linkage between lamina and its binding partners (which eventually interact with the cytoskeletal elements) might be affected.

The mechanical properties of the cell body, however, are not only defined by F-actin but also by the networks formed by different types of IFs (for example vimentin, keratin) which play a key role in determining the mechanical response of the cytoplasm [55], [99], [82], [100]. The fibroblasts are derived from the connective tissue present in the dermal layer of the skin, which is of mesenchymal origin. They are shown to predominantly express vimentin which reflects their mesodermal origin [101]. The fibroblasts obtained from vimentin$^{-}/^{-}$ mice are found to be much softer as compared to those of wild-type litter-mates. The absence of vimentin is not fatal, but alters the cell migration and mechanical integrity of the cells to a great extent. In addition, the amount of actin in the fibroblasts was also shown to be reduced [102]. Similar to the disruption of actin cytoskeleton in the fibroblasts of the progeria patient, presence of lamin A E145K also might affect the integrity of the vimentin network directly or indirectly as shown in case of other proteins [103], [104]. Several studies have been done so far, to understand the mechanical contribution of lamin A in maintaining the integrity of the cells. The embryonic fibroblasts of lamin A knockout mice show decreased mechanical stiffness due to the absence of lamin A [105]. As discussed before, the cytoplasmic regions of OP and PP fibroblasts are found to be softer than the YP cell cytoplasm in the experiments done in this work. Loss of cellular mechanical stability could be attributed to abnormalities caused due to alterations in the cytoskeletal elements. Further experiments are thus needed to analyze the effect of the progeria mutation on the assembly and structure of these

cytoskeletal elements.

From the AFM measurements obtained in this work, no differences in the mechanical properties of the nuclear regions and the cytoplasmic regions of the fibroblasts were evident. This clearly indicates that the force curves that are generated by AFM probing of intact cells, do not allow a direct judgement of the elastic properties of the nuclei. It might be a mechanical response arising only from the cytoplasmic elements surrounding the nucleus. Further trials were, thus, undertaken to eliminate the contribution of the cytoskeletal elements in living cells allowing direct probing of the nuclei still residing in the cells. It has been observed that cells grown on softer substrates like PA gels coated with fibronectin or collagen, show less spreading and produce less stress fibers [106], [107]. This might render the nucleus more accessible for the AFM probe. To test this, HeLa cells were allowed to grow on collagen coated PA gels and force maps were obtained from the transiently transfected cells expressing either wild-type or progeria mutant lamin A. Due to lack of sufficient amount of data, significant conclusions from these trials could not be obtained.

In another approach, the cells were treated briefly with cytochalasin B to achieve a substantial disassembly of the F-actin network while keeping the cells alive. Disassembly of the actin network reduced the elastic moduli of the nuclear regions of HeLa cells. AFM probing experiments on fibroblasts treated with actin disrupting drugs like jasplakinolide, cytchalasin B, cytchalasin D have been reported before [82]. Each drug was shown to affect mechanical stiffness of cells to different extent depending on the concentration and mode of action of the drug. In general, the stiffness of cells was found to be reduced significantly upon disruption of the actin cytoskeleton. In the few AFM measurements, that were acquired using cytochalasin B treated HeLa cells in this work, the same trend is observed. Since an adequate number of AFM readings could not be recorded for technical reasons mentioned in the results section, no statistically significant outcomes were obtained. From both these attempts carried out using HeLa cells, statistically relevant conclusions could not be obtained. Isolation of the nuclei from fibroblast samples was, thus, necessary for assessment of the effect of the lamin A E145K progeria mutant on the nuclear mechanics.

4.2 Effect of progeria mutation on the mechanics of isolated nuclei

To directly measure the mechanical properties of the nuclei, it was necessary to isolate them from the cells to exclude the influence of cytoskeletal elements. The isolation procedure involved a mild detergent treatment to release the nuclei from surrounding cytoplasm. Isolated nuclei were allowed to settle down in a dish containing PBS to maintain physiologically relevant buffer conditions while recording the AFM force curves. The nuclei were isolated from every passage of OP, PP and YP cell samples. Removal of nuclear membranes upon detergent treatment has been previously reported [89], [90]. Transmission electron micrographs of the nuclei isolated from the YP cell sample in this work, are in accordance with the previous reports about membrane removal upon detergent treatment. The nucleoplasmic contents are heavily extracted during isolation procedure leaving the nuclei with a lamina layer along with the chromatin. Although the membranes are completely removed, the nuclei maintain their shape due to the presence of a mechanically stable lamina. Lamina has been shown to be resistant to extraction by non ionic detergents [89], [90]. The probing of the isolated nuclei was done using low loading forces in the piconewton range to avoid sample destruction. Several force maps were obtained on different regions of each nucleus for an unbiased estimation of the stiffness of the entire nucleus. The TEM analysis of isolated nuclei suggests that these demembranated nuclei can be considered as a thin elastic shell as the mechanical answer to indentation would arise only from the lamina layer which acts as an elastic shell. Experiments performed by Schäpe et al. [72], with *Xenopus* oocyte nuclei have shown that ectopically overexpressed lamin A builds a thick lamina beneath oocyte nuclear membranes, which acts as an elastic shell. AFM probing of these nuclei generated force curves that fitted better with the model curves predicted by an elastic shell model instead of the Hertz model [72].

The stiffness of nuclei analyzed in this work, was expressed as a log of the spring constant values obtained by analysis of the corresponding force curves. The force curves generated by indentation of the isolated nuclei reveal, that, the initial part of the curve, after contact establishment between sample and the tip is linear. This

linearity is considered to be the corresponding elastic response of the lamina layer to an indentation by a pyramidal tip. The occurrence of a linear region in the force curves justifies the use of the elastic shell model for data analysis instead of the Hertzian model. The stiffness of nuclei was, thus, calculated using only the linear regions of the force curves. Taimen et al. (2009), have shown that the severity of nuclear lobulations in progeria cells correlates with corresponding increase in the passage numbers of the cells [26]. Comparison of Log k values indicated that the stiffness of the nuclei does not change as a function of increasing passage number. The AFM measurements were obtained on lobulated and non lobulated nuclei of progeria cells, both of which, however, had stiffer spring constant values. This means that presence of nuclear lobulations does not influence the mechanical properties of the nuclei. As no correlation between nuclear stiffness and corresponding passage number is seen, all the Log k values belonging to one cell type were compared cumulatively to the Log k values of the others as is represented by the histograms (similar to the comparisons for adherent cells data).

The comparison of histograms, which show distribution as well as frequency of Log k values, indicates that the spring constant values of the nuclei isolated from OP and PP cell samples are significantly higher than those of YP cells. The histogram depicting the nuclear stiffness of the OP cells shows two peaks. This possibly indicates a presence of two cell populations within the gradually aged OP cell sample, one group with a higher Log k value, which might be at a later stage of aging, whereas, the other group might consist of a healthier (younger) group of cells. Accumulation of progerin has been reported even in the nuclei of naturally aging cells [91]. Such gradual changes in the lamina composition, as the age increases might also affect the mechanical properties of the nuclei. Nuclei of the cells obtained from progeria patient are very stiff in comparison to the nuclei of YP cells. Such alterations in the mechanical properties might occur due to modifications in the lamin A filament assembly. The progeria mutation in lamin A protein is situated in the coil 1B of the protein, where it replaces a negatively charged amino acid residue, glutamate (E), to a positively charged residue, lysine (K). Fluctuations in the conserved region of the lamin A rod domain do not affect lamin dimerization but have deleterious effects on the further assembly of lamin filaments and their further

lateral association as shown in the in vitro assembly experiments of E145K lamin A [26]. Although these observations were recorded by in vitro experiments, they support the fact that the progeria mutation alters lamin filament assembly pathway. In the experiments presented here, the AFM force curves obtained on the nuclei of PP cells give a fair idea about the mechanical properties of the lamin filaments that might have assembled in a modified manner in vivo, due to the presence of E145K mutant lamin A. This indicates that the progeria mutation in lamin A alters the filament assembly in such a way, that results into a stiffer lamina.

An altered lamina might further affect the interaction between the lamins and their nucleoplasmic binding partners like transcription factors, receptor proteins etc. Such changes could lead to activation or suppression of a cascade of processes simultaneously undergoing in the nucleoplasm. The distribution of DNA replication foci has been found to be altered in the fibroblasts of progeria patient which exhibit very low proliferation capacity [26]. A changed assembly might mask the protein binding regions in the lamins or reveal novel regions of the proteins which ultimately could explain the phenomenon of mislocalization of telomeres and clustering of centromeres in the center of the progeria cell nuclei. The HGPS mutation also causes a persistent activation of checkpoints that control DNA damage in the nuclei [108]. This indicates that either the progeria mutation is directly responsible for causing the DNA damage, or the activation of damage checkpoints is triggered because of false signaling.

Additionally, the mutation E145K in lamin A protein might have adverse effects on expression and regulation of B-type lamins. A depletion of lamin B1 in the healthy dermal fibroblasts results into blebbing of the nuclear envelope. Moreover, in the blebs, only lamin A is present while lamin B2 is absent [109]. In a study by Taimen et al. (2009), the total amount of lamin B1 in the dermal fibroblasts of E145K progeria patient cells, was found to be drastically reduced while a reduction in the amount of lamin B2 was not significant. These alterations might be responsible for the lobulations of the nuclei [26]. Shimi et al. (2008), have also shown that the lamin A blebs devoid of B-type lamins, are enriched with the gene rich euchromatic regions of chromosomes. Studies done on chromosome territories indicate that the chromosomes with gene rich regions usually are found in the central nucleoplasmic compartment

of the nucleus while the pericentric regions are occupied by the transcriptionally inactive chromatin [109]. Disturbances in the lamina meshwork either caused by the absence of one of the lamin proteins or because of the presence of a mutated lamin protein thus dramatically changes chromatin organization. In case of the nuclei with E145K mutant lamin A, a possible depletion of B-type lamins would also generate severe nuclear lobulations. Under the assumption that these lobules would only contain a lamina made up of lamin A, the AFM data obtained in this work, might have revealed elastic properties of the lamina mainly made up of lamin A.

Furthermore in this work, the transmission electron micrographs of all three types of fibroblasts were analyzed in order to measure the thickness of the nuclear lamina. No significant differences in the thickness of the lamina layers of the three cell categories were evident. In case of the PP nuclei, two subgroups (on the basis of differences in lamina thickness) could be distinguished, but no apparent reasons for this difference can be stated. Additionally, the difference between lamina thicknesses of these subgroups is not highly significant. This implies that the nuclei of same lamina thickness but with a lamina layer containing mutant lamin A E145K are stiffer than the purely wild-type lamin A bearing nuclei. Such a composition of the lamina resembles the lamina of the nuclei of *Xenopus* oocytes ectopically expressing E145K lamin A [47], and the results of this work corroborate the outcome of the work done by Kaufmann et al. [47].

The atomic force microscopy technique has thus been successfully used to study the mechanical properties of nuclei of aging cells. The assessment of the changes in the nuclear mechanics caused by the progeria mutation E145K in the lamin A, could only be achieved upon their isolation from the cells. The AFM probing of adherent cells on the other hand, revealed changes occurring in the mechanics of the cytoskeletal elements. Hence, it can be concluded that the phenomenon of aging, either natural or abnormal, increases the stiffness of the nuclei and isolation of nuclei is a necessary prerequisite to measure their stiffness by AFM.

Bibliography

[1] Stewart, E. J., R. Madden, G. Paul, and F. Taddei. 2005. Aging and death in an organism that reproduces by morphologically symmetric division. *PLoS Biol.* 3:295-300.

[2] Messaris, E., P. Kekis, N. Memos, E. Chatzigianni, E. Menenakos, E. Leandros, and M. Konstadoulakis. 2007. Sepsis: Prognostic Role of Apoptosis Regulators in Gastrointestinal Cells. *World J Surg* 31:787-794.

[3] Bhardwaj, R. D., M. A. Curtis, K. L. Spalding, B. A. Buchholz, D. Fink, T. Bjrk-Eriksson, C. Nordborg, F. H. Gage, H. Druid, P. S. Eriksson, and J. Frisn. 2006. Neocortical neurogenesis in humans is restricted to development. *Proc. Natl. Acad. Sci. U.S.A.* 103:12564-12568.

[4] Moss, F. P., and C. P. Leblond. 1970. Nature of dividing nuclei in skeletal muscle of growing rats. *J. Cell Biol.* 44:459-461.

[5] Bergmann, O., R. D. Bhardwaj, S. Bernard, S. Zdunek, F. Barnab-Heider, S. Walsh, J. Zupicich, K. Alkass, B. A. Buchholz, H. Druid, S. Jovinge, and J. Frisn. 2009. Evidence for Cardiomyocyte Renewal in Humans. *Science* 324:98-102.

[6] Mecocci, P., G. Fan, S. Fulle, U. MacGarvey, L. Shinobu, M. Polidori, A. Cherubini, J. Vecchiet, U. Senin, and M. Beal. 1999. Age-dependent increases in oxidative damage to DNA, lipids, and proteins in human skeletal muscle. *Free Radic. Biol. Med.* 26:303-308.

[7] Navarro, C. L., P. Cau, and N. Lévy. 2006. Molecular bases of progeroid syndromes. *Hum. Mol. Genet.* 15:R151-R161.

[8] Hirschfeld, G., M. Berneburg, C. v. Arnim, S. Iben, A. C. Ludolph, and K. Scharffetter-Kochanek. 2007. Progeroid Syndromes: Clinical Symptoms and Molecular Causes of Premature Aging. *Dtsch Arztebl Int* 104:A-346.

[9] Mounkes, L. C., and C. L. Stewart. 2004. Aging and nuclear organization: lamins and progeria. *Curr. Opin. Cell Biol.* 16:322-327.

[10] De Sandre-Giovannoli, A., R. Bernard, P. Cau, C. Navarro, J. Amiel, I. Boccaccio, S. Lyonnet, C. L. Stewart, A. Munnich, M. Le Merrer, and N. Lévy. 2003. Lamin A Truncation in Hutchinson-Gilford Progeria. *Science* 300:2055.

[11] Oshima, J. 2000. The Werner syndrome protein: an update. *BioEssays* 22:894-901.

[12] Bonne, G., M. R. D. Barletta, S. Varnous, H.-M. Becane, E.-H. Hammouda, L. Merlini, F. Muntoni, C. R. Greenberg, F. Gary, J.-A. Urtizberea, D. Duboc, M. Fardeau, D. Toniolo, and K. Schwartz. 1999. Mutations in the gene encoding lamin A/C cause autosomal dominant Emery-Dreifuss muscular dystrophy. *Nat. Genet.* 21:285-288.

[13] Rankin, J., and S. Ellard. 2006. The laminopathies: a clinical review. *Clin. Genet.* 70:261-274.

[14] Worman, H. J. 2012. Nuclear lamins and laminopathies. *J. Pathol.* 226:316-25.

[15] Cao, H., and R. A. Hegele. 2000. Nuclear lamin A/C R482Q mutation in Canadian kindreds with Dunnigan-type familial partial lipodystrophy. *Hum. Mol. Genet.* 9:109-112.

[16] Shackleton, S., D. J. Lloyd, S. N. Jackson, R. Evans, M. F. Niermeijer, B. M. Singh, H. Schmidt, G. Brabant, S. Kumar, P. N. Durrington, S. Gregory, S. O'Rahilly, and R. C. Trembath. 2000. *LMNA*, encoding lamin A/C, is mutated in partial lipodystrophy. *Nat. Genet.* 24:153-156.

[17] De Sandre-Giovannoli, A., M. Chaouch, S. Kozlov, J. M. Vallat, M. Tazir, N. Kassouri, P. Szepetowski, T. Hammadouche, A. Vandenberghe, C. L. Stewart, D. Grid, and N. Lévy. 2002. Homozygous Defects in *LMNA*, Encoding Lamin A/C Nuclear-Envelope Proteins, Cause Autosomal Recessive Axonal Neuropathy in Human (Charcot-Marie-Tooth Disorder Type 2) and Mouse. *Am. J. Hum. Genet.* 70:726-736.

[18] Padiath, Q. S., K. Saigoh, R. Schiffmann, H. Asahara, T. Yamada, A. Koeppen, K. Hogan, L. J. Ptáček, and Y.-H. Fu. 2006. Lamin B1 duplications cause autosomal dominant leukodystrophy. *Nat. Genet.* 38:1114-1123.

[19] Hegele, R. A., H. Cao, D. M. Liu, G. A. Costain, V. Charlton-Menys, N. W. Rodger, and P. N. Durrington. 2006. Sequencing of the Reannotated *LMNB2* Gene Reveals Novel Mutations in Patients with Acquired Partial Lipodystrophy. *Am. J. Hum. Genet.* 79:383-389.

[20] Harborth, J., S. M. Elbashir, K. Bechert, T. Tuschl, and K. Weber. 2001. Identification of essential genes in cultured mammalian cells using small interfering RNAs. *J. Cell. Sci.* 114:4557-4565.

[21] Dreesen, O., A. Chojnowski, P. F. Ong, T. Y. Zhao, J. E. Common, D. Lunny, E. B. Lane, S. J. Lee, L. a. Vardy, C. L. Stewart, and A. Colman. 2013. Lamin B1 fluctuations have differential effects on cellular proliferation and senescence. *J. Cell Biol.* 200:605-617.

[22] Chen, L., L. Lee, B. Kudlow, and H. D. Santos. 2003. *LMNA* mutations in atypical Werner's syndrome. *The Lancet* 362:440-445.

[23] Eriksson, M., W. T. Brown, L. B. Gordon, M. W. Glynn, J. Singer, L. Scott, M. R. Erdos, C. M. Robbins, T. Y. Moses, P. Berglund, A. Dutra, E. Pak, S. Durkin, A. B. Csoka, M. Boehnke, T. W. Glover, and F. S. Collins. 2003. Recurrent de novo point mutations in lamin A cause Hutchinson-Gilford progeria syndrome. *Nature* 423:293-298.

[24] Baker, P. B., N. Baba, and C. P. Boesel. 1981. Cardiovascular abnormalities in progeria. Case report and review of the literature. *Arch. Pathol. Lab. Med.* 105:384-386.

[25] Goldman, R. D., D. K. Shumaker, M. R. Erdos, M. Eriksson, A. E. Goldman, L. B. Gordon, Y. Gruenbaum, S. Khuon, M. Mendez, R. Varga, and F. S. Collins. 2004. Accumulation of mutant lamin A causes progressive changes in nuclear architecture in Hutchinson-Gilford progeria syndrome. *Proc. Natl. Acad. Sci. U.S.A.* 101:8963-8968.

[26] Taimen, P., K. Pfleghaar, T. Shimi, D. Möller, K. Ben-Harush, M. R. Erdos, S. Adam, H. Herrmann, O. Medalia, F. S. Collins, A. E. Goldman, and R. D. Goldman. 2009. A progeria mutation reveals functions for lamin A in nuclear assembly, architecture, and chromosome organization. *Proc. Natl. Acad. Sci. U.S.A.* 106:20788-20793.

[27] Weber, K., U. Plessmann, and P. Traub. 1989. Maturation of nuclear lamin A involves a specific carboxy-terminal trimming, which removes the polyisoprenylation site from the precursor; implications for the structure of the nuclear lamina. *FEBS Lett.* 257:411-414.

[28] Goldman, R. D., Y. Gruenbaum, R. D. Moir, D. K. Shumaker, and T. P. Spann. 2002. Nuclear lamins: building blocks of nuclear architecture. *Genes Dev.* 16:533-547.

[29] Guelen, L., L. Pagie, E. Brasset, W. Meuleman, M. B. Faza, W. Talhout, B. H. Eussen, A. de Klein, L. Wessels, and W. de Laat. 2008. Domain organization of human chromosomes revealed by mapping of nuclear lamina interactions. *Nature* 453:948-951.

[30] Dahl, K., S. Kahn, K. Wilson, and D. Discher. 2004. The nuclear envelope lamina network has elasticity and a compressibility limit suggestive of a molecular shock absorber. *J. Cell. Sci.* 117:4779-4786.

[31] Burke, B., and C. L. Stewart. 2002. Life at the edge: the nuclear envelope and human disease. *Nat. Rev. Mol. Cell Biol.* 3:575-585.

[32] Levy, D. L., and R. Heald. 2010. Nuclear Size Is Regulated by Importin α and Ntf2 in *Xenopus*. *Cell* 143:288-298.

[33] Vaughan, O., W. Whitfield, and C. Hutchison. 2000. Functions of the nuclear lamins. *Protoplasma* 211:1-7.

[34] Döring, V., and R. Stick. 1990. Gene structure of nuclear lamin LIII of *Xenopus laevis*; a model for the evolution of IF proteins from a lamin-like ancestor. *EMBO J.* 9:4073-4081.

[35] Herrmann, H., and U. Aebi. 2004. INTERMEDIATE FILAMENTS: Molecular Structure, Assembly Mechanism, and Integration Into Functionally Distinct Intracellular Scaffolds. *Annu. Rev. Biochem.* 73:749-789.

[36] Peter, A., and R. Stick. 2012. Evolution of the lamin protein family: What introns can tell. *Nucleus* 3:44-59.

[37] Dhe-Paganon, S., E. D. Werner, Y.-I. Chi, and S. E. Shoelson. 2002. Structure of the Globular Tail of Nuclear Lamin. *J. Biol. Chem.* 277:17381-17384.

[38] Krimm, Isabelle Östlund, C., B. Gilquin, J. Couprie, P. Hossenlopp, J.-P. Mornon, G. Bonne, J.-C. Courvalin, H. J. Worman, and S. Zinn-Justin. 2002. The Ig-like Structure of the C-Terminal Domain of Lamin A/C, Mutated in Muscular Dystrophies, Cardiomyopathy, and Partial Lipodystrophy. *Structure* 10:811-823.

[39] Rusiñol, A. E., and M. S. Sinensky. 2006. Farnesylated lamins, progeroid syndromes and farnesyl transferase inhibitors. *J. Cell. Sci.* 119:3265-3272.

[40] Prokocimer, M., M. Davidovich, M. Nissim-Rafinia, N. Wiesel-Motiuk, D. Z. Bar, R. Barkan, E. Meshorer, and Y. Gruenbaum. 2009. Nuclear lamins: key regulators of nuclear structure and activities. *J. Cell. Mol. Med.* 13:1059-1085.

[41] Lin, F., and H. J. Worman. 1993. Structural organization of the human gene encoding nuclear lamin A and nuclear lamin C. *J. Biol. Chem.* 268:16321-16326.

[42] Furukawa, K., H. Inagaki, and Y. Hotta. 1994. Identification and Cloning of an mRNA Coding for a Germ Cell-Specific A-Type Lamin in Mice. *Exp. Cell Res.* 212:426-430.

[43] Stick, R. 1992. The gene structure of *Xenopus* nuclear lamin A: A model for the evolution of A-type from B-type lamins by exon shuffling. *Chromosoma* 101:566-574.

[44] Peter, A., and R. Stick. 2008. Ectopic expression of prelamin A in early *Xenopus* embryos induces apoptosis. *Eur. J. Cell Biol.* 87:879-891.

[45] Firmbach-Kraft, I., and R. Stick. 1995. Analysis of nuclear lamin isoprenylation in *Xenopus* oocytes: isoprenylation of lamin B3 precedes its uptake into the nucleus. *J. Cell Biol.* 129:17-24.

[46] Krohne, G., I. Waizenegger, and T. H. Hger. 1989. The conserved carboxy-terminal cysteine of nuclear lamins is essential for lamin association with the nuclear envelope. *J. Cell Biol.* 109:2003-2011.

[47] Kaufmann, A., F. Heinemann, M. Radmacher, and R. Stick. 2011. Amphibian oocyte nuclei expressing lamin A with the progeria mutation E145K exhibit an increased elastic modulus. *Nucleus* 2:310-319.

[48] Parry, D. A. D., and P. M. Steinert. 1999. Intermediate filaments: molecular architecture, assembly, dynamics and polymorphism. *Q. Rev. Biophys.* 32:99-187.

[49] Ben-Harush, K., N. Wiesel, D. Frenkiel-Krispin, D. Moeller, E. Soreq, U. Aebi, H. Herrmann, Y. Gruenbaum, and O. Medalia. 2009. The supramolecular organization of the *C. elegans* nuclear lamin filament. *J. Mol. Biol.* 386:1392-1402.

[50] Karabinos, A., J. Schönemann, M. Meyer, U. Aebi, and K. Weber. 2003. The Single Nuclear Lamin of *Caenorhabditis elegans* Forms In Vitro Stable Intermediate Filaments and Paracrystals with a Reduced Axial Periodicity. *J. Mol. Biol.* 325:241-247.

[51] Imai, S., S. Nishibayashi, K. Takao, M. Tomifuji, T. Fujino, M. Hasegawa, and T. Takano. 1997. Dissociation of Oct-1 from the Nuclear Peripheral Structure Induces the Cellular Aging-associated Collagenase Gene Expression. *Mol. Biol. Cell* 8:2407-2419.

[52] Hutchison, C. J., and H. J. Worman. 2004. A-type lamins: guardians of the soma? *Nat. Cell Biol.* 6:1062-1067.

[53] Chambliss, A. B., S. B. Khatau, N. Erdenberger, D. K. Robinson, D. Hodzic, G. D. Longmore, and D. Wirtz. 2013. The LINC-anchored actin cap connects the extracellular milieu to the nucleus for ultrafast mechanotransduction. *Sci Rep* 3:1-9.

[54] Wojtanik, K. M., K. Edgemon, S. Viswanadha, B. Lindsey, M. Haluzik, W. Chen, G. Poy, M. Reitman, and C. Londos. 2009. The role of LMNA in adipose: a novel mouse model of lipodystrophy based on the Dunnigan-type familial partial lipodystrophy mutation. *J. Lipid Res.* 50:1068-1079.

[55] Chahine, N. O., C. Blanchette, C. B. Thomas, J. Lu, D. Haudenschild, and G. G. Loots. 2013. Effect of age and cytoskeletal elements on the indentation-dependent mechanical properties of chondrocytes. *PLoS ONE* 8:1-12.

[56] Crisp, M., Q. Liu, K. Roux, J. B. Rattner, C. Shanahan, B. Burke, P. D. Stahl, and D. Hodzic. 2006. Coupling of the nucleus and cytoplasm: role of the LINC complex. *J. Cell Biol.* 172:41-53.

[57] Razafsky, D., and D. Hodzic. 2009. Bringing KASH under the SUN: the many faces of nucleo-cytoskeletal connections. *J. Cell Biol.* 186:461-472.

[58] Yang, L., M. Munck, K. Swaminathan, L. E. Kapinos, A. a. Noegel, and S. Neumann. 2013. Mutations in *LMNA* Modulate the Lamin A - Nesprin-2 Interaction and Cause LINC Complex Alterations. *PLoS ONE* 8:e71850.

[59] Zwerger, M., D. E. Jaalouk, M. L. Lombardi, P. Isermann, M. Mauermann, G. Dialynas, H. Herrmann, L. L. Wallrath, and J. Lammerding. 2013. Myopathic lamin mutations impair nuclear stability in cells and tissue and disrupt nucleo-cytoskeletal coupling. *Hum. Mol. Genet.* 22:2335-2349.

[60] Khatau, S. B., C. M. Hale, P. J. Stewart-Hutchinson, M. S. Patel, C. L. Stewart, P. C. Searson, D. Hodzic, and D. Wirtz. 2009. A perinuclear actin cap regulates nuclear shape. *Proc. Natl. Acad. Sci. U.S.A.* 106:19017-19022.

[61] Khatau, S. B., D.-H. Kim, C. M. Hale, R. J. Bloom, and D. Wirtz. 2010. The perinuclear actin cap in health and disease. *Nucleus* 1:337-342.

[62] Hale, C. M., A. L. Shrestha, S. B. Khatau, P. Stewart-Hutchinson, L. Hernandez, C. L. Stewart, D. Hodzic, and D. Wirtz. 2008. Dysfunctional connections between the nucleus and the actin and microtubule networks in laminopathic models. *Biophys. J.* 95:5462-5475.

[63] Lee, J. S., C. M. Hale, P. Panorchan, S. B. Khatau, J. P. George, Y. Tseng, C. L. Stewart, D. Hodzic, and D. Wirtz. 2007. Nuclear lamin A/C deficiency induces defects in cell mechanics, polarization, and migration. *Biophys. J.* 93:2542-2552.

[64] Swift, J., I. L. Ivanovska, A. Buxboim, T. Harada, P. C. D. P. Dingal, J. Pinter, J. D. Pajerowski, K. R. Spinler, J.-W. Shin, M. Tewari, F. Rehfeldt, D. W. Speicher, and D. E. Discher. 2013. Nuclear lamin-A scales with tissue stiffness and enhances matrix-directed differentiation. *Science* 341:1240104-1-1240104-15.

[65] Hochmuth, R. M. 2000. Micropipette aspiration of living cells. *J Biomech* 33:15-22.

[66] Guck, J., R. Ananthakrishnan, H. Mahmood, T. J. Moon, C. C. Cunningham, and J. Ks. 2001. The Optical Stretcher: A Novel Laser Tool to Micromanipulate Cells. *Biophys. J.* 81:767-784.

[67] Caille, N., O. Thoumine, Y. Tardy, and J.-J. Meister. 2002. Contribution of the nucleus to the mechanical properties of endothelial cells. *J Biomech* 35:177-187.

[68] Tao, N. J., S. M. Lindsay, and S. Lees. 1992. Measuring the microelastic properties of biological material. *Biophys. J.* 1165-1169.

[69] Radmacher, M., J. P. Cleveland, M. Fritz, H. G. Hansma, and P. K. Hansma. 1994. Mapping interaction forces with the atomic force microscope. *Biophys. J.* 66:2159-2165.

[70] Binnig, G., C. Quate, and C. Gerber. 1986. Atomic Force Microscope. *Phys. Rev. Lett.* 56:930-933.

[71] Radmacher, M., M. Fritz, C. M. Kacher, J. P. Cleveland, and P. K. Hansma. 1996. Measuring the viscoelastic properties of human platelets with the atomic force microscope. *Biophys. J.* 70:556-567.

[72] Schäpe, J., S. Prausse, M. Radmacher, and R. Stick. 2009. Influence of lamin A on the mechanical properties of amphibian oocyte nuclei measured by atomic force microscopy. *Biophys. J.* 96:4319-4325.

[73] Lemkine, G., and B. Demeneix. 2001. Polyethylenimines for in vivo gene delivery. *Curr. Opin. Mol. Ther.* 3:178-182.

[74] Stick, R. 1988. cDNA cloning of the developmentally regulated lamin LIII of *Xenopus laevis*. *EMBO J.* 7:3189-3197.

[75] Radmacher, M. 2007. Studying the Mechanics of Cellular Processes by Atomic Force Microscopy. *Methods Cell Biol.* 83:347-372.

[76] West, P. 2006. Introduction to Atomic Force Microscopy: Theory Practice Applications. Oxford University Press.

[77] Hertz, H. 1882. Über die Berührung fester elastischer Körper. *J. Reine Angew. Math.* 92:156-171.

[78] Sneddon, I. N. 1965. The relation between load and penetration in the axisymmetric boussinesq problem for a punch of arbitrary profile. *Int J Eng Sci* 3:47-57.

[79] Arnoldi, M., C. Kacher, E. Bäuerlein, M. Radmacher, and M. Fritz. 1998. Elastic properties of the cell wall of *Magnetospirillum gryphiswaldense* investigated by atomic force microscopy. *Appl Phys A Mater Sci Process* 66:S613-S617.

[80] McClintock, D., L. B. Gordon, and K. Djabali. 2006. Hutchinson-Gilford progeria mutant lamin A primarily targets human vascular cells as detected by an anti-Lamin A G608G antibody. *Proc. Natl. Acad. Sci. U.S.A.* 103:2154-2159.

[81] Radmacher, M. 1997. Measuring the elastic properties of biological samples with the AFM. *IEEE Eng Med Biol Mag, IEEE* 16:47-57.

[82] Rotsch, C., and M. Radmacher. 2000. Drug-induced changes of cytoskeletal structure and mechanics in fibroblasts: an atomic force microscopy study. *Biophys. J.* 78:520-535.

[83] Bendre, S. 2013. The effect of transient expression of a lamin A mutant on the nuclear structure and mechanics in different human cell lines. Master's thesis. University of Bremen.

[84] Moir, R. D., M. Yoon, S. Khuon, and R. D. Goldman. 2000. Nuclear lamins A and B1: different pathways of assembly during nuclear envelope formation in living cells. *J. Cell Biol.* 151:1155-1168.

[85] Liu, J., T. Rolef Ben-Shahar, D. Riemer, M. Treinin, P. Spann, K. Weber, A. Fire, and Y. Gruenbaum. 2000. Essential roles for *Caenorhabditis elegans* lamin gene in nuclear organization, cell cycle progression, and spatial organization of nuclear pore complexes. *Mol. Biol. Cell* 11:3937-3947.

[86] Zhang, Q., J. N. Skepper, F. Yang, J. D. Davies, L. Hegyi, R. G. Roberts, P. L. Weissberg, J. a. Ellis, and C. M. Shanahan. 2001. Nesprins: a novel family of

spectrin-repeat-containing proteins that localize to the nuclear membrane in multiple tissues. *J. Cell. Sci.* 114:4485-4498.

[87] Beer, M., and C. R. Zobel. 1961. Electron stains II: Electron microscopic studies on the visibility of stained DNA molecules. *J. Mol. Biol.* 3:717-726.

[88] MacLean-Fletcher, S., and T. D. Pollard. 1980. Mechanism of Action of Cytochalasin B on Actin. *Cell* 20:329-341.

[89] Aaronson, R. P., and G. Blobel. 1974. ON THE ATTACHMENT OF THE NUCLEAR PORE COMPLEX. *J. Cell Biol.* 62:746-754.

[90] Aaronson, R. P., and G. Blobel. 1975. Isolation of nuclear pore complexes in association with a lamina. *Proc. Natl. Acad. Sci. U.S.A.* 72:1007-1011.

[91] Zahn, J. T., I. Louban, S. Jungbauer, M. Bissinger, D. Kaufmann, R. Kemkemer, and J. P. Spatz. 2011. Age-dependent changes in microscale stiffness and mechanoresponses of cells. *Small* 7:1480-1487.

[92] Schulze, C., F. Wetzel, T. Kueper, A. Malsen, G. Muhr, S. Jaspers, T. Blatt, K.-P. Wittern, H. Wenck, and J. a. Käs. 2010. Stiffening of human skin fibroblasts with age. *Biophys. J.* 99:2434-2442.

[93] McClintock, D., D. Ratner, M. Lokuge, D. M. Owens, L. B. Gordon, F. S. Collins, and K. Djabali. 2007. The mutant form of lamin A that causes Hutchinson-Gilford progeria is a biomarker of cellular aging in human skin. *PLoS ONE* 2:1-10.

[94] Foeger, N., N. Wiesel, D. Lotsch, N. Mücke, L. Kreplak, U. Aebi, Y. Gruenbaum, and H. Herrmann. 2006. Solubility properties and specific assembly pathways of the B-type lamin from *Caenorhabditis elegans*. *J. Struct. Biol.* 155:340-350.

[95] Wiesel, N., A. Mattout, S. Melcer, N. Melamed-Book, H. Herrmann, O. Medalia, U. Aebi, and Y. Gruenbaum. 2008. Laminopathic mutations interfere with the assembly, localization, and dynamics of nuclear lamins. *Proc. Natl. Acad. Sci. U.S.A.* 105:180-185.

[96] Shroff, S. G., D. R. Saner, and R. Lal. 1995. Dynamic micromechanical properties of cultured rat atrial myocytes measured by atomic force microscopy. *Am. J. Physiol., Cell Physiol.* 269:C286-C292.

[97] Costa, K. D., and F. C. P. Yin. 1999. Analysis of Indentation: Implications for Measuring Mechanical Properties With Atomic Force Microscopy. *J Biomech Eng* 121:462-471.

[98] Münter, S., J. Enninga, R. Vazquez-Martinez, E. Delbarre, B. David-Watine, U. Nehrbass, and S. L. Shorte. 2006. Actin polymerisation at the cytoplasmic face of eukaryotic nuclei. *BMC Cell Biol.* 7:23.

[99] Rotsch, C., F. Braet, E. Wisse, and M. Radmacher. 1997. AFM imaging and elasticity measurements on living rat liver macrophages. *Cell Biol. Int.* 21:685-696.

[100] Ouyang, H., E. Nauman, and R. Shi. 2010. Contribution of Cytoskeletal Elements to the Mechanical Property of Axons. *In* Micro/Nano Symposium (UGIM), 2010 18th Biennial University/Government/Industry. IEEE. 1-5.

[101] Weissman-Shomer, P., and M. Fry. 1975. Chick embryo fibroblasts senescence in vitro: Pattern of cell division and life span as a function of cell density. *Mech. Ageing Dev.* 4:159-166.

[102] Eckes, B., D. Dogic, E. Colucci-Guyon, N. Wang, A. Maniotis, D. Ingber, A. Merckling, F. Langa, M. Aumailley, A. Delouvée, V. Koteliansky, C. Babinet, and T. Krieg. 1998. Impaired mechanical stability, migration and contractile capacity in vimentin-deficient fibroblasts. *J. Cell. Sci.* 111:1897-1907.

[103] Cary, R. B., M. W. Klymkowsky, R. M. Evans, A. Domingo, J. A. Dent, and L. E. Backhus. 1994. Vimentin's tail interacts with actin-containing structures in vivo. *J. Cell. Sci.* 1622:1609-1622.

[104] Tolstonog, G. V., M. Sabasch, and P. Traub. 2002. Cytoplasmic intermediate filaments are stably associated with nuclear matrices and potentially modulate their DNA-binding function. *DNA Cell Biol.* 21:213-239.

[105] Broers, J. L., E. A. Peeters, H. J. Kuijpers, J. Endert, C. V. Bouten, C. W. Oomens, F. P. Baaijens, and F. C. Ramaekers. 2004. Decreased mechanical stiffness in $LMNA^{-/-}$ cells is caused by defective nucleo-cytoskeletal integrity: implications for the development of laminopathies. *Hum. Mol. Genet.* 13:2567-2580.

[106] Yeung, T., P. C. Georges, L. A. Flanagan, B. Marg, M. Ortiz, M. Funaki, N. Zahir, W. Ming, V. Weaver, and P. A. Janmey. 2005. Effects of substrate stiffness on cell morphology, cytoskeletal structure, and adhesion. *Cell Motil. Cytoskeleton* 60:24-34.

[107] Pelham, R., and Y. Wang. 1997. Cell locomotion and focal adhesions are regulated by substrate flexibility. *Proc. Natl. Acad. Sci. U.S.A.* 94:13661-13665.

[108] Liu, Y., A. Rusinol, M. Sinensky, Y. Wang, and Y. Zou. 2006. DNA damage responses in progeroid syndromes arise from defective maturation of prelamin A. *J. Cell. Sci.* 119:4644-4649.

[109] Shimi, T., K. Pfleghaar, S. Kojima, C. G. Pack, I. Solovei, A. E. Goldman, S. A. Adam, D. K. Shumaker, M. Kinjo, T. Cremer, and R. D. Goldman. 2008. The A- and B-type nuclear lamin networks : microdomains involved in chromatin organization and transcription. *Genes Dev.* 22:3409-3421.

Appendices

Appendix A

A.1 Cotransfection of HeLa cells

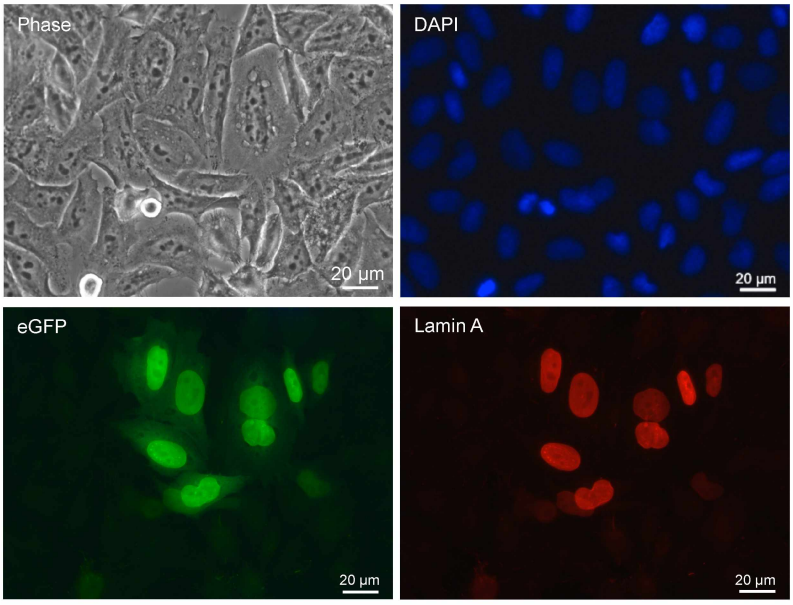

FIGURE A.1 Cotransfection of HeLa cells with plasmids encoding *Xenopus* Flag lamin A and eGFP. To confirm the success of coexpression of two proteins encoded by different plasmids, cotransfection of HeLa cells was done using plasmids encoding *Xenopus* Flag lamin A and eGFP. Cells were fixed and stained for indirect immunofluorescence microscopy. 99% of the cells expressing eGFP show presence of Flag tagged lamin A which was detected by a Flag tag specific monoclonal antibody M2. The secondary antibody was conjugated with Cy3. DAPI staining was done to detect chromatin. The phase contrast image *(Phase)* shows the total number of cells in the field of view.

A.2 An experiment wise graph for HeLa cells

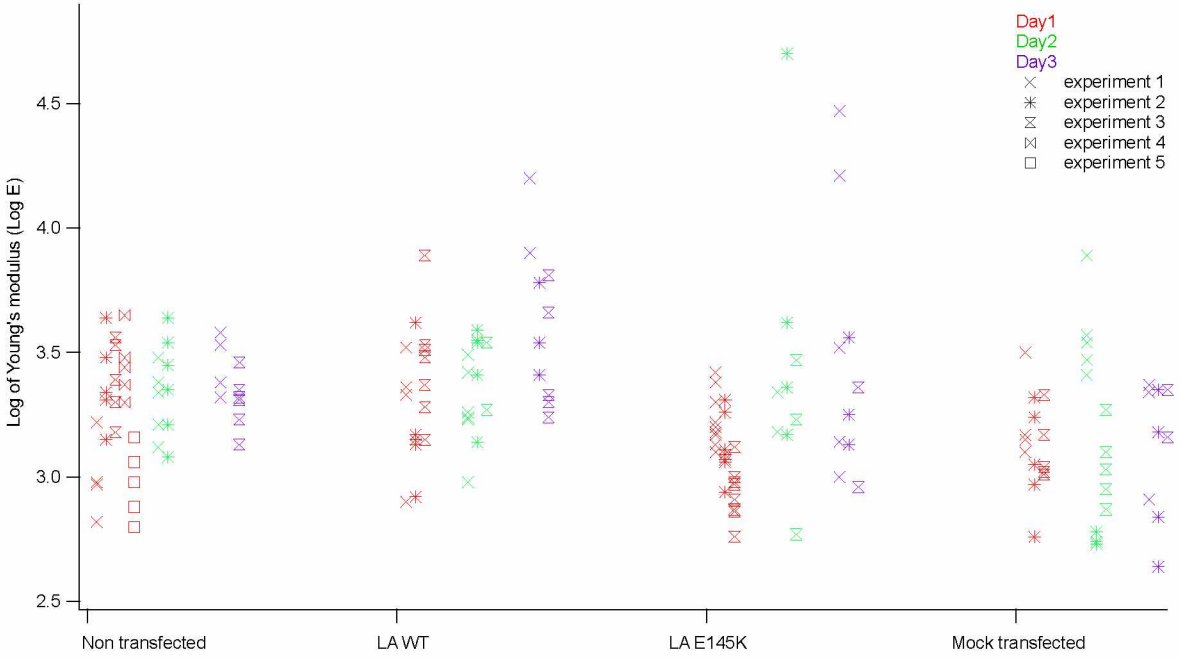

FIGURE A.2 HeLa cells probed by pyramidal tip. The graph shows Log E values plotted for the cell samples mentioned on the x axis according to independent experiments. The legend shows corresponding symbols for each experiment number. Minor variations in Log E values are seen from experiment to experiment.

A.3 Step response

Force curves were obtained on the fibroblasts by indentation due to a point force under low loading forces and the elastic moduli of the cells were calculated. In another approach, the viscoelastic properties of the cells were determined using a "step response" method developed by Prof. Dr. Manfred Radmacher (Institute for Biophysics, NW1, Univeristy of Bremen). This method is currently in a preliminary stage of development. In the step response approach information about the viscosity of the sample is obtained along with its elastic properties. This is achieved by an additional indentation of the sample when it is already in contact with the tip. After contact establishment with the tip, the sample is further moved towards the tip in a single 50 nm step (in this case). The creep response of the cell is recorded for some time (0.5 s in this case), before the sample is retracted in a sudden step (50 nm here) followed by monitoring the creep response after retraction (0.5 s). The entire z step measurement thus lasted for 1 s in this case. This creep response is due to the viscoelastic properties of the cell. The force curves that are recorded as a result of the sample indentation without z step give information about the elastic modulus of the sample. The step response curves that are obtained upon additional indentation of sample by the z step of 50 nm, are used to determine the viscosity (η) of the sample that is also dependent on the time constant (τ) of decay, that is recorded in the step response data. Hence, with the step response approach, not only the mechanical properties of cells (as elastic moduli) can be determined but also their response to an additional indentation can be measured (as viscosity).

Dermal fibroblasts of a progeria patient, an old person and a young person were used for obtaining the step response data. This data were collected on the same cells on which force maps were obtained for calculation of the elastic moduli. The data was acquired along a single line, mostly consisting of 15 points. Generally two sets of data were acquired for each cell, either along length and breadth of the cell, or along the diagonal axes of the cell. Figure A.3 shows a typical step response curve generated on the cell. The data can be analyzed by simple mechanical models (for example, Maxwell model, Kelvin-Voigt model) that describe viscoelastic behavior of the sample. According to Kelvin-Voigt model, a combination of a spring and a

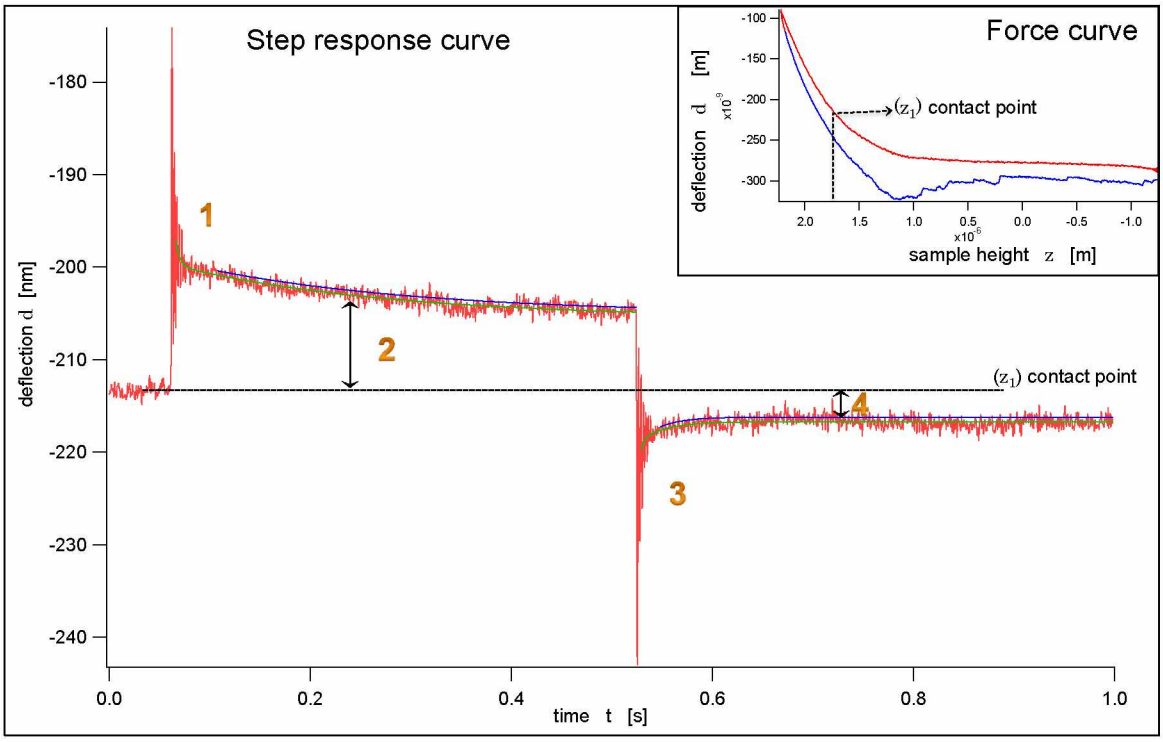

FIGURE A.3 Typical step response curve generated on a fibroblast. After contact establishment, the cell is further indented due to movement of the sample towards the tip by 50 nm step in the z direction. The red curve is experimental data, the blue lines are single exponential fits and the green lines are the double exponential fits. Parts of the curve denoted as 1 and 2 represent the response of the cell during approach in the z step and the parts 3 and 4 represent the response of the cell during retraction from the z step. The total time allowed for the z step of 50 nm was 1 s.

dashpot in parallel (spring is the elastic element and the dashpot is a Kelvin element or a damper which is the viscous element) show an exponential creep response. Since the step response data obtained with cells often show a fast and a slow creep responses, single (blue lines in Figure A.3) and double exponential fits (green lines in Figure A.3) were applied to the experimental data (red line in Figure A.3), corresponding to the combination of two Kelvin elements. As a result, three values, namely k, η and τ can be calculated from both, the approach (plus) and retract (minus) curves separately. At this stage of analysis only the data from the approach step was taken into further consideration. The k is the spring constant of the sample obtained from the step response curves. The viscosity of the sample, i.e., $\eta 1$, is the value according to the single exponential fit. $\eta 2$a and 2b are obtained when the double exponential fit is applied. Similarly the time constant $\tau 1$ and $\tau 2$a and 2b are also calculated. Both the double headed arrows shown in the figure give the effective change in the deflection from the contact point z_1, which is taken into account for data analysis. As shown in the figure, the single exponential fit only analyses the slower responses on the cell along the time scale (x axis). The double exponential, on the other hand, takes into account, the faster response and the slower response of the cell. But while considering the faster cell response, the noise in the deflection generated due to the sudden step interferes with the analysis. Hence, both the fits are equally considered for the analysis at this stage of the development of the step response approach.

Figures A.4, A.5 and A.6 show the outcome of the analysis of step response data obtained on the fibroblasts. Whole cells were used for data acquisition. The x axis in all panels shows the cell passage numbers according to the color code for OP, PP and YP. No differences in the spring constant (k) values (in Figure A.4) and the viscosity (η) values (in Figure A.6) with corresponding τ values (in Figure A.5) are evident from the comparison. Such a result is not surprising, as the AFM probing of whole cells also resulted into non significant differences between the elastic moduli of OP, PP and YP samples.

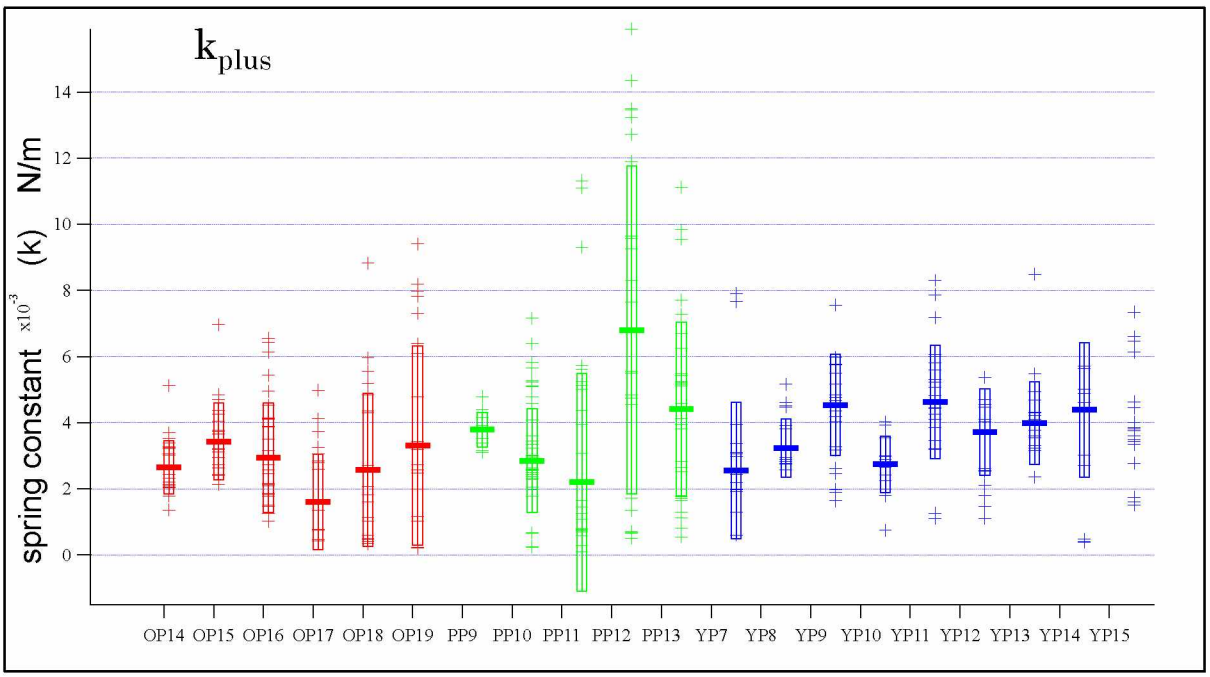

FIGURE A.4 Preliminary results of step response data analysis. The spring constant (k) values calculated from the step response curves obtained on different passages of OP *(red)*, PP *(green)* and YP cells *(blue)*.

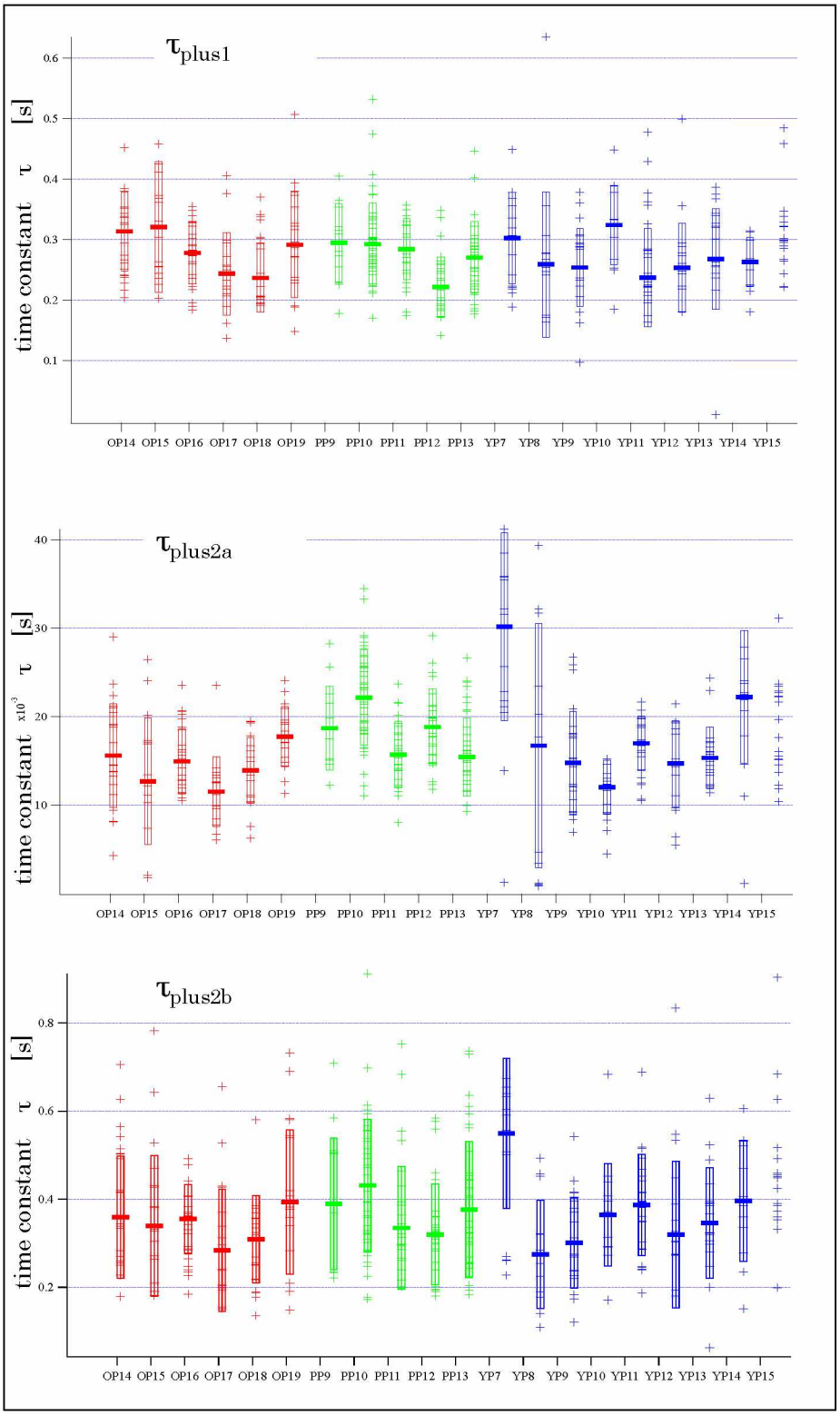

FIGURE A.5 Preliminary results of step response data analysis. The time constant values (τ) of different fibroblasts obtained from OP *(red)*, PP *(green)* and YP cells *(blue)*.

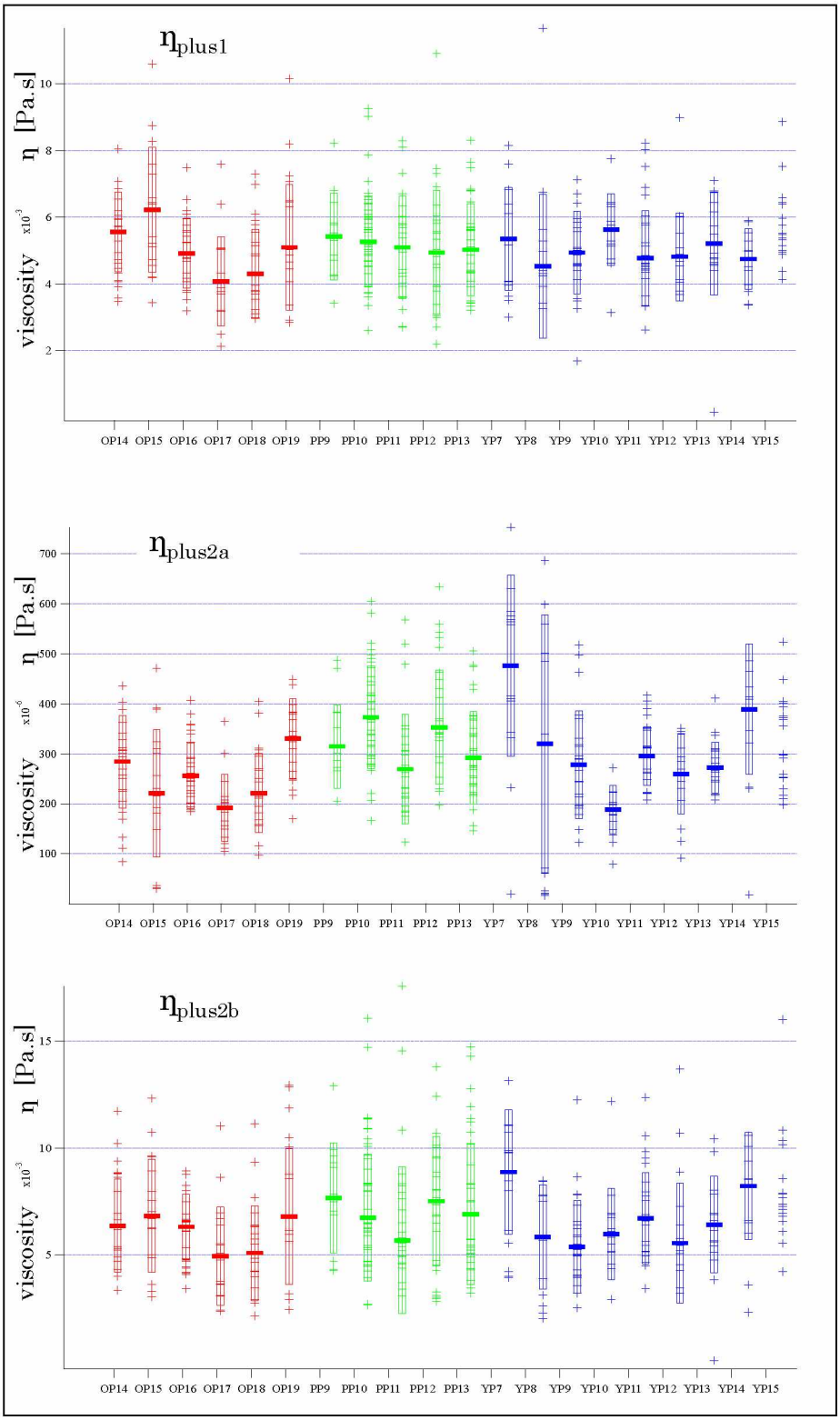

FIGURE A.6 Preliminary results of step response data analysis. The viscosity (η) of different fibroblasts of OP *(red)*, PP *(green)* and YP cells *(blue)*.

A.4 Analysis of TEM images for height measurements

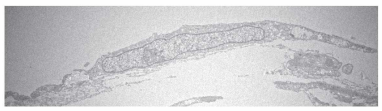

OP15_14.10.13/Image 01_3k
cell height: 2 µm
distance to nucleus from top: 0.3 µm
distance to nucleus from bottom: 0.3 µm
nucleus height: 1.2 µm
nucleus length: 12.3 µm
cell length: 26.2 µm

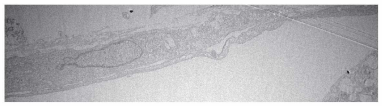

OP15_14.10.13/Image 31_3k
cell height: 2.3 µm
distance to nucleus from top: 0.2 µm
distance to nucleus from bottom: 0.3 µm
nucleus height: 1.4 µm
nucleus length: 6.3 µm
cell length: 20.7 µm

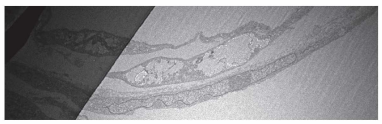

OP15_14.10.13/Image 49a_3k
cell height: 1.2 µm
distance to nucleus from top: 0.3 µm
distance to nucleus from bottom: 0.2 µm
nucleus height: 1 µm
nucleus length: 14.4 µm
cell length: 26.6 µm

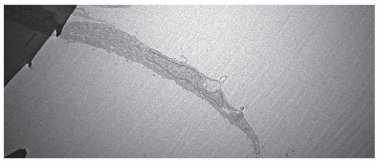

OP15_14.10.13/Image 49b_3k
cell height: 1.4 µm
distance to nucleus from top: 0.2 µm
distance to nucleus from bottom: 0.5 µm
nucleus height: 0.9 µm
nucleus length: 6.8 µm
cell length: 18.6 µm

OP15_9.10.13/Image 35_3k
cell height: 1.6 µm
distance to nucleus from top: 0.4 µm
distance to nucleus from bottom: 0.3 µm
nucleus height: 1 µm
nucleus length: 15.7 µm
cell length: 26.8 µm

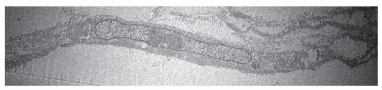

OP15_9.10.13/Image 02_3k
cell height: 2.3 µm
distance to nucleus from top: 0.3 µm
distance to nucleus from bottom: 0.6 µm
nucleus height: 1.4 µm
nucleus length: 11.8 µm
cell length: 27.3 µm

FIGURE A.7 TEM images of cells obtained from an old person

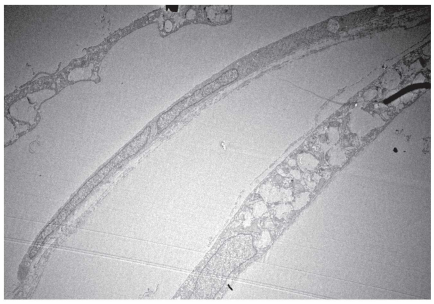

OP15_9.10.13/Image 08_3k
cell height: 1 µm
distance to nucleus from top: 0.2 µm
distance to nucleus from bottom: 0.1 µm
nucleus height: 0.6 µm
nucleus length: 18 µm
cell length: 30 µm

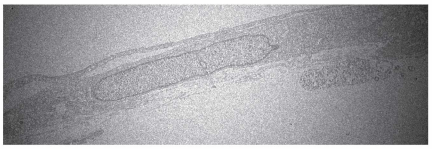

OP15_9.10.13/Image 19_3k
cell height: 2.3 µm
distance to nucleus from top: 0.3 µm
distance to nucleus from bottom: 0.1µm
nucleus height: 1.6 µm
nucleus length: 12.4 µm
cell length: 28.6 µm

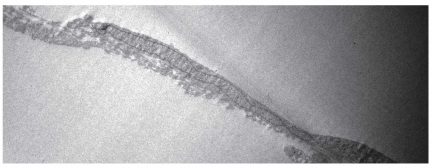

OP15_18.7.13/Image 01_3k
cell height: 1.3 µm
distance to nucleus from top: 0.2 µm
distance to nucleus from bottom: 0.2 µm
nucleus height: 0.8 µm
nucleus length: 15.6 µm

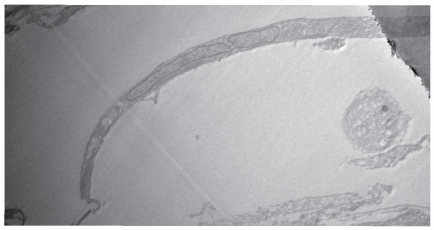

OP15_18.7.13/Image 03_3k
cell height: 1.3 µm
distance to nucleus from top: 0.25 µm
distance to nucleus from bottom: 0.4 µm
nucleus height: 0.7 µm
nucleus length: 10.8 µm

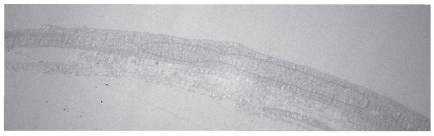

OP15_18.7.13/Image 30_3k
cell height: 1.8 µm
distance to nucleus from top: 0.4 µm
distance to nucleus from bottom: 0.3 µm
nucleus height: 1 µm
nucleus length: 14.8 µm

FIGURE A.8 TEM images of cells obtained from an old person

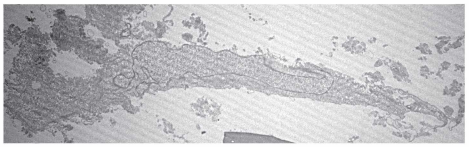

PP10_15.07.13/Image 62_3k
cell height: 2.5 µm
distance to nucleus from top: 0.5 µm
distance to nucleus from bottom: 0.5 µm
nucleus height: 1.6 µm
nucleus length: 13.1 µm
cell length: 26 µm

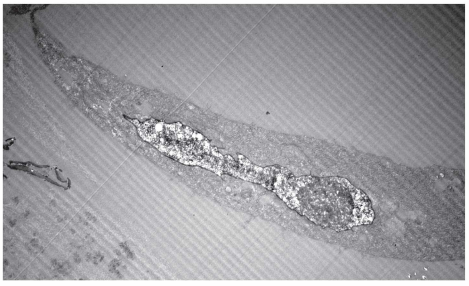

PP10_19.07.13/Image 13_3k
cell height: 5.7 µm
distance to nucleus from top: 1.9 µm
distance to nucleus from bottom: 0.8 µm
nucleus height: 3 µm
nucleus length: 16.2 µm
cell length: 27.3 µm

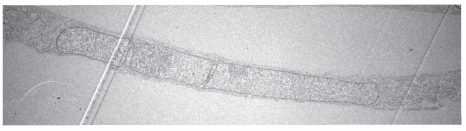

PP10new_a_17.09.13/Image 01_3k
cell height: 2.1 µm
distance to nucleus from top: 0.2 µm
distance to nucleus from bottom: 0.13 µm
nucleus height: 1.6 µm
nucleus length: 19.6 µm
cell length: 28.1 µm

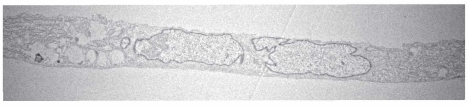

PP10new_a_17.09.13/Image064_3k
cell height: 2.4 µm
distance to nucleus from top: 0.1 µm
distance to nucleus from bottom: 0.4 µm
nucleus height: 1.7 µm
nucleus length: 15.2 µm
cell length: 27.8 µm

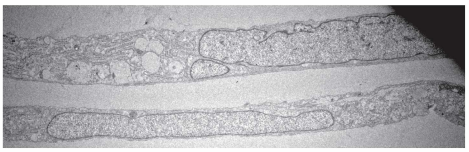

(a) PP10new_a_17.09.13/Image 65_3k
cell height: 2.9 µm
distance to nucleus from top: 0.3 µm
distance to nucleus from bottom: 0.3 µm
nucleus height: 2 µm
nucleus length: 15.2 µm
cell length: 23.3 µm

(a)

(b)

(b) PP10new_a_17.09.13/Image 65_3k
cell height: 1.8 µm
distance to nucleus from top: 0.2 µm
distance to nucleus from bottom: 0.13 µm
nucleus height: 1.3 µm
nucleus length: 17.2 µm
cell length: 27.7 µm

FIGURE A.9 TEM images of cells obtained from a progeria patient

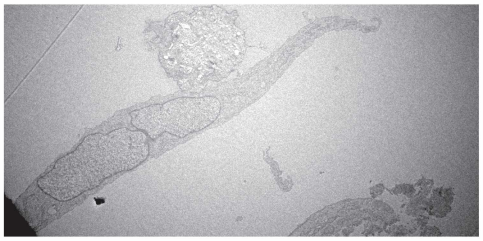

PP10new_b_8.10.13/Image 3k
cell height: 3.4 µm
distance to nucleus from top: 0.2 µm
distance to nucleus from bottom: 0.28 µm
nucleus height: 2.3 µm
nucleus length: 11.3 µm
cell length: 23.2 µm

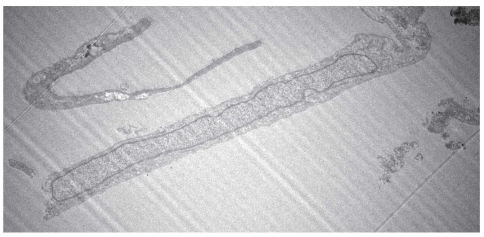

PP10new_b_8.10.13/Image 1_3k
cell height: 2.1 µm
distance to nucleus from top: 0.35 µm
distance to nucleus from bottom: 0.4 µm
nucleus height: 1.2 µm
nucleus length: 20.2 µm
cell length: 26 µm

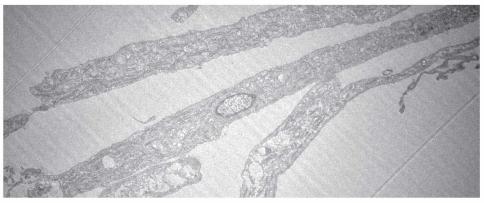

PP10new_b_8.10.13/Image 2_3k
cell height: 2 µm
distance to nucleus from top: 0.5 µm
distance to nucleus from bottom: 0.3 µm
nucleus height: 1 µm
nucleus length: 2.2 µm
cell length: 29.8 µm

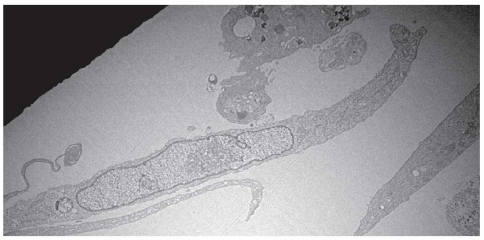

PP10new_b_8.10.13/Image19_3k
cell height: 2.8 µm
distance to nucleus from top: 0.2 µm
distance to nucleus from bottom: 0.3 µm
nucleus height: 2.3 µm
nucleus length: 13.1 µm
cell length: 26.3 µm

FIGURE A.10 TEM images of cells obtained from a progeria patient

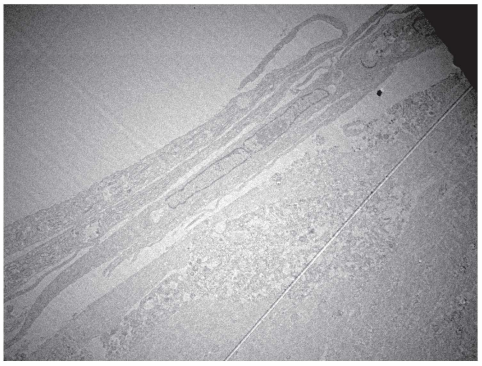

PP10new_b_8.10.13/Image 20_3k
cell height: 2.1 µm
distance to nucleus from top: 0.3 µm
distance to nucleus from bottom: 0.7 µm
nucleus height: 1 µm
nucleus length: 11.4 µm
cell length: 33.8 µm

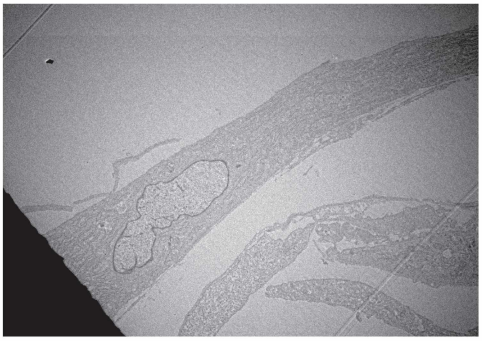

PP10new_b_8.10.13/Image 32_3k
cell height: 5.8 µm
distance to nucleus from top: 0.7 µm
distance to nucleus from bottom: 1.7 µm
nucleus height: 2.4 µm
nucleus length: 8.9 µm
cell length: 25.7 µm

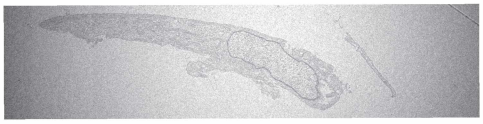

PP10new_b_8.10.13/Image 54_3k
cell height: 2.6 µm
distance to nucleus from top: 0.6 µm
distance to nucleus from bottom: 0.3 µm
nucleus height: 1.6 µm
nucleus length: 6.2 µm
cell length: 17 µm

FIGURE A.11 TEM images of cells obtained from a progeria patient

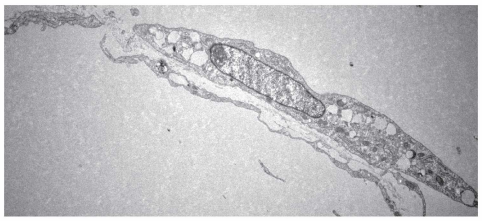

YP10_9.10.13/Image 22_3k
cell height: 2.8 µm
distance to nucleus from top: 0.8 µm
distance to nucleus from bottom: 0.3 µm
nucleus height: 1.6 µm
nucleus length: 7.6 µm
cell length: 22.4 µm

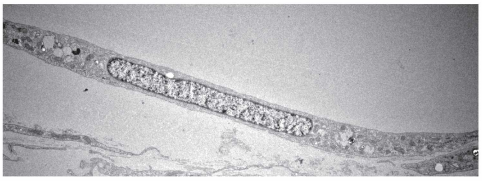

YP10_9.10.13/Image 37_3k
cell height: 1.8 µm
distance to nucleus from top: 0.3 µm
distance to nucleus from bottom: 0.3 µm
nucleus height: 1.1 µm
nucleus length: 12.4 µm
cell length: 28.5 µm

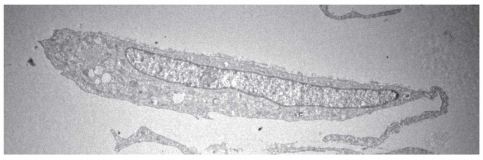

YP11_9.10.13/Image 02_3k
cell height: 3.3 µm
distance to nucleus from top: 0.7 µm
distance to nucleus from bottom: 1.5, 0.7 µm
nucleus height: 1.2 µm
nucleus length: 16 µm
cell length: 22 µm

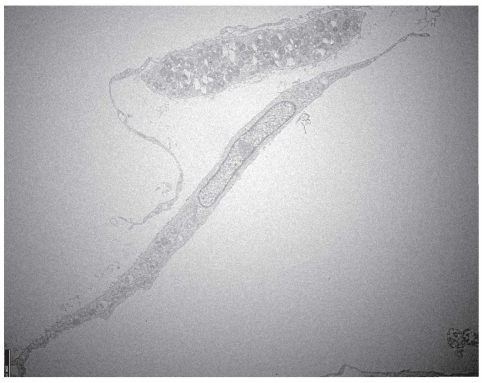

YP11_9.10.13/Image 16_3k
cell height: 1.8 µm
distance to nucleus from top: 0.3 µm
distance to nucleus from bottom: 0.3 µm
nucleus height: 1.1 µm
nucleus length: 7.9 µm
cell length: 30.9 µm

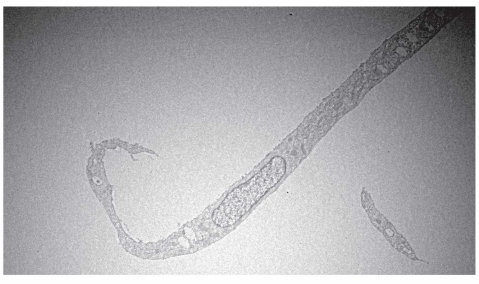

YP11_9.10.13/Image 23_3k
cell height: 1.8 µm
distance to nucleus from top: 0.25 µm
distance to nucleus from bottom: 0.23 µm
nucleus height: 1.4 µm
nucleus length: 5.4 µm
cell length: 26.3 µm

FIGURE A.12 TEM images of cells obtained from a young person

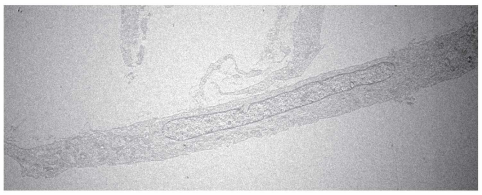

YP11_9.10.13/Image 44_3k
cell height: 2.5 µm
distance to nucleus from top: 0.5 µm
distance to nucleus from bottom: 1 µm
nucleus height: 1 µm
nucleus length: 14 µm
cell length: 28 µm

YP11_9.10.13/Image 30_3k
cell height: 2.3 µm
distance to nucleus from top: 0.3 µm
distance to nucleus from bottom: 0.5 µm
nucleus height: 1 µm
nucleus length: 22.6 µm
cell length: 31.5 µm

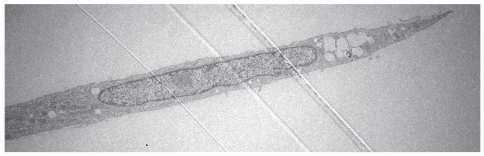

YP11_18.07.13/Image 39_3k
cell height: 2.3 µm
distance to nucleus from top: 0.4 µm
distance to nucleus from bottom: 0.3 µm
nucleus height: 1.5 µm
nucleus length: 12.9 µm
cell length: 26.6 µm

YP11_18.07.13/Image 40_3k
cell height: 3 µm
distance to nucleus from top: 0.5 µm
distance to nucleus from bottom: 0.54 µm
nucleus height: 1.9 µm
nucleus length: 7 µm

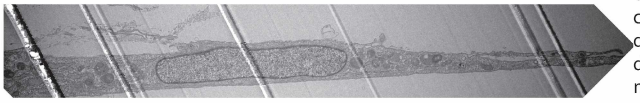

YP11_9.10.13/Image 23_3k
cell height: 2.5 µm
distance to nucleus from top: 0.5 µm
distance to nucleus from bottom: 0.4 µm
nucleus height: 1.7 µm
nucleus length: 11 µm
cell length: 38.2 µm

FIGURE A.13 TEM images of cells obtained from a young person

A.5 Phase contrast images of the isolated nuclei used for AFM data acquisition

The representative phase contrast images of the isolated nuclei on which AFM data were recorded are shown in the following panels. Note that the nuclei of progeria cells retained their shape even after isolation from cytoplasmic components. The scale bar in each panel denotes 20 µm.

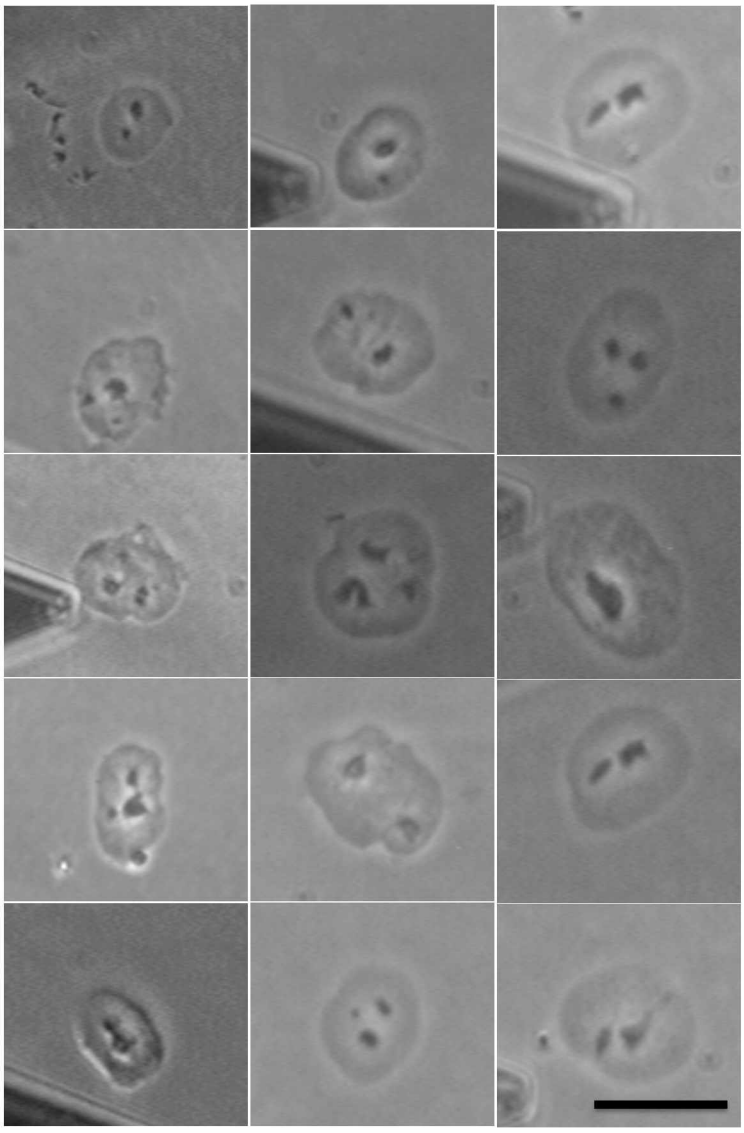

FIGURE A.14 Nuclei isolated from dermal fibroblasts of the old person.

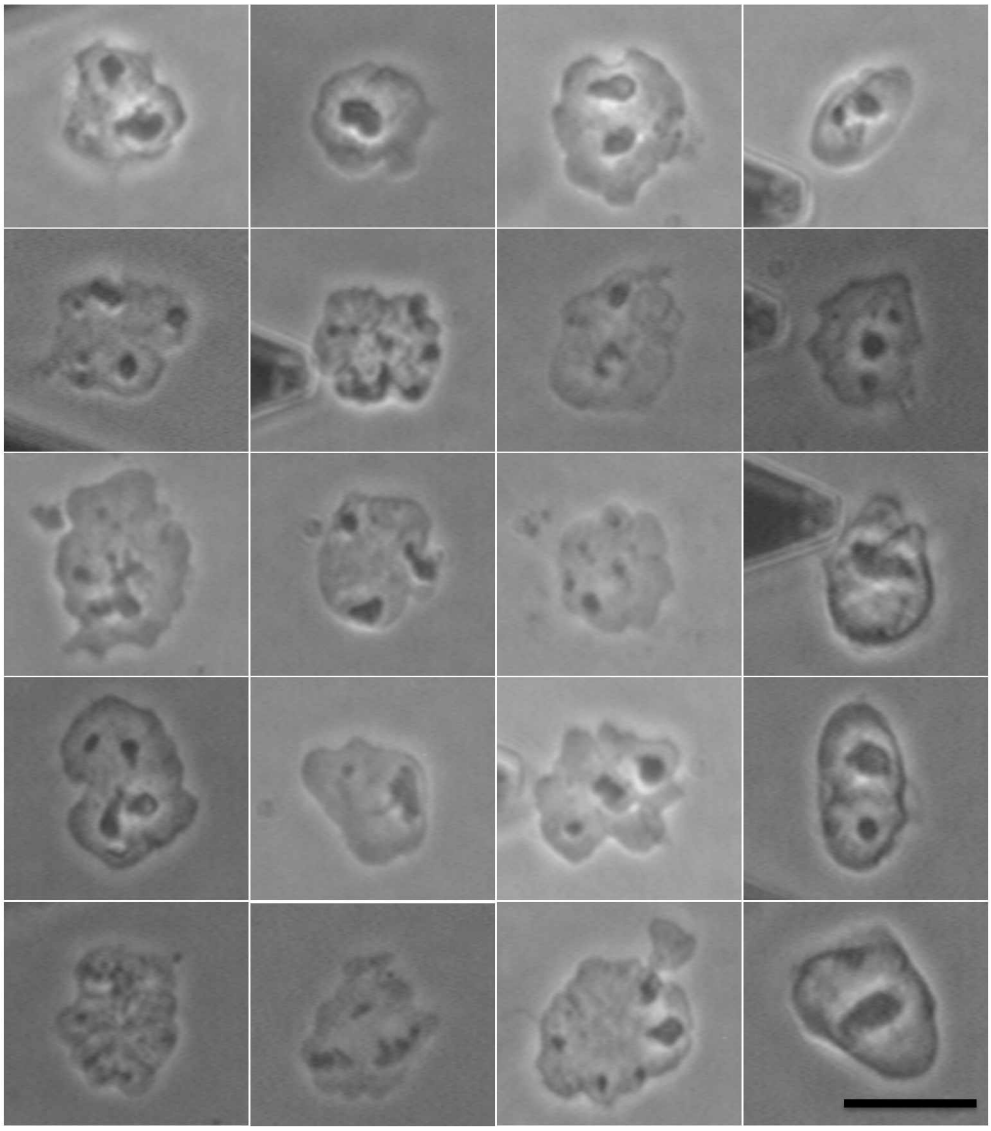

FIGURE A.15 Nuclei isolated from dermal fibroblasts of the progeria patient.

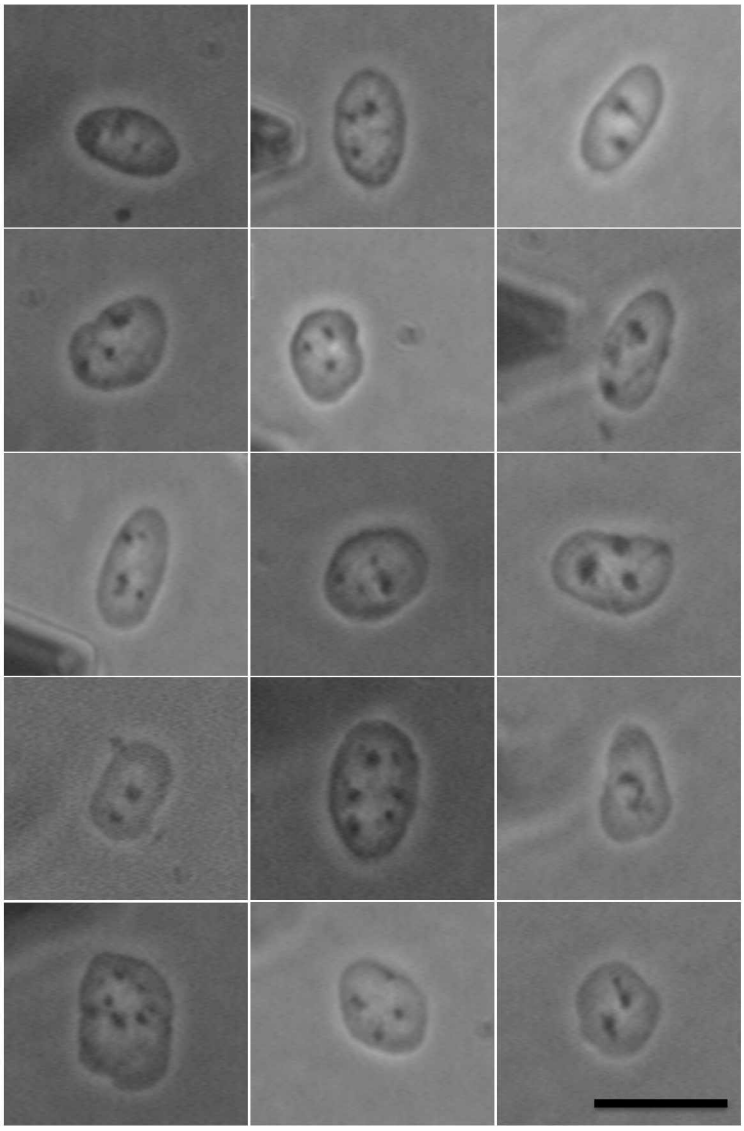

FIGURE A.16 Nuclei isolated from dermal fibroblasts of the young person.

A.6 Experimental data for selection of nuclear and cytoplasmic regions on the basis of sample z height

To assess the mechanical properties of the nuclear region of the cells, the corresponding Log E values could be selected roughly, on the basis of the sample height z recorded while obtaining force curves. From each force map, the z height points corresponding only to the nuclear region (top of cell to periphery of nucleus) were selected and an average of the Log E from only these data points was calculated. The stiffness of the nuclear region of each cell is thus represented by the average Log E values of selected data points.

For analyzing the stiffnesses of only the cytoplasmic region of the cells, an approximate z height range was chosen from the base of the cell till the periphery of the nucleus, excluding data of the nuclear region and the substrate. The average Log E of these selected data points represents the stiffness of cytoplasmic region of each cell. The experimental data for each force map of each experiment is given here. OP denotes old person, PP denotes progeria patient, YP denotes young person. Each number indicates the corresponding file name of each force volume. In each reading, lower height and upper height values represent the selected z range corresponding to either nuclear region or cytoplasmic region. datapoints indicates the total number of force curves in that range. Average is the Log E average value calculated from only those force curves in the range along with the standard deviation (Stand. dev.).

Nuclear region

OP14
0268
 lower height: 1.81711e-06
 upper height: 2.60868e-06
 datapoints: 114
 Average: 4.06368
 Stand. dev.: 0.293283
0552
 lower height: 8.27343e-07
 upper height: 1.35949e-06
 datapoints: 59
 Average: 3.87675
 Stand. dev.: 0.147817
0836
 lower height: 8.16793e-07
 upper height: 2.61646e-06
 datapoints: 184
 Average: 3.78838
 Stand. dev.: 0.172449
1125
 lower height: -8.73495e-07
 upper height: 9.90283e-07
 datapoints: 111
 Average: 3.80372
 Stand. dev.: 0.240815
1440
 lower height: -1.1253e-08
 upper height: 1.24156e-06
 datapoints: 62
 Average: 3.39467
 Stand. dev.: 0.307878
1573
 lower height: 1.46381e-07
 upper height: 1.25935e-06
 datapoints: 32
 Average: 3.3196
 Stand. dev.: 0.221064
0175
 lower height: -4.12302e-07
 upper height: 2.64928e-06
 datapoints: 146
 Average: 3.42691
 Stand. dev.: 0.565163
0261
 lower height: -1.88456e-06
 upper height: 8.87069e-07
 datapoints: 73
 Average: 3.38512
 Stand. dev.: 0.333758
0383
 lower height: 2.87344e-07
 upper height: 1.8517e-06
 datapoints: 38
 Average: 3.36275
 Stand. dev.: 0.442252
0608
 lower height: -1.05068e-06
 upper height: 2.43738e-06
 datapoints: 141
 Average: 3.63906
 Stand. dev.: 0.304727
0761
 lower height: 3.56151e-07
 upper height: 1.70502e-06
 datapoints: 180
 Average: 3.64195
 Stand. dev.: 0.166447

OP15
0118
 lower height: -2.22449e-06
 upper height: 2.40244e-07
 datapoints: 188
 Average: 3.65903
 Stand. dev.: 0.212941
0302
 lower height: 1.46193e-07
 upper height: 2.4278e-06
 datapoints: 119
 Average: 3.61774
 Stand. dev.: 0.3152
0603
 lower height: 1.74636e-06
 upper height: 2.88941e-06
 datapoints: 99
 Average: 3.93874
 Stand. dev.: 0.209509
0683
 lower height: 3.32127e-07
 upper height: 2.01214e-06
 datapoints: 122
 Average: 3.62713
 Stand. dev.: 0.26649
0769
 lower height: -2.29641e-07
 upper height: 1.01527e-06
 datapoints: 78
 Average: 3.92655
 Stand. dev.: 0.287453
0994
 lower height: -2.07368e-06
 upper height: -7.74894e-07
 datapoints: 152
 Average: 4.19096
 Stand. dev.: 0.263819
1122
 lower height: -6.37783e-08
 upper height: 2.64843e-06
 datapoints: 109
 Average: 3.95237
 Stand. dev.: 0.320655
1299
 lower height: 7.44804e-07
 upper height: 3.74444e-06
 datapoints: 35
 Average: 3.30122
 Stand. dev.: 0.163085

OP16
0199
 lower height: -4.52019e-06
 upper height: 4.54922e-07
 datapoints: 124
 Average: 3.29036
 Stand. dev.: 0.361452
0364
 lower height: 5.13855e-07
 upper height: 1.82723e-06
 datapoints: 161
 Average: 3.54029
 Stand. dev.: 0.188308
0520
 lower height: 1.05956e-06
 upper height: 2.94644e-06
 datapoints: 144
 Average: 4.02234
 Stand. dev.: 0.380736
0672
 lower height: -1.74118e-06
 upper height: 9.9596e-07
 datapoints: 117
 Average: 3.80048
 Stand. dev.: 0.394244
0902
 lower height: 1.86017e-06
 upper height: 3.16036e-06
 datapoints: 107
 Average: 3.40404
 Stand. dev.: 0.165288
1057
 lower height: -2.11523e-06
 upper height: 3.03191e-07
 datapoints: 127
 Average: 3.71049
 Stand. dev.: 0.444618
1205
 lower height: -1.16807e-06
 upper height: 1.05597e-06
 datapoints: 136
 Average: 3.80802
 Stand. dev.: 0.394454
1314
 lower height: 1.32527e-06
 upper height: 2.1243e-06
 datapoints: 106
 Average: 4.31418
 Stand. dev.: 0.169256
1418
 lower height: 2.24798e-06
 upper height: 3.56773e-06
 datapoints: 54
 Average: 3.65209
 Stand. dev.: 0.294274
1660
lower height: 7.54278e-07
 upper height: 2.09601e-06
 datapoints: 190
 Average: 4.18635
 Stand. dev.: 0.225596
1914
 lower height: 9.01612e-07
 upper height: 1.98048e-06
 datapoints: 128
 Average: 4.02284
 Stand. dev.: 0.115866

OP17
1454
 lower height: -2.03615e-06
 upper height: 6.5961e-08
 datapoints: 166
 Average: 3.85881
 Stand. dev.: 0.173915
1551
 lower height: 1.46993e-06
 upper height: 2.93279e-06
 datapoints: 191
 Average: 3.83296
 Stand. dev.: 0.139488
1691
 lower height: 2.17707e-06
 upper height: 3.56428e-06
 datapoints: 146
 Average: 4.11872
 Stand. dev.: 0.252706
1760
 lower height: 1.32586e-07
 upper height: 2.63816e-06
 datapoints: 168
 Average: 4.31102
 Stand. dev.: 0.4619
1869
 lower height: 1.7219e-06
 upper height: 3.85942e-06
 datapoints: 144
 Average: 3.72986
 Stand. dev.: 0.406921
1953

lower height: 1.25976e-06
upper height: 2.76078e-06
datapoints: 118
Average: 3.383
Stand. dev.: 0.131782
2086
lower height: -1.10289e-06
upper height: 1.30893e-06
datapoints: 38
Average: 2.76533
Stand. dev.: 0.183737
2207
lower height: -6.73744e-07
upper height: 1.69774e-06
datapoints: 99
Average: 3.14693
Stand. dev.: 0.169898

OP18
0164
lower height: -7.34244e-07
upper height: 2.46133e-06
datapoints: 127
Average: 3.30711
Stand. dev.: 0.42388
0622
lower height: -1.1594e-06
upper height: -1.3981e-07
datapoints: 157
Average: 4.2739
Stand. dev.: 0.298699
0767
lower height: -1.88954e-06
upper height: 8.79969e-07
datapoints: 42
Average: 3.93593
Stand. dev.: 0.481901
0857
lower height: -3.44687e-06
upper height: 1.12015e-06
datapoints: 45
Average: 3.03833
Stand. dev.: 0.458195
0966
lower height: 1.87384e-06
upper height: 3.46161e-06
datapoints: 113
Average: 4.11013
Stand. dev.: 0.305056
1054
lower height: 6.80004e-07
upper height: 2.4107e-06
datapoints: 138
Average: 3.29884
Stand. dev.: 0.18875
1264
lower height: -4.35318e-07
upper height: 1.58613e-06
datapoints: 121
Average: 3.26918
Stand. dev.: 0.241895
1364
lower height: 2.21601e-06
upper height: 3.44285e-06
datapoints: 102
Average: 3.95692
Stand. dev.: 0.302731
1448
lower height: -1.31723e-06
upper height: -9.59246e-09
datapoints: 116
Average: 3.77836
Stand. dev.: 0.305703
1551
lower height: -1.09711e-06
upper height: 1.07463e-06
datapoints: 77
Average: 3.14654
Stand. dev.: 0.354529

OP19
0197
lower height: -3.58027e-07
upper height: 2.05662e-06
datapoints: 115
Average: 4.12957
Stand. dev.: 0.353728
0324
lower height: -3.98042e-06
upper height: -2.82264e-06
datapoints: 173
Average: 4.24779
Stand. dev.: 0.502161
0424
lower height: -1.3096e-06
upper height: -1.20507e-09
datapoints: 149
Average: 3.83666
Stand. dev.: 0.166956
0534
lower height: 7.61735e-08
upper height: 2.85069e-06
datapoints: 90
Average: 2.95683
Stand. dev.: 0.213222
0620
lower height: 2.16453e-06
upper height: 3.62678e-06
datapoints: 175
Average: 3.70679
Stand. dev.: 0.261936
0698
lower height: 9.95225e-07
upper height: 3.53534e-06
datapoints: 64
Average: 4.02665
Stand. dev.: 0.543588
0768
lower height: 6.11957e-08
upper height: 2.20854e-06
datapoints: 144
Average: 3.77742
Stand. dev.: 0.279973
0839
lower height: 9.75163e-09
upper height: 3.1118e-06
datapoints: 246
Average: 3.44928
Stand. dev.: 0.230401
0922
lower height: 1.72904e-06
upper height: 2.78504e-06
datapoints: 119
Average: 4.31988
Stand. dev.: 0.186495

PP10old
0558
lower height: -1.63362e-06
upper height: -1.20225e-07
datapoints: 174
Average: 4.16249
Stand. dev.: 0.454952
0711
lower height: -1.91043e-06
upper height: 1.17944e-06
datapoints: 147
Average: 3.59577
Stand. dev.: 0.305917
1036
lower height: -2.43278e-06
upper height: 3.00886e-08
datapoints: 146
Average: 3.53661
Stand. dev.: 0.226115
1211
lower height: -2.3763e-06
upper height: -8.33301e-07
datapoints: 119
Average: 4.08959
Stand. dev.: 0.258585
1355
lower height: -2.12533e-06
upper height: 1.0365e-06
datapoints: 246
Average: 3.30014
Stand. dev.: 0.297182
1498
lower height: 1.62105e-06
upper height: 3.18493e-06
datapoints: 290
Average: 3.62195
Stand. dev.: 0.261738
1596
lower height: -9.36616e-07
upper height: 1.43735e-06
datapoints: 206
Average: 3.5647
Stand. dev.: 0.273264
1833
lower height: -1.24579e-06
upper height: 7.51504e-07
datapoints: 132
Average: 3.63473
Stand. dev.: 0.411059
1972
lower height: -2.89529e-07
upper height: 1.8662e-06
datapoints: 104
Average: 3.75499
Stand. dev.: 0.215442
2128
lower height: 1.75844e-06
upper height: 3.32456e-06
datapoints: 247
Average: 3.95346
Stand. dev.: 0.268671

PP10new
0092
lower height: -3.89839e-06
upper height: -1.53444e-06
datapoints: 232
Average: 3.4954
Stand. dev.: 0.215539
0309
low er height: 1.05228e-06
upper height: 2.79791e-06
datapoints: 160
Average: 3.52158
Stand. dev.: 0.372216
0463
lower height: 4.01152e-07
upper height: 2.46398e-06
datapoints: 83
Average: 3.73877
Stand. dev.: 0.200416
0627
lower height: 8.10652e-07
upper height: 2.4578e-06
datapoints: 149

Average: 3.58959
Stand. dev.: 0.220949
0823
lower height: 2.16419e-06
upper height: 3.0384e-06
datapoints: 120
Average: 3.55793
Stand. dev.: 0.192368
1186
lower height: 2.45095e-08
upper height: 2.65612e-06
datapoints: 198
Average: 3.22569
Stand. dev.: 0.129993
1396
lower height: -9.68459e-07
upper height: 1.44942e-06
datapoints: 144
Average: 3.5676
Stand. dev.: 0.278525
1582
lower height: 1.18073e-06
upper height: 3.05192e-06
datapoints: 117
Average: 3.03302
Stand. dev.: 0.157623

PP11
0399
lower height: 1.08626e-06
upper height: 2.52947e-06
datapoints: 40
Average: 3.59649
Stand. dev.: 0.516997
0656
lower height: 1.90508e-06
upper height: 3.0723e-06
datapoints: 124
Average: 4.55194
Stand. dev.: 0.209031
1027
lower height: -4.63728e-07
upper height: 9.77371e-07
datapoints: 162
Average: 3.78738
Stand. dev.: 0.566099
1257
lower height: 1.36848e-06
upper height: 2.95934e-06
datapoints: 157
Average: 3.82676
Stand. dev.: 0.362471
1525
lower height: -1.18205e-06
upper height: 1.26312e-06
datapoints: 98
Average: 3.0278
Stand. dev.: 0.260295
1721
lower height: 2.90253e-07
upper height: 2.60758e-06
datapoints: 122
Average: 3.3646
Stand. dev.: 0.42684
1926
lower height: 6.91227e-07
upper height: 2.92986e-06
datapoints: 178
Average: 3.61209
Stand. dev.: 0.509763
2129
lower height: 1.33258e-06
upper height: 3.39403e-06
datapoints: 303

Average: 3.48964
Stand. dev.: 0.741249
2318
lower height: 3.80054e-06
upper height: 4.81017e-06
datapoints: 288
Average: 4.16084
Stand. dev.: 0.449301
2504
lower height: 1.64011e-06
upper height: 3.52367e-06
datapoints: 113
Average: 3.501
Stand. dev.: 0.317434
2694
lower height: -5.51429e-08
upper height: 1.86678e-06
datapoints: 177
Average: 3.26772
Stand. dev.: 0.516844

PP12
0203
lower height: 4.215e-07
upper height: 2.16744e-06
datapoints: 116
Average: 3.55175
Stand. dev.: 0.342692
0357
lower height: -5.54412e-09
upper height: 3.15874e-06
datapoints: 141
Average: 3.97485
Stand. dev.: 0.709893
0359
lower height: -2.73155e-07
upper height: 2.99056e-06
datapoints: 261
Average: 4.30944
Stand. dev.: 0.671922
0585
lower height: -1.73487e-08
upper height: 1.90133e-06
datapoints: 114
Average: 4.51873
Stand. dev.: 0.305095
0865
lower height: -9.60321e-08
upper height: 1.4351e-06
datapoints: 191
Average: 4.07967
Stand. dev.: 0.7685
1148
lower height: 3.47523e-06
upper height: 4.11688e-06
datapoints: 192
Average: 5.11425
Stand. dev.: 0.513718
1327
lower height: -6.40825e-07
upper height: 2.08786e-06
datapoints: 123
Average: 3.66649
Stand. dev.: 0.628285
1520
lower height: 5.86547e-07
upper height: 1.94155e-06
datapoints: 291
Average: 4.67904
Stand. dev.: 0.243748
1673
lower height: 3.50263e-07
upper height: 2.41316e-06
datapoints: 131

Average: 3.353
Stand. dev.: 0.348512
1918
lower height: 4.24865e-06
upper height: 5.21675e-06
datapoints: 240
Average: 5.14565
Stand. dev.: 0.297189
1920
lower height: 4.018e-06
upper height: 5.11398e-06
datapoints: 164
Average: 5.35448
Stand. dev.: 0.240468
2226
lower height: 3.05717e-07
upper height: 2.71943e-06
datapoints: 81
Average: 3.4616
Stand. dev.: 0.379929
2375
lower height: -7.81371e-07
upper height: 2.02184e-06
datapoints: 221
Average: 3.52548
Stand. dev.: 0.475567

PP13
0124
lower height: 2.09385e-06
upper height: 2.88992e-06
datapoints: 170
Average: 4.75469
Stand. dev.: 0.470006
0231
lower height: 2.44888e-06
upper height: 3.02206e-06
datapoints: 166
Average: 4.74828
Stand. dev.: 0.395909
0477
lower height: 1.26263e-06
upper height: 3.11685e-06
datapoints: 120
Average: 3.9399
Stand. dev.: 0.26781
0663
lower height: -5.34891e-06
upper height: -4.06562e-06
datapoints: 195
Average: 4.32882
Stand. dev.: 0.161211
0824
lower height: 1.57908e-06
upper height: 2.7366e-06
datapoints: 261
Average: 4.01052
Stand. dev.: 0.116374
1014
lower height: 3.87633e-07
upper height: 2.81649e-06
datapoints: 286
Average: 4.13602
Stand. dev.: 0.308375
1533
lower height: 1.96788e-06
upper height: 3.1543e-06
datapoints: 154
Average: 3.57978
Stand. dev.: 0.175182
1754
lower height: 1.59855e-06
upper height: 3.08838e-06
datapoints: 200

Average: 4.32934
Stand. dev.: 0.287293
1973
lower height: 1.87373e-06
upper height: 2.50938e-06
datapoints: 120
Average: 4.28762
Stand. dev.: 0.201986
2135
lower height: 1.25728e-06
upper height: 2.95302e-06
datapoints: 194
Average: 3.51586
Stand. dev.: 0.209725
2304
lower height: 2.69625e-06
upper height: 3.43011e-06
datapoints: 186
Average: 3.8456
Stand. dev.: 0.165825
2449
lower height: -1.35256e-07
upper height: 9.60124e-07
datapoints: 155
Average: 3.74012
Stand. dev.: 0.277926
2603
lower height: -1.1282e-06
upper height: 1.22188e-06
datapoints: 240
Average: 3.35066
Stand. dev.: 0.221015

PP9
0180
lower height: -3.26577e-06
upper height: 1.46467e-06
datapoints: 171
Average: 3.68232
Stand. dev.: 0.384917
0352
lower height: -1.5454e-06
upper height: -6.29978e-08
datapoints: 199
Average: 3.78964
Stand. dev.: 0.193211
0539
lower height: 1.50117e-06
upper height: 2.09977e-06
datapoints: 105
Average: 3.82724
Stand. dev.: 0.440274
0691
lower height: 1.39913e-06
upper height: 2.37254e-06
datapoints: 58
Average: 3.58765
Stand. dev.: 0.276197
0874
lower height: -2.32406e-06
upper height: 3.98547e-08
datapoints: 117
Average: 3.74239
Stand. dev.: 0.290289
1042
lower height: 7.06681e-08
upper height: 1.96324e-06
datapoints: 215
Average: 3.83485
Stand. dev.: 0.303436

YP10
0436
lower height: -7.63269e-07
upper height: 9.61938e-07
datapoints: 91
Average: 3.91366
Stand. dev.: 0.273871
0528
lower height: -1.63302e-06
upper height: 3.98545e-07
datapoints: 56
Average: 3.76091
Stand. dev.: 0.407939
0643
lower height: -1.81411e-06
upper height: -5.68614e-07
datapoints: 52
Average: 3.69516
Stand. dev.: 0.313629
0780
lower height: -1.8803e-06
upper height: -6.25113e-07
datapoints: 58
Average: 3.92135
Stand. dev.: 0.272499
0891
lower height: -1.22596e-06
upper height: 3.38822e-07
datapoints: 73
Average: 3.65052
Stand. dev.: 0.442803
1039
lower height: 2.68043e-06
upper height: 3.65397e-06
datapoints: 111
Average: 3.76623
Stand. dev.: 0.175702
1140
lower height: 6.97272e-07
upper height: 2.11376e-06
datapoints: 67
Average: 3.8042
Stand. dev.: 0.271665
1313
lower height: -1.94645e-06
upper height: 1.21228e-06
datapoints: 107
Average: 3.59723
Stand. dev.: 0.261947

YP11
0757
lower height: 3.77989e-06
upper height: 4.65981e-06
datapoints: 80
Average: 4.2598
Stand. dev.: 0.346084
0906
lower height: 1.56268e-06
upper height: 2.1678e-06
datapoints: 60
Average: 3.56332
Stand. dev.: 0.231048
0933
lower height: 1.72051e-06
upper height: 2.86029e-06
datapoints: 187
Average: 4.17897
Stand. dev.: 0.342961
1038
lower height: 1.36548e-06
upper height: 2.19762e-06
datapoints: 234
Average: 4.11341
Stand. dev.: 0.268646
1206
lower height: 7.51423e-07
upper height: 1.93792e-06
datapoints: 125
Average: 3.39415
Stand. dev.: 0.256059
0237
lower height: 3.36836e-06
upper height: 4.42957e-06
datapoints: 163
Average: 4.00413
Stand. dev.: 0.270436
0376
lower height: 1.95319e-06
upper height: 2.95116e-06
datapoints: 54
Average: 3.94146
Stand. dev.: 0.202753
0543
lower height: 1.77397e-06
upper height: 3.41222e-06
datapoints: 229
Average: 4.02398
Stand. dev.: 0.213662
0741
lower height: 4.14625e-06
upper height: 4.82135e-06
datapoints: 130
Average: 4.08848
Stand. dev.: 0.228896
0882
lower height: -1.4677e-07
upper height: 1.18508e-06
datapoints: 115
Average: 4.12971
Stand. dev.: 0.26036
1153
lower height: 1.97753e-06
upper height: 3.04218e-06
datapoints: 126
Average: 4.14315
Stand. dev.: 0.370479
1222
lower height: 2.33732e-06
upper height: 3.02416e-06
datapoints: 108
Average: 4.10936
Stand. dev.: 0.373582

YP12
0160
lower height: 1.43219e-06
upper height: 2.90346e-06
datapoints: 76
Average: 4.04574
Stand. dev.: 0.358137
0347
lower height: 1.03091e-06
upper height: 2.04977e-06
datapoints: 108
Average: 4.18595
Stand. dev.: 0.340894
0479
lower height: 2.03284e-06
upper height: 2.91925e-06
datapoints: 89
Average: 4.18787
Stand. dev.: 0.279486
0575
lower height: 1.01899e-06
upper height: 1.93228e-06
datapoints: 80
Average: 3.97142
Stand. dev.: 0.283765
0701
lower height: 8.51878e-07

upper height: 2.63677e-06
datapoints: 61
Average: 3.4931
Stand. dev.: 0.180831
0801
lower height: 2.29299e-06
upper height: 3.37741e-06
datapoints: 141
Average: 3.96103
Stand. dev.: 0.240741
0970
lower height: -3.20523e-06
upper height: -7.11053e-07
datapoints: 69
Average: 3.53075
Stand. dev.: 0.348266

YP13
0172
lower height: 1.3467e-06
upper height: 2.97611e-06
datapoints: 126
Average: 4.17938
Stand. dev.: 0.184442
0324
lower height: 1.77738e-06
upper height: 3.28746e-06
datapoints: 89
Average: 3.76577
Stand. dev.: 0.296592
0460
lower height: 3.122e-06
upper height: 3.98121e-06
datapoints: 85
Average: 4.06522
Stand. dev.: 0.110137
0596
lower height: 1.8389e-06
upper height: 4.02637e-06
datapoints: 88
Average: 3.91684
Stand. dev.: 0.176381
0737
lower height: 1.33483e-06
upper height: 2.50371e-06
datapoints: 113
Average: 3.72002
Stand. dev.: 0.29267
0829
lower height: 2.21875e-06
upper height: 3.35806e-06
datapoints: 186
Average: 3.8256
Stand. dev.: 0.242433
0985
lower height: -5.15342e-06
upper height: -2.82222e-06
datapoints: 97
Average: 4.09908
Stand. dev.: 0.233192
1101
lower height: -3.2295e-06
upper height: -5.29132e-07
datapoints: 92
Average: 4.38588
Stand. dev.: 0.775434
1233
lower height: 8.68044e-07
upper height: 2.71857e-06
datapoints: 72
Average: 4.03358
Stand. dev.: 0.218151

YP14
0232
lower height: -5.69637e-07
upper height: 1.09089e-06
datapoints: 78
Average: 3.15527
Stand. dev.: 0.178917
0368
lower height: -1.2073e-06
upper height: 3.04318e-07
datapoints: 38
Average: 3.01099
Stand. dev.: 0.201121
0402
lower height: -3.12876e-07
upper height: 8.32148e-07
datapoints: 112
Average: 4.01129
Stand. dev.: 0.343278
0568
lower height: 2.35738e-06
upper height: 3.23482e-06
datapoints: 72
Average: 4.27491
Stand. dev.: 0.223725
0655
lower height: 2.29197e-06
upper height: 3.35132e-06
datapoints: 194
Average: 4.22765
Stand. dev.: 0.25398
0755
lower height: 9.44794e-07
upper height: 2.07668e-06
datapoints: 166
Average: 4.01615
Stand. dev.: 0.245642

YP15
0055
lower height: 1.16352e-06
upper height: 2.24318e-06
datapoints: 34
Average: 3.85257
Stand. dev.: 0.380768
0219
lower height: 2.99839e-07
upper height: 2.13067e-06
datapoints: 64
Average: 3.41392
Stand. dev.: 0.233981
0300
lower height: 9.4189e-07
upper height: 1.73676e-06
datapoints: 74
Average: 4.08708
Stand. dev.: 0.218425
0350
lower height: 6.87873e-07
upper height: 1.77104e-06
datapoints: 54
Average: 3.9164
Stand. dev.: 0.25987
0372
lower height: 2.27206e-06
upper height: 2.99014e-06
datapoints: 89
Average: 4.17827
Stand. dev.: 0.359289
0526
lower height: 1.99437e-06
upper height: 2.98692e-06
datapoints: 83
Average: 3.99183
Stand. dev.: 0.407851
0685
lower height: 2.09678e-06
upper height: 2.62482e-06
datapoints: 55
Average: 4.27038
Stand. dev.: 0.210502
0838
lower height: 1.25967e-06
upper height: 2.96713e-06
datapoints: 80
Average: 3.94411
Stand. dev.: 0.292843
1061
lower height: 2.99754e-06
upper height: 3.69096e-06
datapoints: 114
Average: 4.20642
Stand. dev.: 0.445736
1205
lower height: 3.08823e-06
upper height: 3.89104e-06
datapoints: 228
Average: 4.01681
Stand. dev.: 0.161338

YP7
2346
lower height: -2.61733e-06
upper height: -2.84059e-08
datapoints: 105
Average: 3.68667
Stand. dev.: 0.313351
2464
lower height: 6.89363e-07
upper height: 2.01872e-06
datapoints: 88
Average: 3.6054
Stand. dev.: 0.383528
2648
lower height: 4.67007e-07
upper height: 1.85256e-06
datapoints: 54
Average: 3.54527
Stand. dev.: 0.139562
2738
lower height: -5.01982e-06
upper height: -2.91307e-06
datapoints: 121
Average: 3.95047
Stand. dev.: 0.741044
3243
lower height: 5.90047e-07
upper height: 1.62152e-06
datapoints: 143
Average: 3.42863
Stand. dev.: 0.225063
3543
lower height: -5.29692e-06
upper height: -2.56898e-06
datapoints: 83
Average: 3.08422
Stand. dev.: 0.160849
3616
lower height: -1.27927e-06
upper height: 1.01057e-06
datapoints: 103
Average: 3.27927
Stand. dev.: 0.155532
3678
lower height: -7.61988e-07
upper height: 2.10832e-06
datapoints: 82
Average: 3.47509
Stand. dev.: 0.2085560026

YP8
0026
 lower height: 7.50423e-07
 upper height: 1.86099e-06
 datapoints: 87
 Average: 4.20398
 Stand. dev.: 0.379598
0191
 lower height: 8.26984e-07
 upper height: 2.0893e-06
 datapoints: 120
 Average: 3.168
 Stand. dev.: 0.763875
0358
 lower height: 2.40028e-06
 upper height: 3.86391e-06
 datapoints: 99
 Average: 4.13592
 Stand. dev.: 0.301521
0508
 lower height: 2.26209e-07
 upper height: 1.71253e-06
 datapoints: 62
 Average: 3.65147
 Stand. dev.: 0.209513
0675
 lower height: 2.69967e-06
 upper height: 4.02156e-06
 datapoints: 97
 Average: 3.63383
 Stand. dev.: 0.599251
1015
 lower height: 4.18613e-07
 upper height: 1.83458e-06
 datapoints: 117
 Average: 3.2108
 Stand. dev.: 0.769925

YP9
0222
 lower height: -8.68629e-07
 upper height: 8.10441e-07
 datapoints: 54
 Average: 3.86214
 Stand. dev.: 0.3713
0377
 lower height: 9.7782e-07
 upper height: 3.114e-06
 datapoints: 166
 Average: 3.69974
 Stand. dev.: 0.757804
0593
 lower height: 1.3838e-06
 upper height: 2.01492e-06
 datapoints: 43
 Average: 4.09648
 Stand. dev.: 0.218634
0715
 lower height: 8.53795e-07
 upper height: 1.71261e-06
 datapoints: 117
 Average: 4.02126
 Stand. dev.: 0.286122
0926
 lower height: -1.60949e-06
 upper height: 1.38878e-06
 datapoints: 80
 Average: 2.96412
 Stand. dev.: 0.513395
1059
 lower height: 3.97822e-07
 upper height: 1.44452e-06
 datapoints: 38
 Average: 4.01867
 Stand. dev.: 0.396088
1282
 lower height: -1.60973e-07
 upper height: 1.79793e-06
 datapoints: 49
 Average: 3.66533
 Stand. dev.: 0.625679
1545
 lower height: -2.37661e-06
 upper height: 1.94252e-06
 datapoints: 44
 Average: 3.29119
 Stand. dev.: 0.51629
1861
 lower height: 1.35883e-06
 upper height: 2.11869e-06
 datapoints: 48
 Average: 4.16908
 Stand. dev.: 0.172856
2056
 lower height: 8.89411e-07
 upper height: 2.50011e-06
 datapoints: 64
 Average: 3.35016
 Stand. dev.: 0.877526

Cytoplasmic region

OP14
0268
lower height: 2.55493e-06
upper height: 3.92932e-06
datapoints: 84
Average: 3.79895
Stand. dev.: 0.532245
0552
lower height: 1.35949e-06
upper height: 4.36198e-06
datapoints: 323
Average: 4.24682
Stand. dev.: 0.220667
0836
lower height: 2.61646e-06
upper height: 4.6686e-06
datapoints: 125
Average: 3.74648
Stand. dev.: 0.211873
1125
lower height: 9.97487e-07
upper height: 3.97224e-06
datapoints: 276
Average: 4.36626
Stand. dev.: 0.423557
1440
lower height: 1.24156e-06
upper height: 3.58999e-06
datapoints: 90
Average: 3.47666
Stand. dev.: 0.292826
1573
lower height: 1.25935e-06
upper height: 4.26283e-06
datapoints: 130
Average: 3.57689
Stand. dev.: 0.240147
0175
lower height: 2.60137e-06
upper height: 3.88646e-06
datapoints: 122
Average: 3.46747
Stand. dev.: 0.743905
0261
lower height: 8.87069e-07
upper height: 4.82711e-06
datapoints: 151
Average: 3.57171
Stand. dev.: 0.608546
0383
lower height: 1.84592e-06
upper height: 4.40095e-06
datapoints: 240
Average: 3.7737
Stand. dev.: 0.335715
0608
lower height: 2.43738e-06
upper height: 4.90816e-06
datapoints: 209
Average: 3.97963
Stand. dev.: 0.623748
0761
lower height: 1.74327e-06
upper height: 4.18131e-06
datapoints: 134
Average: 3.66334
Stand. dev.: 0.233997

OP15
0118
lower height: 2.40244e-07
upper height: 3.09766e-06
datapoints: 194
Average: 3.9333
Stand. dev.: 0.197077
0302
lower height: 2.4278e-06
upper height: 4.83482e-06
datapoints: 234
Average: 3.68892
Stand. dev.: 0.360125
0603
lower height: 2.88941e-06
upper height: 4.55571e-06
datapoints: 96
Average: 3.97606
Stand. dev.: 0.332192
0683
lower height: 2.15124e-06
upper height: 4.21731e-06
datapoints: 131
Average: 4.44982
Stand. dev.: 0.463377
0769
lower height: 1.1198e-06
upper height: 3.70245e-06
datapoints: 209
Average: 3.99705
Stand. dev.: 0.582711
0994
lower height: -6.61739e-07
upper height: 1.36278e-06
datapoints: 113
Average: 4.28024
Stand. dev.: 0.30452
1122
lower height: 2.64843e-06
upper height: 4.511e-06
datapoints: 121
Average: 4.14067
Stand. dev.: 0.429053
1299
lower height: 3.73758e-06
upper height: 6.13637e-06
datapoints: 343
Average: 4.21476
Stand. dev.: 0.623505
OP16
0199
lower height: 4.54922e-07
upper height: 5.77099e-06
datapoints: 210
Average: 3.72931
Stand. dev.: 0.344031
0364
lower height: 1.82723e-06
upper height: 4.93378e-06
datapoints: 139
Average: 3.7057
Stand. dev.: 0.339107
0520
lower height: 2.91784e-06
upper height: 5.66149e-06
datapoints: 161
Average: 4.24703
Stand. dev.: 0.452276
0672
lower height: 1.06979e-06
upper height: 3.03032e-06
datapoints: 125
Average: 4.13499
Stand. dev.: 0.39175
0902
lower height: 3.1502e-06
upper height: 5.817e-06
datapoints: 267
Average: 3.49828
Stand. dev.: 0.231139
1057
lower height: 3.03191e-07
upper height: 1.09322e-06
datapoints: 37
Average: 3.7736
Stand. dev.: 0.484873
1205
lower height: 1.06866e-06
upper height: 5.12848e-06
datapoints: 224
Average: 3.84786
Stand. dev.: 0.601808
1314
lower height: 2.11625e-06
upper height: 3.26739e-06
datapoints: 117
Average: 4.38287
Stand. dev.: 0.243766
1418
lower height: 3.59101e-06
upper height: 5.28433e-06
datapoints: 108
Average: 4.16288
Stand. dev.: 0.510731
1660
lower height: 2.06374e-06
upper height: 3.99393e-06
datapoints: 108
Average: 4.27181
Stand. dev.: 0.418533
1914
lower height: 1.90706e-06
upper height: 3.56731e-06
datapoints: 126
Average: 4.04809
Stand. dev.: 0.274011

OP17
1454
lower height: 6.5961e-08
upper height: 1.42845e-06
datapoints: 191
Average: 4.57325
Stand. dev.: 0.509451
1551
lower height: 2.93279e-06
upper height: 5.36196e-06
datapoints: 206
Average: 3.89039
Stand. dev.: 0.137001
1691
lower height: 3.59164e-06
upper height: 5.40882e-06
datapoints: 238
Average: 4.44214
Stand. dev.: 0.359627
1760
lower height: 2.64683e-06
upper height: 4.12926e-06
datapoints: 210
Average: 4.7247
Stand. dev.: 0.302552
1869
lower height: 3.85942e-06
upper height: 6.24299e-06
datapoints: 234
Average: 4.25368
Stand. dev.: 0.430152
1953
lower height: 2.76078e-06
upper height: 3.82717e-06

datapoints: 112
Average: 3.44712
Stand. dev.: 0.244793
2086
lower height: 1.30893e-06
upper height: 5.01156e-06
datapoints: 214
Average: 3.32493
Stand. dev.: 0.274809
2207
lower height: 1.64472e-06
upper height: 5.52212e-06
datapoints: 267
Average: 3.4951
Stand. dev.: 0.294412

OP18
0164
lower height: 2.40406e-06
upper height: 5.15675e-06
datapoints: 186
Average: 3.98406
Stand. dev.: 0.397029
0622
lower height: -1.68629e-07
upper height: 2.36258e-06
datapoints: 134
Average: 4.35935
Stand. dev.: 0.419034
0767
lower height: 8.79969e-07
upper height: 4.20426e-06
datapoints: 179
Average: 4.13842
Stand. dev.: 0.49842
0857
lower height: 1.21084e-06
upper height: 5.18154e-06
datapoints: 318
Average: 4.25532
Stand. dev.: 0.50624
0966
lower height: 3.44236e-06
upper height: 5.89734e-06
datapoints: 249
Average: 4.36085
Stand. dev.: 0.288633
1054
lower height: 2.55569e-06
upper height: 5.5694e-06
datapoints: 161
Average: 3.51991
Stand. dev.: 0.187035
1264
lower height: 1.47478e-06
upper height: 3.07154e-06
datapoints: 121
Average: 3.51159
Stand. dev.: 0.312003
1364
lower height: 3.40422e-06
upper height: 4.92423e-06
datapoints: 93
Average: 4.06524
Stand. dev.: 0.317942
1448
lower height: -9.59246e-09
upper height: 1.93233e-06
datapoints: 154
Average: 3.83822
Stand. dev.: 0.313129
1551
lower height: 1.0551e-06
upper height: 4.79586e-06
datapoints: 273
Average: 3.63193
Stand. dev.: 0.314591

OP19
0197
lower height: 2.08505e-06
upper height: 3.9562e-06
datapoints: 173
Average: 4.41915
Stand. dev.: 0.489811
0324
lower height: -2.75725e-06
upper height: 9.55412e-07
datapoints: 166
Average: 4.30468
Stand. dev.: 0.452866
0424
lower height: -1.20507e-09
upper height: 4.02064e-06
datapoints: 199
Average: 4.17359
Stand. dev.: 0.458802
0534
lower height: 2.82964e-06
upper height: 5.2726e-06
datapoints: 127
Average: 3.30382
Stand. dev.: 0.194235
0620
lower height: 3.66469e-06
upper height: 4.8089e-06
datapoints: 73
Average: 3.80429
Stand. dev.: 0.262014
0698
lower height: 3.54185e-06
upper height: 5.93378e-06
datapoints: 234
Average: 4.42294
Stand. dev.: 0.37456
0768
lower height: 2.20854e-06
upper height: 4.93479e-06
datapoints: 245
Average: 4.26275
Stand. dev.: 0.267642
0839
lower height: 3.18828e-06
upper height: 5.09212e-06
datapoints: 70
Average: 3.62639
Stand. dev.: 0.212702
0922
lower height: 2.76531e-06
upper height: 4.8002e-06
datapoints: 170
Average: 4.35778
Stand. dev.: 0.213876

PP10old
0558
lower height: -1.38377e-07
upper height: 2.07333e-06
datapoints: 61
Average: 4.05339
Stand. dev.: 0.444115
0711
lower height: 1.11524e-06
upper height: 3.91639e-06
datapoints: 100
Average: 3.82406
Stand. dev.: 0.392583
1036
lower height: 3.00886e-08
upper height: 4.29182e-06
datapoints: 221
Average: 3.52028
Stand. dev.: 0.606215
1211
lower height: -7.16524e-07
upper height: 3.93628e-06
datapoints: 247
Average: 3.57199
Stand. dev.: 0.580207
1355
lower height: 1.0365e-06
upper height: 5.49867e-06
datapoints: 147
Average: 3.40098
Stand. dev.: 0.305119
1498
lower height: 3.18189e-06
upper height: 5.52552e-06
datapoints: 78
Average: 3.74581
Stand. dev.: 0.230872
1596
lower height: 1.48963e-06
upper height: 4.79893e-06
datapoints: 157
Average: 3.90834
Stand. dev.: 0.303052
1833
lower height: 7.51504e-07
upper height: 3.97822e-06
datapoints: 155
Average: 3.82394
Stand. dev.: 0.443499
1972
lower height: 1.8662e-06
upper height: 4.81713e-06
datapoints: 125
Average: 3.44449
Stand. dev.: 0.394459
2128
lower height: 3.32741e-06
upper height: 5.28414e-06
datapoints: 62
Average: 4.01339
Stand. dev.: 0.396887

PP10new
0092
lower height: -1.53862e-06
upper height: 3.47662e-06
datapoints: 141
Average: 3.4665
Stand. dev.: 0.328969
0309
lower height: 2.75319e-06
upper height: 5.00328e-06
datapoints: 182
Average: 3.65377
Stand. dev.: 0.478422
0463
lower height: 2.46398e-06
upper height: 5.63426e-06
datapoints: 249
Average: 4.01567
Stand. dev.: 0.599665
0627
lower height: 2.4578e-06
upper height: 5.13232e-06
datapoints: 203
Average: 3.75245
Stand. dev.: 0.167526
0823

lower height: 3.05913e-06
upper height: 5.28242e-06
datapoints: 218
Average: 3.72291
Stand. dev.: 0.269985
1186
lower height: 2.69019e-06
upper height: 4.32122e-06
datapoints: 168
Average: 3.35809
Stand. dev.: 0.127189
1396
lower height: 1.44942e-06
upper height: 5.48398e-06
datapoints: 154
Average: 4.02057
Stand. dev.: 0.404859
1582
lower height: 2.97828e-06
upper height: 4.36851e-06
datapoints: 136
Average: 3.16805
Stand. dev.: 0.244604

PP11
0399
lower height: 2.52947e-06
upper height: 5.29183e-06
datapoints: 136
Average: 4.25049
Stand. dev.: 0.59957
0656
lower height: 3.05372e-06
upper height: 4.82941e-06
datapoints: 156
Average: 4.62724
Stand. dev.: 0.310407
1027
lower height: -9.15832e-07
upper height: 3.08455e-06
datapoints: 277
Average: 3.80078
Stand. dev.: 0.695659
1257
lower height: 2.96364e-06
upper height: 4.76107e-06
datapoints: 231
Average: 4.28506
Stand. dev.: 0.286211
1525
lower height: 1.26312e-06
upper height: 4.42077e-06
datapoints: 149
Average: 2.95965
Stand. dev.: 0.339637
1721
lower height: 2.68165e-06
upper height: 4.51626e-06
datapoints: 121
Average: 3.17441
Stand. dev.: 0.478077
1926
lower height: 2.92986e-06
upper height: 5.54401e-06
datapoints: 146
Average: 3.58596
Stand. dev.: 0.493133
2129
lower height: 3.39403e-06
upper height: 5.42831e-06
datapoints: 53
Average: 3.00159
Stand. dev.: 0.351543
2318
lower height: 4.87501e-06
upper height: 6.83433e-06
datapoints: 76
Average: 4.4328
Stand. dev.: 0.262114
2504
lower height: 3.37613e-06
upper height: 6.5123e-06
datapoints: 273
Average: 3.84086
Stand. dev.: 0.672394
2694
lower height: 1.90406e-06
upper height: 3.90192e-06
datapoints: 123
Average: 3.6849
Stand. dev.: 0.224814
PP12
0203
lower height: 2.19268e-06
upper height: 3.79681e-06
datapoints: 102
Average: 3.45295
Stand. dev.: 0.409081
0357
lower height: 3.16186e-06
upper height: 5.22524e-06
datapoints: 166
Average: 4.29851
Stand. dev.: 0.456065
0359
lower height: 2.98405e-06
upper height: 4.87942e-06
datapoints: 115
Average: 4.55458
Stand. dev.: 0.436028
0585
lower height: 2.0855e-06
upper height: 4.04706e-06
datapoints: 94
Average: 4.61614
Stand. dev.: 0.448442
0865
lower height: 1.42242e-06
upper height: 4.8882e-06
datapoints: 130
Average: 4.41388
Stand. dev.: 0.763558
1148
lower height: 4.11688e-06
upper height: 4.72867e-06
datapoints: 136
Average: 5.2985
Stand. dev.: 0.487452
1327
lower height: 2.15292e-06
upper height: 4.82418e-06
datapoints: 143
Average: 3.90787
Stand. dev.: 0.451871
1520
lower height: 2.01943e-06
upper height: 3.34988e-06
datapoints: 81
Average: 4.87925
Stand. dev.: 0.216036
1673
lower height: 2.40201e-06
upper height: 3.62053e-06
datapoints: 87
Average: 3.72065
Stand. dev.: 0.348109
1918
lower height: 5.21675e-06
upper height: 6.02466e-06
datapoints: 156
Average: 5.31582
Stand. dev.: 0.237931
1920
lower height: 5.35201e-06
upper height: 6.64582e-06
datapoints: 214
Average: 5.13365
Stand. dev.: 0.246375
2226
lower height: 2.85952e-06
upper height: 5.0665e-06
datapoints: 232
Average: 4.39178
Stand. dev.: 0.466331
2375
lower height: 2.12901e-06
upper height: 4.45461e-06
datapoints: 89
Average: 3.73983
Stand. dev.: 0.436053
PP13
0124
lower height: 2.75998e-06
upper height: 4.1644e-06
datapoints: 204
Average: 4.62944
Stand. dev.: 0.303725
0231
lower height: 3.16486e-06
upper height: 4.31725e-06
datapoints: 194
Average: 4.71467
Stand. dev.: 0.305813
0477
lower height: 3.16948e-06
upper height: 5.53703e-06
datapoints: 238
Average: 4.47725
Stand. dev.: 0.396346
0663
lower height: -4.06562e-06
upper height: -1.15896e-06
datapoints: 151
Average: 4.17244
Stand. dev.: 0.127074
0824
lower height: 2.7366e-06
upper height: 4.78084e-06
datapoints: 111
Average: 4.06724
Stand. dev.: 0.100673
1014
lower height: 2.80666e-06
upper height: 5.4921e-06
datapoints: 92
Average: 4.14418
Stand. dev.: 0.193329
1533
lower height: 3.1543e-06
upper height: 5.18131e-06
datapoints: 239
Average: 3.70662
Stand. dev.: 0.170134
1754
lower height: 3.06405e-06
upper height: 3.83354e-06
datapoints: 76
Average: 4.55816
Stand. dev.: 0.322022
1973
lower height: 2.59388e-06
upper height: 4.31815e-06

datapoints: 141
Average: 4.37257
Stand. dev.: 0.329434
2135
lower height: 2.90938e-06
upper height: 4.67294e-06
datapoints: 135
Average: 3.81347
Stand. dev.: 0.23435
2304
lower height: 3.41579e-06
upper height: 4.7654e-06
datapoints: 202
Average: 3.99593
Stand. dev.: 0.170802
2449
lower height: 9.76269e-07
upper height: 4.30236e-06
datapoints: 159
Average: 3.77032
Stand. dev.: 0.307325
2603
lower height: 1.22188e-06
upper height: 3.64479e-06
datapoints: 97
Average: 3.53676
Stand. dev.: 0.0920444
PP9
0180
lower height: 1.46467e-06
upper height: 3.92151e-06
datapoints: 96
Average: 3.82759
Stand. dev.: 0.406804
0352
lower height: -6.29978e-08
upper height: 4.1725e-06
datapoints: 171
Average: 3.93243
Stand. dev.: 0.198085
0539
lower height: 2.10827e-06
upper height: 4.85469e-06
datapoints: 228
Average: 4.14597
Stand. dev.: 0.473099
0691
lower height: 2.38878e-06
upper height: 3.71704e-06
datapoints: 87
Average: 3.67232
Stand. dev.: 0.295971
0874
lower height: 3.98547e-08
upper height: 2.40455e-06
datapoints: 104
Average: 3.87404
Stand. dev.: 0.378253
1042
lower height: 1.90039e-06
upper height: 3.73752e-06
datapoints: 109
Average: 3.90494
Stand. dev.: 0.291983

YP10
0436
lower height: 9.61938e-07
upper height: 3.19585e-06
datapoints: 65
Average: 4.14842
Stand. dev.: 0.343042
0528
lower height: 3.98545e-07
upper height: 2.95133e-06
datapoints: 143
Average: 4.89082
Stand. dev.: 1.59682
0643
lower height: -5.68614e-07
upper height: 1.1791e-06
datapoints: 116
Average: 4.97824
Stand. dev.: 1.47017
0780
lower height: -6.11147e-07
upper height: 3.02655e-06
datapoints: 206
Average: 4.97888
Stand. dev.: 1.00201
0891
lower height: 3.50272e-07
upper height: 2.67699e-06
datapoints: 85
Average: 3.79675
Stand. dev.: 0.447585
1039
lower height: 3.50748e-06
upper height: 5.02981e-06
datapoints: 143
Average: 4.08197
Stand. dev.: 0.382505
1140
lower height: 2.25104e-06
upper height: 4.10059e-06
datapoints: 61
Average: 4.00225
Stand. dev.: 0.267787
1313
lower height: 1.21228e-06
upper height: 3.70976e-06
datapoints: 134
Average: 4.019
Stand. dev.: 0.368323

YP11
0757
lower height: 4.65981e-06
upper height: 6.03559e-06
datapoints: 307
Average: 4.35146
Stand. dev.: 0.47552
0906
lower height: 2.11065e-06
upper height: 4.33588e-06
datapoints: 304
Average: 3.90946
Stand. dev.: 0.316834
0933
lower height: 2.81252e-06
upper height: 4.4791e-06
datapoints: 170
Average: 4.24257
Stand. dev.: 0.353395
1038
lower height: 2.10607e-06
upper height: 3.13444e-06
datapoints: 156
Average: 4.26538
Stand. dev.: 0.28039
1206
lower height: 2.14732e-06
upper height: 4.11001e-06
datapoints: 87
Average: 3.66875
Stand. dev.: 0.355167
0237
lower height: 4.47129e-06
upper height: 6.03095e-06
datapoints: 208
Average: 3.93871
Stand. dev.: 0.263501
0376
lower height: 3.12159e-06
upper height: 4.73431e-06
datapoints: 176
Average: 3.98556
Stand. dev.: 0.248024
0543
lower height: 3.50109e-06
upper height: 4.93276e-06
datapoints: 116
Average: 4.09464
Stand. dev.: 0.264484
0741
lower height: 4.9327e-06
upper height: 5.62396e-06
datapoints: 179
Average: 4.21454
Stand. dev.: 0.233895
0882
lower height: 1.23295e-06
upper height: 2.27987e-06
datapoints: 45
Average: 4.12606
Stand. dev.: 0.342739
1153
lower height: 3.07677e-06
upper height: 4.49437e-06
datapoints: 100
Average: 4.21488
Stand. dev.: 0.374121
1222
lower height: 3.03083e-06
upper height: 4.41789e-06
datapoints: 109
Average: 4.20494
Stand. dev.: 0.353497

YP12
0160
lower height: 3.0338e-06
upper height: 4.29267e-06
datapoints: 43
Average: 4.21884
Stand. dev.: 0.215371
0347
lower height: 2.33448e-06
upper height: 4.24342e-06
datapoints: 122
Average: 4.1061
Stand. dev.: 0.604832
0479
lower height: 2.93256e-06
upper height: 4.29699e-06
datapoints: 92
Average: 4.45888
Stand. dev.: 0.31945
0575
lower height: 2.11544e-06
upper height: 4.09679e-06
datapoints: 86
Average: 4.11771
Stand. dev.: 0.318777
0701
lower height: 2.69293e-06
upper height: 5.63314e-06
datapoints: 173
Average: 4.0891
Stand. dev.: 0.722492
0801

lower height: 3.39431e-06
upper height: 4.63576e-06
datapoints: 80
Average: 4.15893
Stand. dev.: 0.276264
0970
lower height: -6.12414e-07
upper height: 1.90869e-06
datapoints: 147
Average: 4.07842
Stand. dev.: 0.395313

YP13
0172
lower height: 2.97611e-06
upper height: 5.05786e-06
datapoints: 150
Average: 4.26295
Stand. dev.: 0.440537
0324
lower height: 3.28746e-06
upper height: 4.46607e-06
datapoints: 137
Average: 4.11152
Stand. dev.: 0.231755
0460
lower height: 4.02163e-06
upper height: 4.6322e-06
datapoints: 76
Average: 4.07383
Stand. dev.: 0.161097
0596
lower height: 4.02637e-06
upper height: 5.26994e-06
datapoints: 80
Average: 4.16523
Stand. dev.: 0.468577
0737
lower height: 2.50371e-06
upper height: 4.42643e-06
datapoints: 253
Average: 4.02506
Stand. dev.: 0.225692
0829
lower height: 3.35806e-06
upper height: 4.48141e-06
datapoints: 79
Average: 3.74038
Stand. dev.: 0.242531
0985
lower height: -2.76397e-06
upper height: 3.47569e-06
datapoints: 130
Average: 4.20897
Stand. dev.: 0.600482
1101
lower height: -5.29132e-07
upper height: 4.40821e-06
datapoints: 104
Average: 4.4538
Stand. dev.: 0.45652
1233
lower height: 2.73944e-06
upper height: 4.0845e-06
datapoints: 152
Average: 4.19886
Stand. dev.: 0.452869

YP14
0232
lower height: 1.09089e-06
upper height: 4.29502e-06
datapoints: 139
Average: 3.54569
Stand. dev.: 0.335589
0368
lower height: 4.85532e-07
upper height: 4.93429e-06
datapoints: 198
Average: 3.37312
Stand. dev.: 0.269076
0402
lower height: 8.32148e-07
upper height: 2.88055e-06
datapoints: 91
Average: 4.28967
Stand. dev.: 0.552117
0568
lower height: 3.23329e-06
upper height: 5.79473e-06
datapoints: 170
Average: 4.20543
Stand. dev.: 0.433005
0655
lower height: 2.88598e-06
upper height: 3.60771e-06
datapoints: 73
Average: 4.29824
Stand. dev.: 0.217575
0755
lower height: 2.07668e-06
upper height: 3.87721e-06
datapoints: 107
Average: 4.12319
Stand. dev.: 0.293137

YP15
0055
lower height: 2.31431e-06
upper height: 5.11859e-06
datapoints: 137
Average: 4.06117
Stand. dev.: 0.451315
0219
lower height: 3.20374e-06
upper height: 4.73374e-06
datapoints: 82
Average: 3.94593
Stand. dev.: 0.436377
0300
lower height: 1.79919e-06
upper height: 4.44169e-06
datapoints: 111
Average: 4.22976
Stand. dev.: 0.333776
0350
lower height: 1.85111e-06
upper height: 4.55653e-06
datapoints: 170
Average: 4.11507
Stand. dev.: 0.332767
0372
lower height: 2.9914e-06
upper height: 4.86224e-06
datapoints: 265
Average: 4.17159
Stand. dev.: 0.261887
0526
lower height: 3.10459e-06
upper height: 5.68444e-06
datapoints: 252
Average: 4.29499
Stand. dev.: 0.397959
0685
lower height: 2.85512e-06
upper height: 5.03814e-06
datapoints: 110
Average: 4.42341
Stand. dev.: 0.573515
0838
lower height: 3.03975e-06
upper height: 5.62142e-06
datapoints: 259
Average: 4.31113
Stand. dev.: 0.303475
1061
lower height: 3.7293e-06
upper height: 5.85316e-06
datapoints: 205
Average: 4.25427
Stand. dev.: 0.317746
1205
lower height: 3.89646e-06
upper height: 5.51134e-06
datapoints: 94
Average: 4.01122
Stand. dev.: 0.247891

YP7
2346
lower height: -3.29795e-07
upper height: 4.32572e-06
datapoints: 234
Average: 3.79032
Stand. dev.: 0.731166
2464
lower height: 2.01872e-06
upper height: 5.00578e-06
datapoints: 109
Average: 3.94914
Stand. dev.: 0.478385
2648
lower height: 2.08999e-06
upper height: 4.52567e-06
datapoints: 62
Average: 3.87226
Stand. dev.: 0.241372
2738
lower height: -2.92731e-06
upper height: 1.46668e-06
datapoints: 176
Average: 3.97587
Stand. dev.: 0.885227
3243
lower height: 1.70999e-06
upper height: 4.6242e-06
datapoints: 182
Average: 3.51088
Stand. dev.: 0.305278
3543
lower height: -2.65377e-06
upper height: 6.37612e-07
datapoints: 190
Average: 3.36211
Stand. dev.: 0.262685
3616
lower height: 1.03493e-06
upper height: 4.52631e-06
datapoints: 227
Average: 3.94985
Stand. dev.: 0.39205
3678
lower height: 2.20738e-06
upper height: 4.82546e-06
datapoints: 94
Average: 3.65649
Stand. dev.: 0.35949
YP8
0026
lower height: 1.86099e-06
upper height: 3.63125e-06
datapoints: 204

```
  Average:   4.38457
  Stand. dev.:   0.399584
0191
  lower height:   2.05872e-06
  upper height:   4.92959e-06
  datapoints:   187
  Average:   3.76577
  Stand. dev.:   0.495712
0358
  lower height:   3.92934e-06
  upper height:   5.59363e-06
  datapoints:   109
  Average:   4.31692
  Stand. dev.:   0.507661
0508
  lower height:   1.77584e-06
  upper height:   4.04657e-06
  datapoints:   195
  Average:   4.12535
  Stand. dev.:   0.3415
```

Appendix B

Statistical tests

AFM probing of HeLa cells with pyramidal tip

Mann-Whitney U test (Wilcoxon test)
Cell types:

0 non transfected
1 Lamin A wild-type
2 Lamin A E145K
3 mock transfected

==========

comparing celltypes: 0 1
comparing days: 1 1

T-Test P-values
0.198461

Wilcoxon P-values
0.146821 0.856109 0.293643

==========

comparing celltypes: 0 2
comparing days: 1 1

T-Test P-values
0.0353214

Wilcoxon P-values
0.976147 0.0244025 0.0488049

==========

comparing celltypes: 0 3
comparing days: 1 1

T-Test P-values
0.153046

Wilcoxon P-values
0.895947 0.106743 0.213489

==========

comparing celltypes: 1 2
comparing days: 1 1

T-Test P-values
0.00213041

Wilcoxon P-values
0.999412 0.000617347 0.00123472

==========

comparing celltypes: 1 3
comparing days: 1 1

T-Test P-values
0.0124874

Wilcoxon P-values
0.992007 0.00848506 0.0169669

==========

comparing celltypes: 2 3
comparing days: 1 1

T-Test P-values
0.626052

Wilcoxon P-values
0.355196 0.650014 0.710389
==========

comparing celltypes: 0 1
comparing days: 2 2

T-Test P-values
0.862773

Wilcoxon P-values
0.318727 0.6905 0.637644
==========

comparing celltypes: 0 2
comparing days: 2 2

T-Test P-values
0.67115

Wilcoxon P-values
0.56629 0.448261 0.896571
==========

comparing celltypes: 0 3
comparing days: 2 2

T-Test P-values
0.218629

Wilcoxon P-values
0.825301 0.181439 0.362895
==========

comparing celltypes: 1 2
comparing days: 2 2

T-Test P-values
0.720469

Wilcoxon P-values
0.658687 0.353359 0.706735
==========

comparing celltypes: 1 3
comparing days: 2 2

T-Test P-values
0.175637

Wilcoxon P-values
0.898064 0.106 0.212027
==========

comparing celltypes: 2 3
comparing days: 2 2

T-Test P-values
0.301569

Wilcoxon P-values
0.764037 0.245684 0.490779
==========

comparing celltypes: 0 1
comparing days: 3 3

T-Test P-values
0.0329685

Wilcoxon P-values
0.0300937 0.972569 0.0601875
==========

comparing celltypes: 0 2
comparing days: 3 3

T-Test P-values
0.610415

Wilcoxon P-values
0.679385 0.33305 0.66621
==========

comparing celltypes: 0 3
comparing days: 3 3

T-Test P-values
0.0234036

Wilcoxon P-values
0.972872 0.0298827 0.0597653
==========

comparing celltypes: 1 2
comparing days: 3 3

T-Test P-values
0.331437

Wilcoxon P-values
0.931631 0.0733026 0.146475
==========

comparing celltypes: 1 3
comparing days: 3 3

T-Test P-values
0.00122706

Wilcoxon P-values
0.998885 0.00133149 0.00266297
==========

comparing celltypes: 2 3
comparing days: 3 3

T-Test P-values
0.0818701

Wilcoxon P-values
0.89844 0.107925 0.215956
==========

comparing celltypes: 0 0
comparing days: 1 2

T-Test P-values
0.148514

Wilcoxon P-values
0.128773 0.874823 0.25755
==========

comparing celltypes: 0 0
comparing days: 1 3

T-Test P-values
0.0698947

Wilcoxon P-values

0.0974271 0.905639 0.194883
==========

comparing celltypes: 0 0
comparing days: 2 3

T-Test P-values
0.822336

Wilcoxon P-values
0.451976 0.561696 0.903996
==========

comparing celltypes: 1 1
comparing days: 1 2

T-Test P-values
0.826175

Wilcoxon P-values
0.336216 0.671289 0.672431
==========

comparing celltypes: 1 1
comparing days: 1 3

T-Test P-values
0.0292912

Wilcoxon P-values
0.0160087 0.985045 0.0320058
==========

comparing celltypes: 1 1
comparing days: 2 3

T-Test P-values
0.0348527

Wilcoxon P-values
0.023538 0.978192 0.0471179
==========

comparing celltypes: 2 2
comparing days: 1 2

T-Test P-values
0.107206

Wilcoxon P-values
0.00522459 0.995067 0.0104584
==========

comparing celltypes: 2 2
comparing days: 1 3

T-Test P-values
0.0452015

Wilcoxon P-values
0.00851376 0.991894 0.0170261
==========

comparing celltypes: 2 2
comparing days: 2 3

T-Test P-values
0.951414

Wilcoxon P-values
0.566397 0.448333 0.896565
==========

comparing celltypes: 3 3

comparing days: 1 2

T-Test P-values
0.445221

Wilcoxon P-values
0.284148 0.723106 0.568299
==========

comparing celltypes: 3 3
comparing days: 1 3

T-Test P-values
0.994013

Wilcoxon P-values
0.287371 0.722391 0.574749
==========

comparing celltypes: 3 3
comparing days: 2 3

T-Test P-values
0.509846

Wilcoxon P-values
0.797902 0.209922 0.419871

AFM probing of HeLa cells with a glass bead

Mann-Whitney U test (Wilcoxon test)
Cell types:
1 : Lamin A wild-type
2 : Lamin A E145K

Days:
-1 : non transfected
0 : 4 hours post transfection
1 : day 1
2 : day 2
3 : day 3

==========

comparing celltypes: 1 1
comparing days: -1 0

T-Test P-values
0.928241

Wilcoxon P-values
0.549819 0.461282 0.922565

==========

comparing celltypes: 1 1
comparing days: -1 1

T-Test P-values
0.182642

Wilcoxon P-values
0.0869822 0.917882 0.173996

==========

comparing celltypes: 1 1
comparing days: -1 2

T-Test P-values
0.210179

Wilcoxon P-values
0.117454 0.887809 0.234876

==========

comparing celltypes: 1 1
comparing days: -1 3

T-Test P-values
0.723715

Wilcoxon P-values
0.390212 0.623839 0.780358

==========

comparing celltypes: 1 1
comparing days: 0 1

T-Test P-values
0.100737

Wilcoxon P-values
0.0374999 0.964227 0.0749989

```
==========================================

comparing celltypes:    1  1
comparing days:                 0  2

T-Test P-values
0.101986

Wilcoxon P-values
0.050378  0.9515  0.10245
==========================================

comparing celltypes:    1  1
comparing days:                 0  3

T-Test P-values
0.646236

Wilcoxon P-values
0.466134  0.543516  0.932301
==========================================

comparing celltypes:    1  1
comparing days:                 1  2

T-Test P-values
0.824384

Wilcoxon P-values
0.711733  0.295014  0.590021
==========================================

comparing celltypes:    1  1
comparing days:                 1  3

T-Test P-values
0.445626

Wilcoxon P-values
0.817296  0.190011  0.380034
==========================================

comparing celltypes:    1  1
comparing days:                 2  3

T-Test P-values
0.521585

Wilcoxon P-values
0.788392  0.218439  0.436885
==========================================

comparing celltypes:    2  2
comparing days:                 -1  0

T-Test P-values
0.201915

Wilcoxon P-values
0.782306  0.227778  0.456047
==========================================
comparing celltypes:    2  2
comparing days:                 -1  1

T-Test P-values
```

0.00671655

Wilcoxon P-values
0.996633 0.00375631 0.0075188
==========

comparing celltypes: 2 2
comparing days: -1 2

T-Test P-values
0.0675087

Wilcoxon P-values
0.962607 0.0405652 0.0811163
==========

comparing celltypes: 2 2
comparing days: -1 3

T-Test P-values
0.141139

Wilcoxon P-values
0.940817 0.0628062 0.125632
==========
comparing celltypes: 2 2
comparing days: 0 1

T-Test P-values
0.0254352

Wilcoxon P-values
0.990168 0.0107412 0.0215106
==========

comparing celltypes: 2 2
comparing days: 0 2

T-Test P-values
0.307578

Wilcoxon P-values
0.804418 0.204714 0.409429
==========

comparing celltypes: 2 2
comparing days: 0 3

T-Test P-values
0.617721

Wilcoxon P-values
0.57993 0.430639 0.861235
==========
comparing celltypes: 2 2
comparing days: 1 2

T-Test P-values
0.128126

Wilcoxon P-values
0.0870164 0.917806 0.17404
==========
comparing celltypes: 2 2
comparing days: 1 3

T-Test P-values
0.0741293

Wilcoxon P-values
0.0486277 0.954093 0.0971715
==========

comparing celltypes: 2 2
comparing days: 2 3

T-Test P-values
0.677786

Wilcoxon P-values
0.318807 0.690867 0.637626
==========

comparing celltypes: 1 2
comparing days: -1 -1

T-Test P-values
0.129186

Wilcoxon P-values
0.0874018 0.919353 0.174998
==========

comparing celltypes: 1 2
comparing days: 0 0

T-Test P-values
0.345987

Wilcoxon P-values
0.0826778 0.921138 0.165367
==========
comparing celltypes: 1 2
comparing days: 1 1

T-Test P-values
0.00861393

Wilcoxon P-values
0.997666 0.00256044 0.00512006
==========

comparing celltypes: 1 2
comparing days: 2 2

T-Test P-values
0.0972857

Wilcoxon P-values
0.943559 0.0592454 0.118511
==========

comparing celltypes: 1 2
comparing days: 3 3

T-Test P-values
0.811652

Wilcoxon P-values
0.441204 0.569417 0.882433

Nuclear region of whole fibroblasts

CompareCellTypes
==========

comparing celltypes: 2 3 Progeria vs Young
Sample 1: AuxData1
Number of Points=61
Mean=3.85075
Stdv=501723
Degrees of Freedom=60

Sample 2: AuxData2
Number of Points=76
Mean=3.83155
Stdv=340506
Degrees of Freedom=75

Combined effective degrees of freedom: 101.47
T-Test Statistic: 0.255463
Lower Critical Value: -1.98362
Upper Critical Value: 1.98362
H0: avg1=avg2 H0 Acceptance range (0.025000,0.975000)
==> H0 Accepted

Mann-Whitney Wilcoxon Test:
m = 61
n = 76
totalPoints = 137
U_statistic = 2085
Up_statistic = 2551

Using improved normal approximation (no ties).
Lower tail P-value is: 0.157001
Upper tail P-value is: 0.842999
Two tailed P-value is: 0.314003
==========

comparing celltypes: 1 2 Old vs Progeria
Sample 1: AuxData1
Number of Points=57
Mean=3.70843
Stdv=372769
Degrees of Freedom=56

Sample 2: AuxData2
Number of Points=61
Mean=3.85075
Stdv=501723
Degrees of Freedom=60

Combined effective degrees of freedom: 110.51
T-Test Statistic: -1.75661
Lower Critical Value: -1.98166
Upper Critical Value: 1.98166
H0: avg1=avg2 H0 Acceptance range (0.025000,0.975000)
==> H0 Accepted

Mann-Whitney Wilcoxon Test:
m = 57
n = 61
totalPoints = 118
U_statistic = 1593
Up_statistic = 1884

Using improved normal approximation (no ties).
Lower tail P-value is: 0.217351
Upper tail P-value is: 0.782649
Two tailed P-value is: 0.434702
==========

comparing celltypes: 1 3 Old vs Young
Sample 1: AuxData1
Number of Points=57
Mean=3.70843
Stdv=372769
Degrees of Freedom=56

Sample 2: AuxData2
Number of Points=76
Mean=3.83155
Stdv=340506
Degrees of Freedom=75

Combined effective degrees of freedom: 114.53
T-Test Statistic: -1.95562
Lower Critical Value: -1.98089
Upper Critical Value: 1.98089
H0: avg1=avg2 H0 Acceptance range (0.025000,0.975000)
==> H0 Accepted

Mann-Whitney Wilcoxon Test:
m = 57
n = 76
totalPoints = 133
U_statistic = 1738
Up_statistic = 2594

Using improved normal approximation (no ties).
Lower tail P-value is: 0.0257204
Upper tail P-value is: 0.97428
Two tailed P-value is: 0.0514407

Cytoplasmic region of whole fibroblasts

```
 comparing celltypes:    1  2              Old vs. Progeria
 Sample 1: AuxData1
       Number of Points=57
       Mean=3.97619e+06
       Stdv=355404
       Degrees of Freedom=56

 Sample 2: AuxData2
       Number of Points=61
       Mean=3.98604e+06
       Stdv=515137
       Degrees of Freedom=60

 Combined effective degrees of freedom: 106.96
 T-Test Statistic: -0.121521
       Lower Critical Value: -1.98239
       Upper Critical Value: 1.98239
       H0: avg1=avg2          H0 Acceptance range (0.025000,0.975000)
==> H0 Accepted

 Mann-Whitney Wilcoxon Test:
 m = 57
 n = 61
 totalPoints = 118
 U_statistic = 1771
 Up_statistic = 1706

 Using improved normal approximation (no ties).
 Lower tail P-value is: 0.569208
 Upper tail P-value is: 0.430792
 Two tailed P-value is: 0.861583
• CompareTwoCellTypes(LogYoungAvgCytoplasm, CellType, 1, 3)
 ==========================================

 comparing celltypes:    1  3              Old vs. Young
 Sample 1: AuxData1
       Number of Points=57
       Mean=3.97619e+06
       Stdv=355404
       Degrees of Freedom=56

 Sample 2: AuxData2
       Number of Points=76
       Mean=4.09217e+06
       Stdv=303703
       Degrees of Freedom=75

 Combined effective degrees of freedom: 109.59
 T-Test Statistic: -1.98051
```

Lower Critical Value: -1.98185
Upper Critical Value: 1.98185
H0: avg1=avg2 H0 Acceptance range (0.025000,0.975000)
==> H0 Accepted

Mann-Whitney Wilcoxon Test:
m = 57
n = 76
totalPoints = 133
U_statistic = 1847
Up_statistic = 2485

Using improved normal approximation (no ties).
Lower tail P-value is: 0.0736882
Upper tail P-value is: 0.926312
Two tailed P-value is: 0.147376
• CompareTwoCellTypes(LogYoungAvgCytoplasm, CellType, 2, 3)
==========

comparing celltypes: 2 3 Progeria vs. Young
Sample 1: AuxData1
Number of Points=61
Mean=3.98604e+06
Stdv=515137
Degrees of Freedom=60

Sample 2: AuxData2
Number of Points=76
Mean=4.09217e+06
Stdv=303703
Degrees of Freedom=75

Combined effective degrees of freedom: 92.39
T-Test Statistic: -1.42291
Lower Critical Value: -1.98597
Upper Critical Value: 1.98597
H0: avg1=avg2 H0 Acceptance range (0.025000,0.975000)
==> H0 Accepted

Mann-Whitney Wilcoxon Test:
m = 61
n = 76
totalPoints = 137
U_statistic = 1825
Up_statistic = 2811

Using improved normal approximation (no ties).
Lower tail P-value is: 0.016221
Upper tail P-value is: 0.983779
Two tailed P-value is: 0.0324419

AFM probing of isolated nuclei

comparing celltypes: 2 3 Progeria vs. Young
Sample 1: AuxData1
Number of Points=251
Mean=0.000962028
Stdv=0.0011361
Degrees of Freedom=250

Sample 2: AuxData2
Number of Points=200
Mean=0.000503459
Stdv=0.00131202
Degrees of Freedom=199

Combined effective degrees of freedom: 395.46
T-Test Statistic: 3.91078
Lower Critical Value: -1.96598
Upper Critical Value: 1.96598
H0: avg1=avg2 H0 Acceptance range (0.025000,0.975000)
==> H0 Rejected

Mann-Whitney Wilcoxon Test:
m = 251
n = 200
totalPoints = 451
U_statistic = 38283
Up_statistic = 11917

Using improved normal approximation (no ties).
Lower tail P-value is: 1
Upper tail P-value is: 0
Two tailed P-value is: 0
==========

comparing celltypes: 1 2 Old vs. Progeria
Sample 1: AuxData1
Number of Points=108
Mean=0.00192707
Stdv=0.00324187
Degrees of Freedom=107

Sample 2: AuxData2
Number of Points=251
Mean=0.000962028
Stdv=0.0011361
Degrees of Freedom=250

Combined effective degrees of freedom: 118.47
T-Test Statistic: 3.01496
Lower Critical Value: -1.98019

```
        Upper Critical Value: 1.98019
        H0: avg1=avg2          H0 Acceptance range (0.025000,0.975000)
==> H0 Rejected

 Mann-Whitney Wilcoxon Test:
 m = 108
 n = 251
 totalPoints = 359
 U_statistic = 13322
 Up_statistic = 13786

 Using improved normal approximation (no ties).
 Lower tail P-value is: 0.39864
 Upper tail P-value is: 0.60136
 Two tailed P-value is: 0.79728
 ============================================

 comparing celltypes:    1  3          Old vs. Young
 Sample 1: AuxData1
        Number of Points=108
        Mean=0.00192707
        Stdv=0.00324187
        Degrees of Freedom=107

 Sample 2: AuxData2
        Number of Points=200
        Mean=0.000503459
        Stdv=0.00131202
        Degrees of Freedom=199

 Combined effective degrees of freedom: 126.23
 T-Test Statistic: 4.37426
        Lower Critical Value: -1.97894
        Upper Critical Value: 1.97894
        H0: avg1=avg2          H0 Acceptance range (0.025000,0.975000)
==> H0 Rejected

 Mann-Whitney Wilcoxon Test:
 m = 108
 n = 200
 totalPoints = 308
 U_statistic = 14671
 Up_statistic = 6929

 Using improved normal approximation (no ties).
 Lower tail P-value is: 1
 Upper tail P-value is: 7.09517e-08
 Two tailed P-value is: 1.41903e-07
```

Statistical test for comparing lamina thickness

	Cell Type	Avg	SDV between nuclei	Error (= SDV within nuclei)	Total Error	DF (deg. of freedom)
OP	1	23.0036	0.991171	3.16441	3.31601	9
PP all	2	19.317	1.8107	2.16785	2.82457	7
PP a	2	20.9029	0.361161	2.3	2.32818	3
PP b	2	17.7311	0.901507	1.8	2.01314	3
YP	3	22.0071	0.902705	2.05077	2.24065	9

MyOwnTTest()
##################

OP
avg: 23.0036
error: 3.31601
DF: 9

PP all
avg: 19.317
error: 2.82457
DF: 7

T: 2.35178
p: 0.0314868

##################

OP
avg: 23.0036
error: 3.31601
DF: 9

PP a
avg: 20.9029
error: 2.32818
DF: 3

T: 1.01689
p: 0.228314

##################

OP
avg: 23.0036
error: 3.31601
DF: 9

PP b
avg: 17.7311
error: 2.01314
DF: 3

T: 2.59896
p: 0.0214462

##################

OP
avg: 23.0036
error: 3.31601
DF: 9

YP
avg: 22.0071
error: 2.24065
DF: 9

T: 0.746991
p: 0.294391

##################

PP all
avg: 19.317
error: 2.82457
DF: 7

PP a
avg: 20.9029
error: 2.32818
DF: 3

T: -0.855838
p: 0.26377

##################

PP all
avg: 19.317
error: 2.82457
DF: 7

PP b
avg: 17.7311
error: 2.01314
DF: 3

T: 0.881278
p: 0.257875

##################

PP all
avg: 19.317
error: 2.82457
DF: 7

YP
avg: 22.0071
error: 2.24065
DF: 9

T: -2.12426
p: 0.0475325

##################

PP a
avg: 20.9029
error: 2.32818
DF: 3

PP b
avg: 17.7311
error: 2.01314
DF: 3

T: 1.78492
p: 0.0861969

##################

PP a
avg: 20.9029
error: 2.32818
DF: 3

YP
avg: 22.0071
error: 2.24065
DF: 9

T: -0.731952
p: 0.294153

##################

PP b
avg: 17.7311
error: 2.01314
DF: 3

YP
avg: 22.0071
error: 2.24065
DF: 9

T: -2.93413
p: 0.0116189